THE EFFECTS OF TRANSVERSE VIBRATION ON THE PERFORMANCE OF AN AXIAL GROOVE WICK HEAT PIPE

THESIS

Kenneth A. Carpenter, Captain, USAF

AFIT/GA/ENY/94D

DEPARTMENT OF THE AIR FORCE
AIR UNIVERSITY
AIR FORCE INSTITUTE OF TECHNOLOGY

Wright-Patterson Air Force Base, Ohio

AFIT/GA/ENY/94D-5

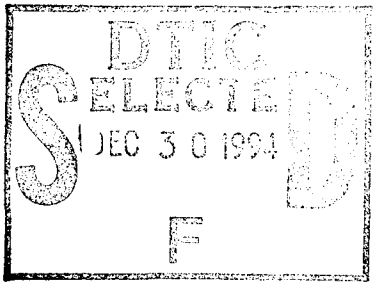

THE EFFECTS OF TRANSVERSE VIBRATION ON THE PERFORMANCE OF AN AXIAL GROOVE WICK HEAT PIPE

THESIS

Kenneth A. Carpenter, Captain, USAF

AFIT/GA/ENY/94D

Approved for public release; distribution unlimited

AFIT/GA/ENY/94D-5

THE EFFECTS OF TRANSVERSE VIBRATION ON THE PERFORMANCE OF AN AXIAL GROOVE WICK HEAT PIPE

THESIS

Presented to the Faculty of the Graduate School of Engineering

of the Air Force Institute of Technology

Air University

in Partial Fulfillment of the

Requirements for the Degree of

Master of Science in Astronautical Engineering

Kenneth A. Carpenter, B.S.

Captain, USAF

December, 1994

Acknowledgments

This thesis has been a long time in the making, and if not for the help and encouragement of several individuals, may never have been. The first of these is Dr. Walter Bienardt of Dynatherm Corporation, who's donation of the heat pipe gave life to this investigation. I'd like to thank Lt. Colonel Jerry Bowman who has been instrumental in keeping me focused, motivated, and heading in the right direction. My thanks also goes out to Mr. Ron Ruley of the AFIT Model Fabrication Center, who's talents and ingenuity turned my vague ideas into usable hardware. A very special thanks goes to Mr. Andy Pitts, Aero/Astro Lab Technician extraordinaire. He spent countless hours helping me track down the assortment of gremlins inherent in any experimental investigation. Finally, my deepest and most heartfelt thank you to my wife, Karen, and my daughter, Katie. Their patience, understanding, and support helped me maintain my perspective and my sanity.

Table of Contents

List of Figures

List of Tables

List of Symbols

Symbol	Definition
A_m	meniscus area (m^2)
A_v	vapor core cross-sectional area (m^2)
A_w	wick cross-sectional area (m^2)
C_p	specific heat of coolant (J/kg-K)
D	characteristic perimeter (m)
DAS	data acquisition system
$DelQ_{max}$	statistical mean performance difference between vibrational case and static baseline (W)
E_{rss}	root-sum square uncertainty value
F	total force (N)
F_l	liquid frictional coefficient
F_v	vapor frictional coefficient
K	effective wick permeability (m^{-2})
L_a	length of adiabatic section (m)
L_c	length of condenser section (m)
L_e	length of evaporator section (m)
L_t	total length of heat pipe (m)
P_c	capillary pressure (N/m^2)
P_l	liquid pressure (N/m^2)
P_v	vapor pressure (N/m^2)
$Q_{b,max}$	boiling heat transport limit (W)
$Q_{c,max}$	capillary heat transport limit (W)
$Q_{e,max}$	entrainment heat transport limit (W)
$Q_{s,max}$	sonic heat transport limit (W)
Q_{max}	experimental heat transport limit (W)
$(QL)_{c,max}$	capillary limit on heat transport factor (W-m)
R_o^2	square of the reliability of the least square curve fit
R_v	vapor gas constant (J/kg-K)
T	tension force (N)
T_i	coolant manifold inlet temperature (°C)
T_o	coolant manifold outlet temperature (°C)
T_O	stagnation temperature (K)
T_{op}	operating temperature (°C)
T_v	vapor temperature (K)

TC	thermocouple
TC1	first TC in evaporator section (top)
TC2	first TC in evaporator section (bottom)
TC3	center TC in evaporator section
TC4	last TC in evaporator section
TC5	first TC in adiabatic section
TC6	center TC in adiabatic section
TC7	last TC in adiabatic section
TC8	first TC in condenser section
TC9	center TC in condenser section
TC10	last TC in condenser section
TC11	coolant manifold inlet
TC12	coolant manifold outlet
a	acceleration (m/sec^2)
f	oscillation frequency (Hz)
f	function of independent variables
$f_v Re_v$	vapor drag coefficient-Reynolds number
g	gravitational force constant (9.81 m/sec^2)
g_{pk}	peak acceleration amplitude (g)
k	half double-amplitude displacement (m)
k_e	effective thermal conductivity of liquid/saturated wick matrix (W/m-K)
k_l	liquid thermal conductivity (W/m-K)
k_w	wall thermal conductivity (W/m-K)
m	mass (kg)
$\dot{m}$	mass flow rate of coolant (kg/sec)
n	number of grooves
$r_{h,s}$	hydraulic radius of wick at vapor/wick interface (m)
$r_{h,v}$	vapor hydraulic radius (m)
r_i	inside radius of heat pipe (m)
r_n	boiling nucleation radius (m)
r_p	effective pore radius (m)
r_v	vapor core radius (m)
t	time (sec)
t_l	groove land thickness (bottom) (m)
u_1	first independent variable
u_2	second independent variable
u_n	nth independent variable
$\dot{v}$	volumetric flow rate (l/min)

w	groove opening (inner radius) (m)
w_b	groove opening (outer radius) (m)
w_f	groove fin thickness (m)
ΔC_p	uncertainty in specific heat of coolant water (J/kg-K)
$\Delta \dot{m}$	uncertainty in mass flow rate (kg/sec)
$\Delta P_\perp$	hydrostatic pressure $\perp$ to heat pipe axis (N/m^2)
ΔQ_{max}	rss uncertainty in maximum heat throughput (W)
ΔT_i	uncertainty in coolant inlet temperature (K)
ΔT_o	uncertainty in coolant outlet temperature (K)
Δu_1	uncertainty in first independent variable
Δu_2	uncertainty in second independent variable
Δu_n	uncertainty in nth independent variable
Φ	heat pipe inclination angle (radians)
α	heat pipe groove angle (degrees)
γ_o	specific gas constant
δ	groove depth (m)
η	unit depth (m)
λ	latent heat of vaporization (J/kg)
σ	surface tension coefficient (N/m)
ρ_l	liquid density (kg/m^3)
ρ_o	vapor density at stagnation temperature (kg/m^3)
ρ_v	vapor density (kg/m^3)
μ_l	liquid viscosity (kg/m-sec)
μ_v	vapor viscosity (kg/m-sec)
ω_o	oscillation frequency (rad/sec)

Abstract

An experimental investigation was performed to determine the effects of transverse vibrations on the performance of an ammonia/aluminum axial groove wick heat pipe. Theoretical calculations predicted a performance degradation due to the working fluid being shaken out of the upper capillary grooves. A benchtop shaker was used to apply transverse, sinusoidal vibrations of 30, 35, and 40 Hertz, corresponding to peak acceleration amplitudes of 1.84g, 2.50g, and 3.27g, respectively. Maximum heat throughput, Q_{max}, of the vibrating heat pipe was measured. A comparison of these values and static Q_{max} values indicated a degradation in heat pipe performance. A mean performance deterioration of 27.6 Watts was measured for the 1.84g case; an average degradation of 12.9 percent from static heat pipe performance. At 2.50g peak acceleration, the degradation rose to 37.3 Watts; an average decrease of 14.8 percent from static performance. An average deterioration in performance of 28.1 percent was recorded for the 3.27g case. This amounted to a mean performance degradation of 69.3 Watts. The results of this investigation revealed that transverse, sinusoidal vibrations have a detrimental impact on the performance of an ammonia/axial groove wick heat pipe. Further, the performance degradation increases with increasing vibrational peak acceleration amplitude.

THE EFFECTS OF TRANSVERSE VIBRATION ON THE PERFORMANCE OF AN AXIAL GROOVE WICK HEAT PIPE

I. Introduction

Background

The heat pipe was first developed in 1963, at the Los Alamos Scientific Laboratory (14). Since then, the heat pipe has been the subject of a great deal of research and experimentation. Early investigations into heat pipe applications centered on space applications because of the heat pipe's low weight to heat transfer ratio and its' mechanical simplicity (10, 11). However, like many new and revolutionary technologies, peripheral uses started emerging almost instantly. Heat pipes have been used in, or proposed for, such diverse applications as nuclear reactor cooling, road/runway/bridge de-icing, electronic component cooling, permafrost temperature maintenance, aircraft leading edge cooling, and spacecraft thermal control (4, 5:211-213, 19:3).

The aerospace industry is particularly attracted to the use of heat pipes in both spacecraft and aircraft (6, 20). One commonality between both of these applications is the use of heat pipes in mechanical systems designed to operate in extremely dynamic environments. Both aircraft

and spacecraft are subject to a wide array of induced vibrations due to their dynamic environments. These vibrations are experienced by all parts of the system, including the heat pipes.

To date, only a limited amount of research has been devoted to evaluating the effects of vibrations on the performance characteristics of heat pipes. The first reported study was conducted in 1967 at the Los Alamos Scientific Laboratory, by Deverall et al (9:3). This study concentrated on determining the effects of a simulated missile launch environment on the performance of a water/stainless steel mesh wick heat pipe. The researchers subjected the test articles to both sinusoidal and random vibrations while in the horizontal position. Additionally, they evaluated heat pipe performance when subjected to sinusoidal vibration while in inclined orientations. The results of their investigation showed no deterioration of the heat pipe performance due to vibrational effects. Instead, they documented a heat pipe performance improvement, due to enhanced wick wetting, as a result of the vibrations. They also recommended applying vibrations to heat pipes as part of the manufacturing process to ensure complete wick wetting (9:7).

A subsequent study disagreed with the findings of the Deverall experiments. This evaluation, accomplished in 1969 by Richardson et al. (18:249), studied the effects of longitudinal, sinusoidal vibrations on the performance of a water/sintered metal wick heat pipe. The researchers

considered a wide range of operating frequencies as well as several acceleration loads. These experiments included both horizontal and inclined heat pipe tests. The data collected in this study indicated there is a detrimental effect on heat pipe performance due to longitudinal vibrations. Additionally, the detrimental effects grew in severity as operating frequency was lowered, and as acceleration load was increased (18:265). A direct comparison to the Deverall study is difficult for two reasons. First, the Deverall study evaluated a different wick configuration; a stainless steel mesh wick as opposed to a sintered metal wick. Second, Deverall does not account for the orientation of the vibration axis with respect to the heat pipe axis.

These two studies, Deverall and Richardson, constituted the sum of all knowledge regarding heat pipes and vibrational effects for the next 20 years. The apparent conflict between the two studies, and the lack of a direct correlation between them, left heat pipe designers with no clear cut answers. While evaluating the potential for using heat pipes to cool the throat area in satellite attitude thrusters, researchers at Aerojet TechSystems were unsure of what to expect when the heat pipes were subjected to the operational environment. They postulated that the vibrations resulting from thruster firing could either "...reduce bubble formation in the evaporator giving greater heat flux capacity." or "...the

vibrations may preclude efficient condensate flow." inhibiting heat flux capacity (8:14).

In most cases, heat pipes were designed, neglecting potential vibrational effects. The performance capabilities of these pipes were then verified experimentally. Current textbooks still endorse this approach. In his book, Silverstein recommends, "When heat pipe operation is required under vibrational conditions, operability should be verified experimentally for the expected vibrational environment." (19:69). More research is obviously needed, and continues, although sporadically.

In 1988, Clark and Glenn studied the effect of random vibrations on the performance characteristics of a sodium/sintered metal wick heat pipe (6). This heat pipe was proposed for use in cooling the leading edges of hypersonic aircraft. The researchers were extremely thorough, basing their test frequencies on MIL-STD-8100, and evaluating the correlation of both heat pipe orientation and vibrational axis in the heat pipe performance tests. As a result of their exhaustive testing, the researchers determined that vibrations have no discernible effect on the performance of the tested heat pipe.

However, more recent studies would seem to indicate otherwise. In 1992, Charlton studied the effects of transverse, sinusoidal vibrations on the capillary heating limit of a water/copper mesh wick heat pipe (3). While he could find no conclusive evidence of a degradation in capillary

limit due to the vibrations, his results appeared to indicate a relationship did exist. However, the magnitude of the change was of the same order as the experimental error. Therefore, no firm conclusions could be drawn (3:6.2).

More rigorous conclusions were drawn from a study done a year later. Following up on the work of Charlton, Huber evaluated the effects of sinusoidal vibrations on a water/copper mesh wick heat pipe. Instead of using transverse vibrations, however, Huber utilized longitudinal vibrations in his evaluations (15). His findings indicated that longitudinal, sinusoidal vibrations degraded the capillary limit temperature of the test article. He also found this degradation increased as the maximum acceleration load increased. Additionally, he recommended those heat pipes with other wick structures, such as axial grooves or sintered metal, be tested (15:6.3).

Purpose and Scope

The purpose of the current experimental study was to broaden the knowledge-base regarding the effects of vibrations on heat pipe performance. This study investigated the effects of sinusoidal, transverse vibrations on an ammonia/axial groove wick heat pipe. To accomplish this, heat pipe performance was measured at three vibrational frequencies, specifically 30, 35, and 40 Hertz, while maintaining a constant oscil-

latory amplitude. These test frequencies corresponded to vibrational acceleration amplitudes of 1.84g, 2.50g, and 3.27g, respectively. The acceleration amplitudes were used to correlate the results of the vibrational test cases. The results of these vibrational test cases were compared to static heat pipe performance data for changes directly attributable to the vibration of the heat pipe. This research was the first to evaluate vibrational effects in an axial groove wick heat pipe.

II. Theoretical Investigations

Heat Pipe Geometry

Heat pipe performance is as much a function of the wick geometry as it is a function of the working fluid. The heat pipe for this experiment was supplied by Dynatherm Corporation. It was an axial groove wick heat pipe of extruded aluminum. For a working fluid, the heat pipe was charged with 8.6 grams of anhydrous ammonia. Fig. 2.1 shows the tested heat pipe in cross section while Table 2.1 presents critical heat pipe dimensions. The tested heat pipe is shown in profile in Fig. 2.2 and includes the dimensions for the evaporator, adiabatic, and the condenser sections (21).

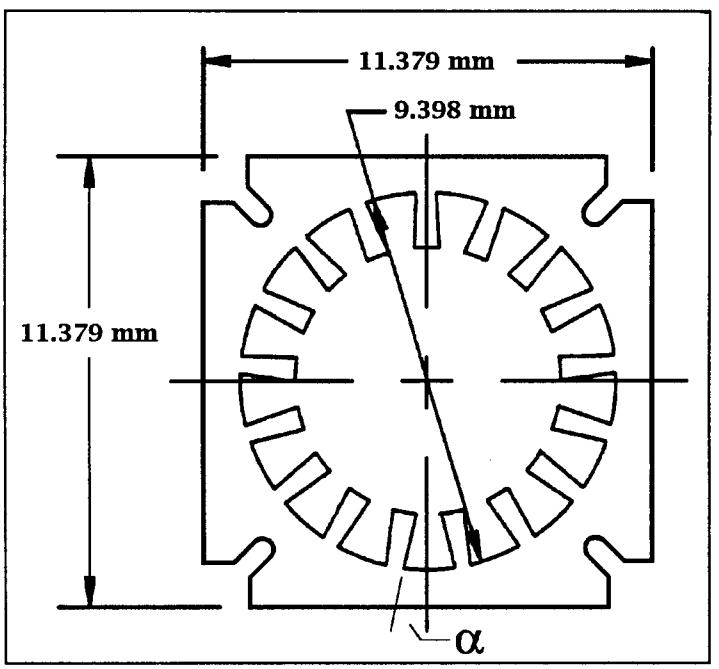

Figure 2.1 Heat Pipe Cross-Sectional Drawing

Table 2.1 Heat Pipe Cross-Section Parameters

Land Thickness (Bottom)	t_l	0.020 in	0.508 mm
Groove Opening (Top)	w	0.025 in	0.635 mm
Groove Opening (Bottom)	w_b	0.048 in	1.219 mm
Groove Depth	δ	0.055 in	1.397 mm
Groove Angle	α	13.9°	0.2426 rad
Number of Grooves	n	17	17

Heat Transport Limits

All heat pipes are constrained by four operating heat transport limits. These are the sonic limit, the entrainment limit, the capillary limit and the boiling limit. The heat transport limits are functions of the heat pipe geometry, the working fluid properties, and the heat pipe operational environment. This last category includes heat pipe inclinations, heat pipe section lengths, and other external influences.

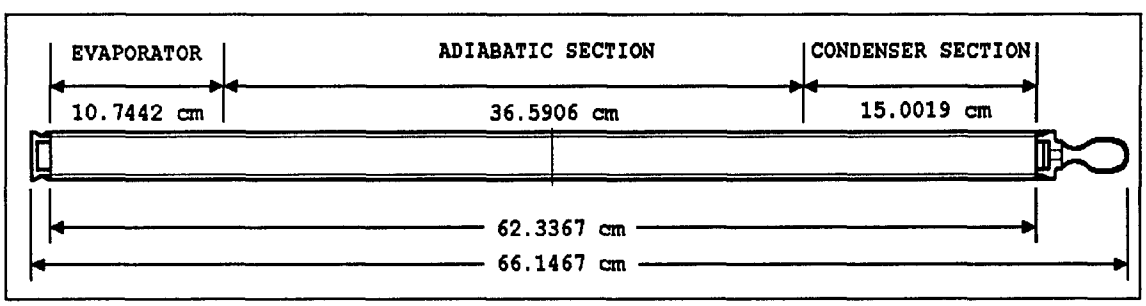

Figure 2.2 Heat Pipe Profile View

The complete explanations and derivations for the heat transport limits of the tested heat pipe are provided in Appendix A. Table 2.2 is a representation of the theoretical operating limits of the tested heat pipe. Column 1 of this table gives the heat pipe operating temperature, which

is the temperature of the adiabatic section of the heat pipe. The remaining columns give the values for the four heat transport limits at the various operating temperatures. An examination of Table 2.2 reveals that for the anticipated operating temperature range of 40 to 80°C, the boiling limit was expected to constrain the maximum heat transport of the test article since it has the lowest heat transport value for the entire operating range. However, as Chi points out (5:89-93), the boiling limit of a heat pipe must be verified experimentally.

Table 2.2 Theoretical Heat Transport Limits

T_{op}	$Q_{s,max}$	$Q_{e,max}$	$Q_{c,max}$	$Q_{b,max}$
Operating Temperature (Celsius)	Sonic Limit (Watts)	Entrainment Limit (Watts)	Capillary Limit (Watts)	Boiling Limit (Watts)
40	99050	529.29	289.09	18.22
50	124740	543.15	263.78	12.69
60	158550	554.04	234.78	8.58
70	202230	558.36	202.64	5.63
80	256760	551.02	168.05	3.59

Experimental investigation showed the theoretical boiling limit to be overly conservative. This agrees with the findings of Brennan and Kroliczek. They point out that boiling limit models are very conservative. In their work, they found the theoretical boiling limit can be an order of magnitude lower than the actual boiling limit (2:44). The true heat transport limit in the operating temperature range of 40 to 80°C proved to be the capillary limit.

Critical Acceleration

The basic premise of this investigation theorized a degradation in heat pipe performance due to transverse vibrations. The hypothesis stated at the right combination of vibrational frequency and vibrational amplitude, a critical acceleration of the working fluid could be achieved. At this critical acceleration, the working fluid would be shaken loose from the upper grooves of the heat pipe. This in turn would lead to early dryout of the upper capillary grooves, and a decrease in maximum heat throughput. This hypothesis was based on the principles of surface tension and droplet formation.

The theoretical investigation of this hypothesis started by examining a cross-section of one of the upper capillary grooves. The groove was assumed to be filled with the working fluid, and was used as a control volume. The sum of the vertical forces acting on this control volume, depicted in Fig. 2.3, is represented by

$$F = ma = T + P_v A_m - mg - P_l A_m \qquad (2\text{-}1)$$

where F = sum of the forces acting on the fluid element (N)
m = mass of the fluid element (kg)
a = acceleration of the fluid element (m/sec^2)
g = gravitational acceleration (9.81 m/sec^2)
P_v = pressure of the surrounding vapor (N/m^2)
P_l = pressure of the fluid (N/m^2)
A_m = meniscus area (m^2)
T = tension force (N)

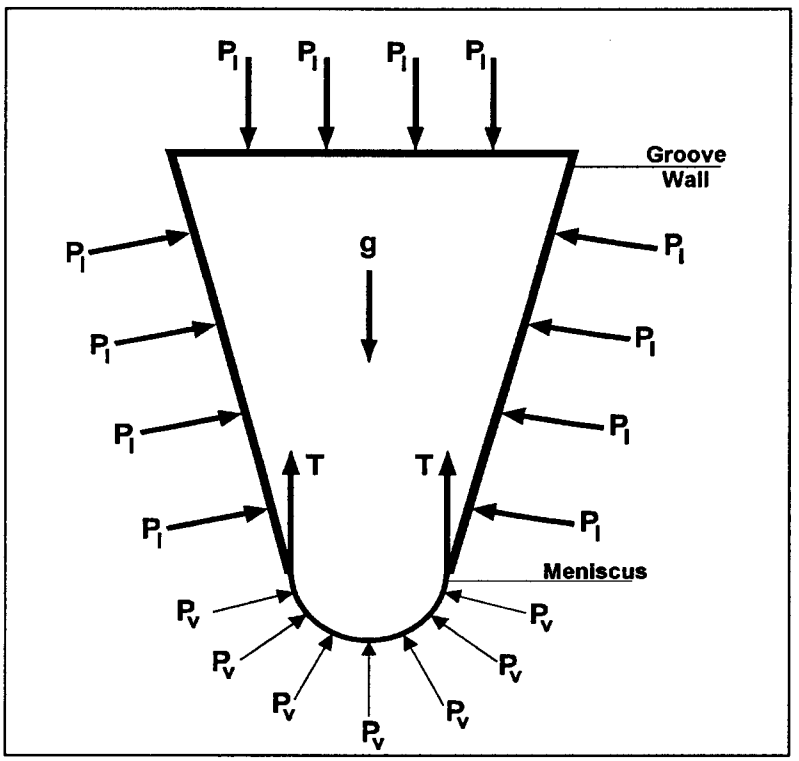

Figure 2.3 Control Volume Force Diagram

Assume the fluid element is of unit depth. Further, assume the two pressure forces are of the same order of magnitude, then Eq. 2-1 becomes:

$$ma \approx T - mg \tag{2-2}$$

In his book, Adam gives an equation for the tension force (T) in terms of the surface tension (σ) and a characteristic perimeter length (D) (1:8).

$$T = \sigma D \tag{2-3}$$

In the tested heat pipe, the perimeter of one groove is a long rectangle with sides the length of the pipe, and the width being the width of the grooves. To simplify the analysis, the control volume end effects are assumed to be negligible. The tension force then reduces to

$$T = 2\eta\sigma \tag{2-4}$$

where η is the unit depth along the groove.

For the shaker used in this experiment, the equation for the acceleration imparted into the test article is given by (22):

$$a = k\omega_o^2 \sin(\omega_o t) \tag{2-5}$$

where a = test article acceleration (m/sec^2)
k = half double-amplitude (DA) displacement (m)
ω_o = oscillation frequency (rad/sec)
t = time (sec)

Now Eq. 2-2, Eq. 2-4 and Eq. 2-5 can be combined, yielding an expression in terms of the fluid properties and the vibrational parameters.

$$\frac{2\sigma\eta}{m} - g \approx k\omega_o^2 \sin(\omega_o t) \tag{2-6}$$

The fluid volume will experience maximum acceleration when $\omega_o t$ is either $\pm \pi/2$. In this case, the equation further simplifies to

$$\frac{2\sigma\eta}{m} - g \approx \pm k\omega_o^2 \tag{2-7}$$

Assuming a constant double-amplitude displacement of 0.04 in. (1.016 mm), Eq. 2-7 can be rearranged to solve for the critical shaker frequency.

$$\omega_o \approx \left[\frac{2\sigma\eta}{km} - \frac{g}{k}\right]^{\frac{1}{2}} \quad \text{and} \quad \omega_o \approx \left[\frac{g}{k} - \frac{2\sigma\eta}{km}\right]^{\frac{1}{2}} \tag{2-8}$$

The derivation continues using the first expression in this equation.

The mass of the fluid element, m, is a function of the groove geometry shown in Fig. 2.4, and the fluid density. The equation for the fluid mass reduces to

$$m = \rho_l \text{Vol.} = \rho_l \left[w\delta + \left((w_b - w)/2 \right)\delta \right]\eta \tag{2-9a}$$

$$m = \rho_l \delta\eta \left(\frac{w_b + w}{2} \right) \tag{2-9b}$$

where ρ_l = fluid liquid density (kg/m^3)
w = inner groove width (m)
w_b = outer groove width (m)
δ = groove depth (m)
η = unit depth

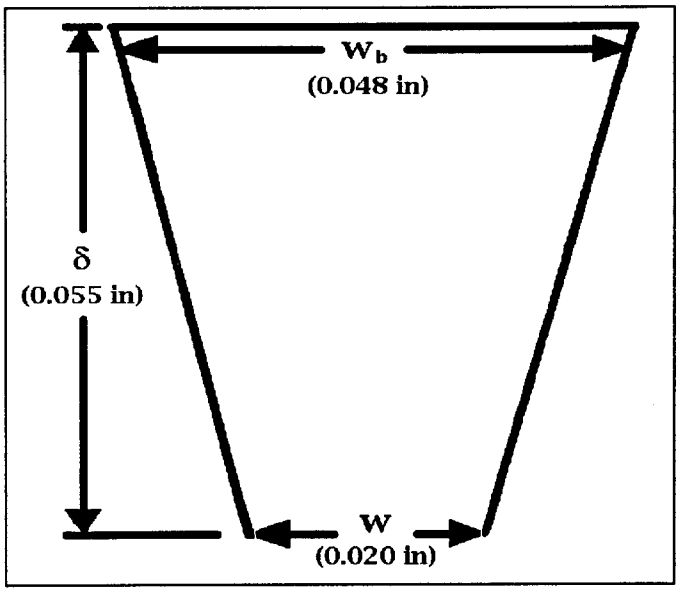

Figure 2.4 Capillary Groove Geometry

Inserting this equation for the fluid mass into the critical frequency equation, Eq. 2-8, results in:

$$\omega_o \approx \left[\frac{1}{k}\left(\frac{2\eta\sigma}{\rho_l \delta \eta\left(\frac{(w_b + w)}{2}\right)} - g\right)\right]^{\frac{1}{2}} \qquad (2\text{-}10a)$$

$$\omega_o \approx \left[\frac{1}{k}\left(\frac{4\sigma}{\rho_l \delta (w_b + w)} - g\right)\right]^{\frac{1}{2}} \qquad (2\text{-}10b)$$

In this equation, there are two temperature dependent terms, σ and ρ_l, with the remainder of the terms being constant. The critical frequency is therefore a function only of operating temperature. Using this

equation, a critical frequency based on operating temperature can be found. The oscillation frequency is then changed from rad/sec to Hertz (cycles/sec) using the relationship

$$f = \left(\frac{\omega_o}{2\pi}\right) \tag{2-11}$$

where f = oscillation frequency in Hertz (cycles/sec)

The final calculation involves computing the peak acceleration amplitude resulting from the given oscillation frequency. This is accomplished by using an equation supplied by the shaker manufacturer (22:A-1). This equation was given as:

$$g_{pk} = 0.0511 \times (2k) f^2 \tag{2-12}$$

where g_{pk} = peak acceleration amplitude in Earth gravity units (g)
k = half double-amplitude (DA) displacement (in)
f = oscillation frequency (Hz)

Combining Eq. 2.10b, Eq. 2.11 and Eq. 2.12, results in an expression for the peak acceleration amplitude in terms of the groove geometry and the working fluid characteristics.

$$g_{pk} = 0.0511(2k)\left\{\frac{\left[\frac{1}{k}\left(\frac{4\sigma}{\rho_l \delta (w_b + w)} - g\right)\right]^{1/2}}{2\pi}\right\}^2 \tag{2-13}$$

$$= 0.0511(2k)\left[\frac{\frac{1}{k}\left(\frac{4\sigma}{\rho_l \delta (w_b + w)} - g\right)}{4\pi^2}\right]$$

$$= 0.0511\left[\frac{\left(\frac{4\sigma}{\rho_l \delta (w_b + w)} - g\right)}{2\pi^2}\right]$$

Using Eq. 2-13, the peak acceleration amplitude of the heat pipe can be found as a function of the operating temperature. At a given operating temperature, the peak acceleration amplitude computed using Eq. 2-13 is the critical acceleration. Vibrating the heat pipe in excess of the critical acceleration will result in the working fluid being shaken out of the upper capillary grooves. The loss of this fluid leads to premature wick dryout, and, therefore, reduced heat pipe performance. The critical acceleration-critical temperature plot for the tested heat pipe is given in Fig. 2.5.

Similar arguments can be made starting with a fixed acceleration amplitude. For a given peak acceleration amplitude, there is a critical operating temperature. Operation of the heat pipe at temperatures in excess of the critical operating temperature will result in the working

fluid being shaken from the capillary grooves. This leads to the same loss of performance described earlier.

It is this second approach, maintaining a constant peak acceleration amplitude and increasing the heat pipe operating temperature, that formed the basis for this investigation.

An examination of Fig. 2.5 shows for an anticipated operating temperature range of 40 to 80 degrees Celsius, the theoretical critical acceleration amplitude ranges from approximately 2.00g to 3.85g. For this investigation, test frequencies of 30 Hz, 35 Hz, and 40 Hz were used. These frequencies corresponded to peak acceleration amplitudes of 1.84g, 2.50g, and 3.27g, respectively.

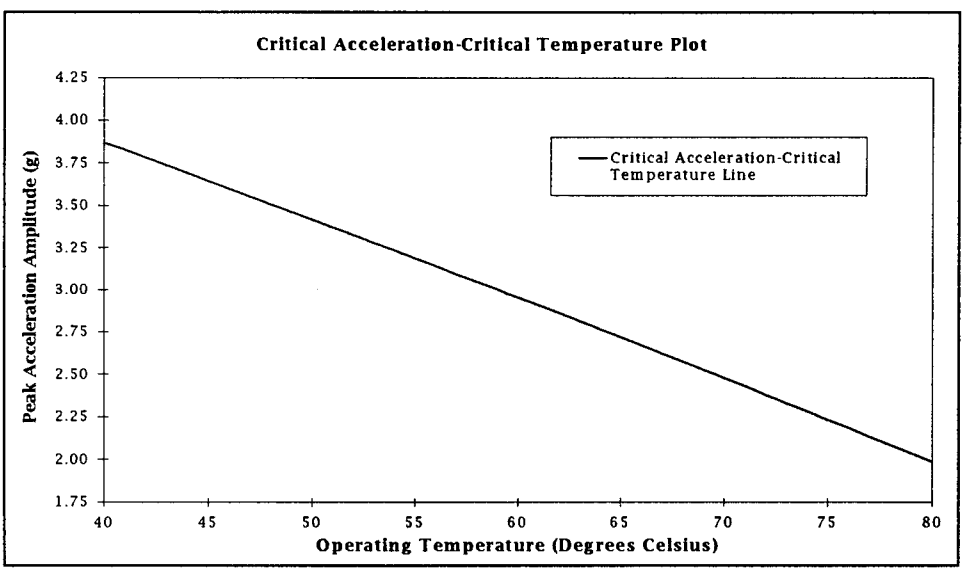

Figure 2.5 Critical Acceleration-Critical Temperature Graph

III. Experimental Investigations

Experimental Equipment

The equipment for this experiment consisted of five major subsystems, in addition to the heat pipe. The first subsystem is the coolant system. The coolant system provided the heat sink to maintain the temperature of the condenser end of the heat pipe. Additionally, by adjusting the coolant temperature and flow rate, the operating temperature of the heat pipe was controlled. The next subsystem is the heater system. The heater system was used to incrementally increase the thermal heat load experienced by the evaporator section of the heat pipe. The vibration system provided the controlled, sinusoidal vibrations for this experiment. The data acquisition system (DAS) was used to display and record pertinent experimental data. The primary components of the DAS were the thermocouples (TCs) mounted to the outside of the heat pipe. These TCs measured and recorded the heat pipe surface temperature during each test run. Fig. 3.1 shows the location and designation of the twelve TCs used in this experiment. Finally, there is the structural subsystem. This system contained the brackets, bolts, and fixtures that supported the other systems and isolated the experiment from outside

influences. A detailed description and schematic of these five subsystems, along with their individual components, is provided in Appendix B.

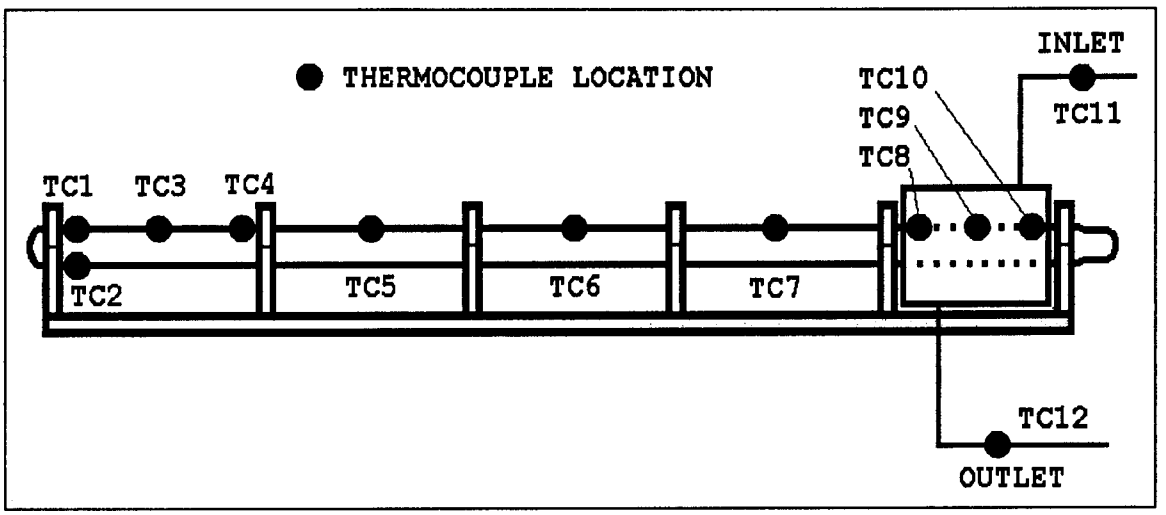

Figure 3.1 Heat Pipe Thermocouple Location

Experimental Process

Several parameters needed to be established and verified before any reliable test data could be collected. The first of these was to ensure the test set-up could not be affected by outside influences. This required the heat pipe to be perfectly level and totally insulated. The former was accomplished using a digital inclinometer, and adding or removing shim stock from the condenser end hinge assembly/stand-off bracket joint, as necessary. The insulation for the coolant manifold, coolant system, and the heater system are detailed in Appendix B. Additionally, the adiabatic section of the heat pipe was insulated using 6.35 mm of RPC-X-AQ Ceramic Fiber Insulation, covered with 9.52 mm of polystyrene foam insula-

tion. These measures, leveling and insulating the heat pipe, were taken to prevent gravity and outside thermal effects from corrupting the test data.

Once the heat pipe was isolated, the issue of wick dryout needed to be addressed. Heat pipe wick dryout is defined in the literature as a condition in which the working fluid is vaporized and cannot be replenished. It is recognized by large, rapid increases in evaporator wall temperatures (3:2.19). There are three primary causes of wick dryout. The first involves the working fluid being swept up into a rapidly moving vapor stream (entrainment limit). Second, the working fluid is being evaporated more rapidly than it can be replaced by capillary action (capillary limit). Finally, rapidly expanding vapor bubbles formed by boiling working fluid may prevent replacement fluid from reaching the heat pipe walls (boiling limit). These three methods of wick dryout represent three of the four heat transport limits discussed in Chapter 2, with the capillary limit governing this experiment.

Safety concerns dictated that wick dryout be avoided at the upper end of the anticipated operating temperature range. Since this heat pipe was designed for use in space applications, it's design operating temperature was 15°C. At the anticipated operating temperature range of 40 to 80°C, the working fluid vapor pressure inside the heat pipe became a real concern. According to the data Ivanovski provided in his book, at

the anticipated upper operating temperature, the saturated vapor pressure of ammonia is over 3.87×10^6 N/m^2 (550 psi) (17:249). This caused concern for heat pipe integrity. Additionally, based on the theoretical calculations of Appendix A, and the capacity of the coolant system, it was not possible to attain heat pipe wick dryout at the lower temperature of the anticipated operating range. Therefore, an alternative to the conventional definition of dryout needed to be developed. This definition needed to give a reliable indication of imminent dryout, but at a reduced temperature and, therefore, internal pressure.

After a series of trial runs were performed, a suitable dryout criteria for this experiment was devised. The dryout criteria selected was based on a temperature difference between TC1 and TC2. These thermocouples are located at the beginning of the evaporator section, with TC1 being on the top of the heat pipe, and TC2 on the bottom. The hypothesis predicted, and experimental investigation showed, the temperature at TC1 would always be greater than, or equal to the temperature at TC2. The temperature difference between these two TCs increased as the heat load of the heat pipe increased. The wick dryout criteria was defined as a temperature difference of 1.1°C, or more, between TC1 and TC2, lasting for at least 10 time intervals. The data acquisition rate used in this experiment was set at 5 seconds to keep the data files to a manageable size.

There were two primary reasons for the selection of this dryout criteria. First, this temperature difference is slightly over twice the uncertainty of the thermocouples temperature response of 0.5 °C. Second, the selected criteria is about three times the nominal temperature difference between the two thermocouples, TC1 and TC2. Both of these reasons result in a 95 percent or better reliability in the identification of wick dryout, based on the assumption of a Gaussian distribution in the both the thermocouple uncertainty and the nominal temperature difference between the two thermocouples, TC1 and TC2.

To ensure the selected definition of dryout was a valid indication of imminent true wick dryout, several trial runs were made. The purpose of these runs was to verify the addition of more heat to the system, once the selected dryout criteria had been met, would indeed result in true wick dryout. These trial runs confirmed wick dryout, as defined in the literature, did occur and that the temperature difference between TC1 and TC2 continued to increase, without ever falling below the 1.1°C threshold previously established. Appendix C contains the data resulting from one of these verification runs.

After establishing the dryout criteria, it was necessary to verify the heat transport limit governing these investigations. Recalling the theoretical work of the previous chapter, the maximum heat throughput was expected to be the boiling heat transport limit. But as Chi pointed out,

the boiling limit must be verified experimentally (5:89-90). To this end, a series of trial runs were completed. Then, with wick dryout as the criterion, the collected data was used to compute the heat throughput of the heat pipe at the time of dryout by means of:

$$Q_{max} = \dot{m} C_p (T_o - T_i) \tag{3-1}$$

where Q_{max} = maximum heat throughput at dryout (W)
$\dot{m}$ = coolant water mass flow rate (kg/sec)
C_p = coolant specific heat (J/kg-K)
T_o = coolant manifold outlet temperature, T12 (K)
T_i = coolant manifold inlet temperature, T11 (K)

This equation is based on the assumption that the specific heat of the coolant (water) is constant between T_o and T_i. In these investigations, this temperature difference was found to be on the order of 15°C or less. Over this limited temperature range, the change in value of the specific heat for water is relatively small, less than 0.2 percent. Therefore, the assumption of constant specific heat is justified.

Once the data from the trial runs had been reduced using Eq. 3-1, it was compared to the theoretical findings plotted in Appendix A. This comparison used the computed maximum heat throughput and defined the heat pipe operating temperature as the average of the first two adiabatic section thermocouples (TC5 and TC6), to verify the heat transport limit for these investigations. The analysis determined the heat trans-

port limit for this experiment was actually the capillary limit, not the boiling limit as predicted by theoretical calculations. This coincides with the findings of Brennan and Kroliczek (2:44).

During the verification runs, a discrepancy was discovered between the temperature being recorded by the DAS and the true temperature at the various test points. These discrepancies were determined by comparing DAS temperature readings to those achieved by connecting the same thermocouple to an Omega Omnical Thermocouple Calibration Unit. Further investigation determined the DAS was adding a bias to the data stream and this bias was channel dependent. The discrepancy in the data was a function of the channel to which a given thermocouple was connected. Based on a series of tests and measurements, the reliability of each channel was determined in terms of measuring a true temperature, and the error associated with a given channel measurement.

With this channel bias data in hand, it then became necessary to analyze the data requirements in an attempt to determine the most critical readings in terms of true temperature measurement accuracy and allowable temperature measurement standard deviation. The most critical thermocouples were determined to be TC1, TC2, TC5, TC6, TC11, and TC12. Of these, TC1 and TC2 needed only an accurate reading of the relative difference between the two TCs. This meant the channels

associated with these two TCs must provide readings with a small standard deviation in temperature measurement, but not necessarily an accurate temperature reading. These were the thermocouples used for determining wick dryout. The other four TCs needed data readings that had both accuracy in true temperature measurement and small temperature measurement standard deviations. The critical thermocouples were then connected to the data channels most nearly matching their data requirements. Additional bias measurements were accomplished as part of each experimental test run to further eliminate the influence of the DAS bias on the final results of the experiment.

The lessons learned while completing the parameter identification and verification portion of the experiment were utilized to develop a test discipline and test procedure to be followed during the actual test runs.

Experimental Procedures

In order to assure each of the test runs was performed in exactly the same manner, a rigorous test procedure was developed and adhered to. This test procedure is listed below.

Experimental Test Procedure

1. Set coolant bath temperature and coolant flow rate.
2. Allow system to come to equilibrium.
3. Set power supply to initial heater setting.
4. For vibrational test runs, set vibrational frequency and amplitude.
5. Allow 10 minutes for system stabilization.

6. Begin test run.
7. Increment heat load by approximately 5 watts.
8. Allow system to stabilize (5 to 10 minutes).
9. Repeat steps 7 and 8 until dryout has been achieved.
10. Record coolant system readings.
11. Allow system to stabilize.
12. Take bias temperature readings.

12a. For vibrational tests;

   i. Shut off shaker.

   ii. Allow system to stabilize, monitoring for heat pipe rewetting (temperature difference between TC1 and TC2 drops below 1.1°C.

   iii. If rewet occurs, heat to dryout, following steps 7 and 8.

13. Decrease power by approximately 15 watts.
14. Verify heat pipe rewet (temperature difference between TC1 and TC2 dropping below 1.1°C).
15. End test run.
16. Shut off heater.

IV. Experimental Results and Analysis

The experimental results from this investigation have been divided into three sections: static data, vibrational data, and an analysis section which includes both an observational and a statistical analysis. The section on vibrational data is further subdivided to examine the results from each of the three vibrational cases; corresponding to peak acceleration amplitudes of 1.84g, 2.50g, and 3.27g. The static data and the vibrational data are presented in both tabular and graphical form. In the analysis section, both observational and statistical methods are used to evaluate the vibrational test data with respect to the experimental static test results. The results of the statistical analysis will be presented in graphical form only. Included with the data will be the uncertainty associated with the data. The details of the uncertainty analysis are provided in Appendix D.

Static Data

The static data presented in this section was used to establish a baseline for heat pipe performance. In the next section, the baseline is used to evaluate the effect of vibrations on heat pipe performance. The data used to establish this baseline was collected during a series of twenty-four static test runs, while the heat pipe was held stationary, in a

horizontal configuration. During the static test runs, a range of coolant flow rates and coolant bath temperatures were used to provide a broad range of heat pipe operating temperatures. Three different coolant bath temperatures, along with eight different coolant flow rate settings, were used to establish the test conditions for the twenty-four static test runs. The coolant bath temperatures used were 0.0°C, 5.0°C, and 10.0°C. The coolant flow rates ranged from 0.20 l/min to 0.55 l/min, in 0.05 l/min increments. These various test conditions resulted in a range of heat pipe operating temperatures from 54.4°C to 72.0°C

A summary of the data collected from all twenty-four static test runs is presented in Table 4.1. Column 1 of this table is the run number for each test. The heat pipe operating temperature at wick dryout is given in Column 2. Column 3 is the maximum heat throughput at wick dryout, Q_{max}. These values were computed using Eq. 3-1. The uncertainty associated with Q_{max} is listed in Column 4. This uncertainty, referred to as ΔQ_{max}, was computed using Eq. D-11.

The static test data is presented graphically in Fig. 4.1. This figure also includes the theoretical operating limit for the heat pipe and a least squares approximation for the static test data. The theoretical operating limit was computed using the equations for the theoretical capillary limit discussed in Appendix A. The least squares approximation was found by applying the method of least squares to the data to establish a

line of minimum deviation. The equation for this least squares approximation is given by:

$$Q_{max} = -2.9767T_{op} + 380.48 \qquad (4\text{-}1)$$

where Q_{max} = maximum heat throughput at wick dryout (W)
T_{op} = heat pipe operating temperature (°C)

Table 4.1 Static Test Run Data

Run #	T_{op} (°C)	Q_{max} (Watts)	ΔQ_{max} (Watts)
1	71.0	169.95	7.7
2	69.3	171.16	7.9
3	67.8	177.36	8.5
4	63.4	189.49	9.4
5	61.9	199.15	9.8
6	58.1	212.43	10.0
7	56.3	221.46	10.6
8	69.5	173.32	9.6
9	68.8	179.12	10.4
10	66.0	186.92	11.6
11	63.0	191.52	12.6
12	60.3	199.84	13.4
13	58.8	198.98	14.3
14	58.2	199.92	15.0
15	57.1	214.02	16.0
16	54.4	204.06	9.1
17	72.0	164.75	12.0
18	70.3	166.86	13.6
19	68.6	175.17	15.3
20	65.3	182.69	17.2
21	62.0	205.39	20.5
22	64.5	190.95	18.8
23	61.1	199.67	22.0
24	59.8	210.35	23.9

This line establishes the performance baseline for the tested heat pipe. It is used to evaluate the vibrational test data and in the statistical analysis of the final section.

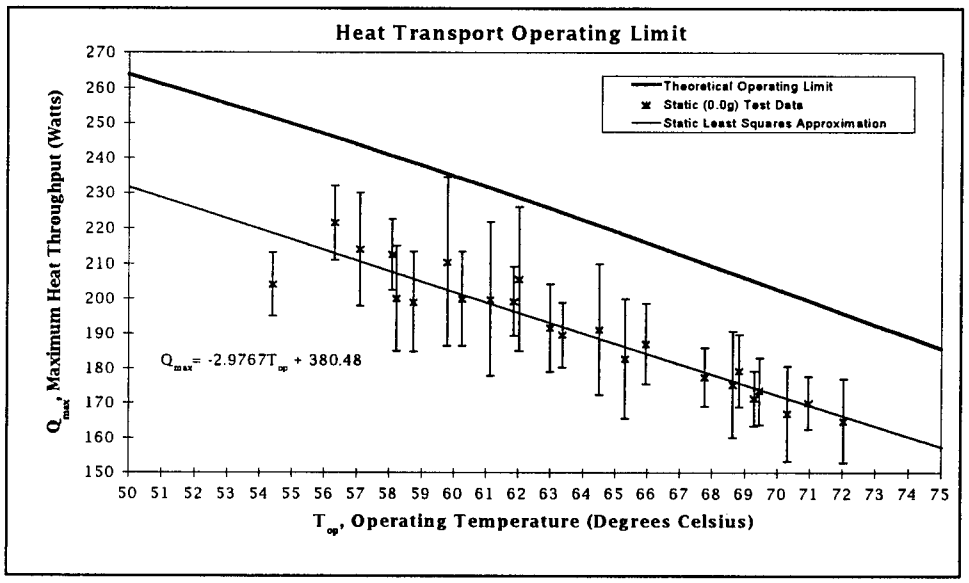

Figure 4.1 Q_{max} versus T_{op}: Static and Theoretical

An examination of the data in Fig. 4.1 reveals the static test data is consistently below the theoretical operating limit of the tested heat pipe. This effect was expected based on the definition of wick dryout used in this investigation. The selected wick dryout criteria was chosen to give an indication of imminent wick dryout, but at a lower operating temperature than established by the conventional definition of wick dryout. The methods and reasons for this selection were explained in Chapter 3. The graphical effect of this selection is a translation of the theoretical operating limit to the left. A translation of this nature results in a lower

Q_{max} for a given operating temperature. Fig. 4.1 displays a close relationship between the theoretical operating limit and the least squares approximation from the static test data. The close correspondence between the slopes of these two lines demonstrates both the validity of the dry-out criteria selected for this investigation, and the reliability of the performance baseline being established by the static least squares approximation.

Vibrational Data

The collection of the vibrational data was similar to the static data collection. The same twenty-four combinations of coolant flow rate and coolant bath temperatures were used. The heat pipe was subjected to a sinusoidal, transverse vibration of fixed frequency and amplitude, rather than being held in a static, horizontal position. The amplitude of the vibration was held fixed at 0.02 in. (0.508 mm) for all three vibrational cases. The vibrational frequency was adjusted for each case. These actions maintained a constant displacement amplitude, but changed the peak acceleration amplitude for each of the three vibrational test cases. The acceleration loads used in this investigation were 1.84g, 2.50g, and 3.27g. These accelerations corresponded to oscillation frequencies of 30, 35, and 40 Hertz, respectively.

1.84g Vibration. In this series of tests, the heat pipe was subjected to a transverse sinusoidal vibration of 30 Hertz. This corresponded to a peak acceleration amplitude of 1.84g. The data resulting from these tests is summarized in Table 4.2. The column designations are the same as for the static test data. Column 1 is the test run number; Column 2, the heat pipe operating temperature at wick dryout; Column 3 shows the maximum heat throughput at wick dryout, Q_{max}; and Column 4 gives the uncertainty of the data, ΔQ_{max}. The values of Q_{max} and ΔQ_{max} are computed using Eq. 3-1 and Eq. D-11, respectively.

The distinction drawn from this table when compared to Table 4.1 is the change in heat pipe operating temperature. For the static test data, the range of operating temperatures was from 54.4 °C to 72.0 °C. Using the same parameters for coolant flow and coolant bath temperature, the 1.84g vibrational test data yielded an operating temperature range of 49.7 °C to 64.7 °C. Although the size of the operational range is comparable, 17.6 °C for the static test data to 15.0 °C for the 1.84g vibrational test data, the whole range has been shifted to the left with respect to the operating temperature range exhibited by the static performance data. This alone indicates that transverse vibrations have an effect on heat pipe performance, but it is when viewing the graphical representation of the data in Fig. 4.2 that the true nature of the effect becomes evident.

Table 4.2 1.84g Vibrational Test Run Data

Run #	T_{op} (°C)	Q_{max} (Watts)	ΔQ_{max} (Watts)
1	64.6	158.79	9.7
2	64.7	162.40	11.0
3	60.8	157.29	12.1
4	61.8	173.41	14.0
5	61.3	173.22	15.4
6	57.1	190.33	16.9
7	56.1	196.68	18.4
8	54.2	197.96	19.7
9	62.7	171.61	7.8
10	62.2	169.99	8.3
11	58.0	172.76	9.0
12	57.5	176.10	9.7
13	56.8	181.20	10.4
14	53.5	192.84	11.3
15	52.8	202.91	12.2
16	51.4	201.29	12.8
17	60.4	175.90	6.2
18	58.6	171.32	6.2
19	54.8	175.27	6.5
20	53.8	180.48	6.8
21	55.7	191.40	7.2
22	51.7	202.72	7.9
23	50.9	208.37	8.0
24	49.7	203.89	8.1

Fig. 4.2 graphically represents the data from Table 4.2 In addition, the theoretical operating limit, the static least squares approximation, and a least squares approximation for the 1.84g vibrational data are included. This data shows a clear degradation in heat pipe performance. It is only the uncertainty in one data point that prevents the entire data set from having a Q_{max} lower than the baseline established using the

static test data. There is a mean decrease in performance of 27.6 Watts. This decrease in Q_{max} indicates that transverse vibration has a detrimental effect on heat pipe operating limits. This assessment is borne out more dramatically in the remaining vibrational test cases.

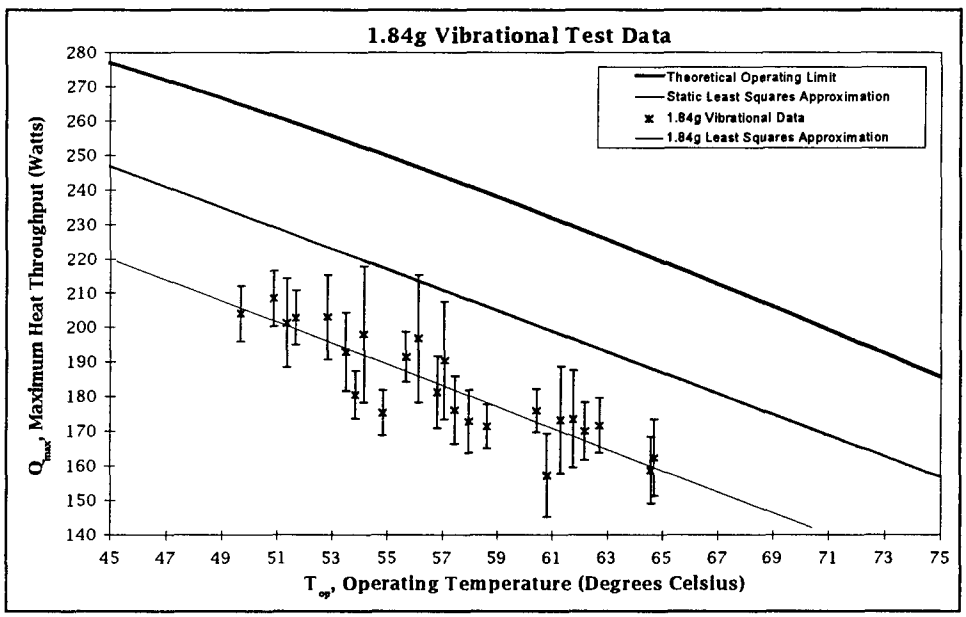

Figure 4.2 Q_{max} versus T_{op}: 1.84g Vibrational Test Case

2.50g Vibration. In this series of tests, the heat pipe was subjected to a transverse sinusoidal vibration of 35 Hertz. This corresponded to a peak acceleration amplitude of 2.50g. The data resulting from these tests is summarized in Table 4.3. The column designations are the same as previously discussed for Table 4.1 and Table 4.2.

While viewing the data in Table 4.3, the shift in the range of heat pipe operating temperature is once again evident. In this case, the range is 48.9 °C to 65.6 °C, with 16.6°C separating the upper and lower limits of

the operating range. While the size of the operating range is comparable to the size of the operating range for the static test data, the entire range has been shifted to the left with respect to the operating temperature range exhibited by the static performance data. The true effects of this shift can be seen in the graphical representation, Fig. 4.3.

Table 4.3 2.50g Vibrational Test Run Data

Run #	T_{op} (°C)	Q_{max} (Watts)	ΔQ_{max} (Watts)
1	65.6	159.74	11.9
2	63.8	168.75	15.4
3	61.8	171.84	17.0
4	57.6	183.62	18.7
5	55.2	179.33	20.3
6	55.5	184.67	22.0
7	53.0	181.43	23.3
8	61.0	162.50	9.4
9	60.1	162.29	10.0
10	57.2	178.77	11.3
11	56.5	163.12	10.9
12	57.8	176.82	12.0
13	55.3	168.14	12.5
14	52.0	176.84	13.4
15	51.0	181.27	14.6
16	49.2	192.84	15.5
17	59.5	174.28	7.2
18	58.5	165.67	7.5
19	55.0	167.47	7.8
20	53.5	182.60	8.4
21	53.1	185.82	8.4
22	50.0	197.28	9.7
23	48.9	197.65	9.7
24	49.2	196.93	10.6

In Fig. 4.3, the 2.50g vibrational data is displayed in graphical form, along with the theoretical operating limit line, the static least squares approximation, and a least squares approximation for the 2.50g vibrational data. This display of the 2.50g vibrational data reveals a greater degradation in heat pipe performance than was seen in Fig. 4.2. In this case, all of the data points lie below the static least squares approximation. The mean of the difference between the 2.50g vibrational data and the static least squares approximation has increased to 37.3 Watts. This is 9.7 Watts, or 34 percent, more than the mean difference seen in the 1.84g vibrational case. These values indicate that heat pipe performance degradation increases with increasing peak acceleration amplitude.

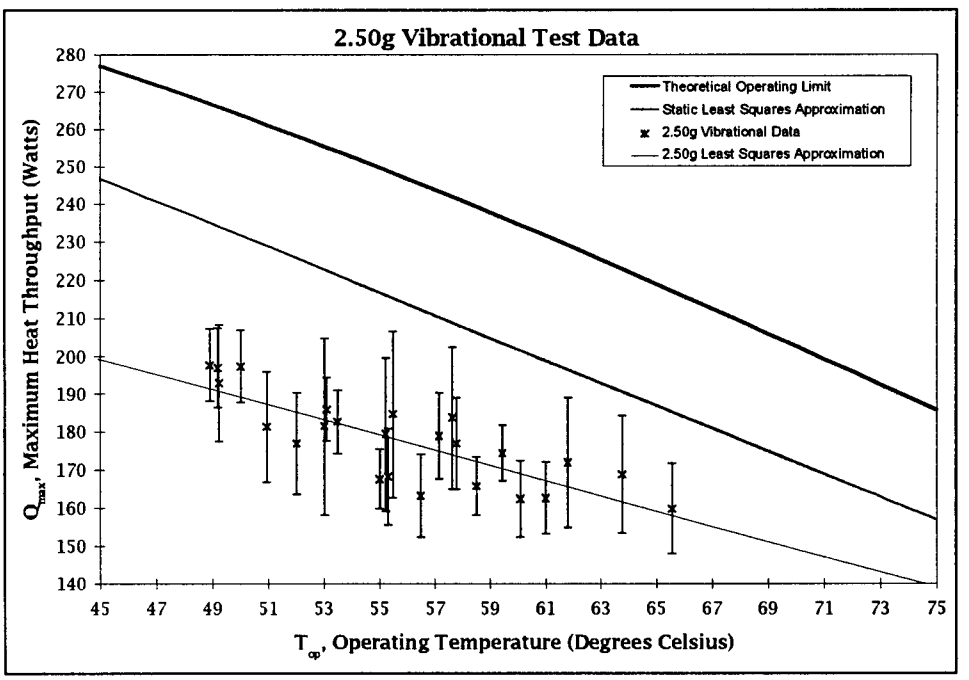

Figure 4.3 Q_{max} versus T_{op}: 2.50g Vibrational Test Case

One caution must be made while examining Fig. 4.3. This involves the apparent convergence of the static least squares approximation and the 2.50g least squares approximation. If the 2.50g test data represented a pure shift in the heat pipe operating limit, one would expect these two lines to run parallel to each other. The fact they do not indicates a lack of exact correspondence between the 2.50g test data and the static test data. Therefore, the 2.50g test data must be viewed with some degree of conservatism. A more exact correspondence between the vibrational data and the static data is more readily apparent in the 3.27g case, to be considered next.

3.27g Vibrational Data. In this series of tests, the heat pipe was subjected to a transverse sinusoidal vibration of 40 Hertz. This corresponded to a peak acceleration amplitude of 3.27g. The data resulting from these tests is summarized in Table 4.4. The column designations are the same previously discussed for Table 4.1 and Table 4.2.

Once again, the shift in the range of heat pipe operating temperature is evident, although in this case the shift is even more pronounced. For the 3.27g vibrational data, the heat pipe operating temperature ranges from 43.3°C to 59.8°C. The size of the operating range is still comparable to the operating range for the static test data, 16.5°C and 17.7°C, respectively. However, the range has been drastically shifted to

the left, with respect to the static performance operating temperature range, for the 3.27g vibrational data, by over 11°C. This indicates the 3.27g vibrations had a significant impact on heat pipe performance. The degree of this effect is more readily seen in the graphical representation of the data, Fig. 4.4.

Table 4.4 3.27g Vibrational Test Run Data

Run #	T_{op} (°C)	Q_{max} (Watts)	ΔQ_{max} (Watts)
1	59.8	146.44	12.8
2	57.3	139.99	14.1
3	52.3	142.57	16.0
4	52.9	150.48	17.6
5	51.5	174.63	20.3
6	50.5	170.66	21.7
7	48.7	166.35	23.4
8	48.6	164.82	24.6
9	54.0	144.18	9.8
10	54.0	152.24	10.9
11	53.3	158.00	11.8
12	51.2	160.05	12.9
13	47.4	172.23	14.0
14	47.2	167.83	14.8
15	46.4	180.16	16.1
16	46.3	167.52	16.4
17	54.5	151.51	7.6
18	53.3	153.56	7.9
19	50.0	163.10	8.5
20	46.2	159.49	8.5
21	44.9	177.71	9.5
22	44.0	172.93	9.4
23	43.3	180.02	10.2
24	44.6	187.14	10.4

Fig. 4.4 graphically represents the data from Table 4.4. In addition, the theoretical operating limit, the static least squares approximation, and a least squares approximation for the 3.27g vibrational data are included. This data reveals an even greater degradation in heat pipe performance than was seen in the previous two vibrational test cases. All of the 3.27g data points fall well below the static least squares approximation. The mean difference between the least squares approximation and the 3.27g least squares approximation has jumped to 69.4 Watts. This is an increase of over 150 percent of the difference seen in the 1.84g case and an increase of more than 85 percent from the 2.50g case. A strong

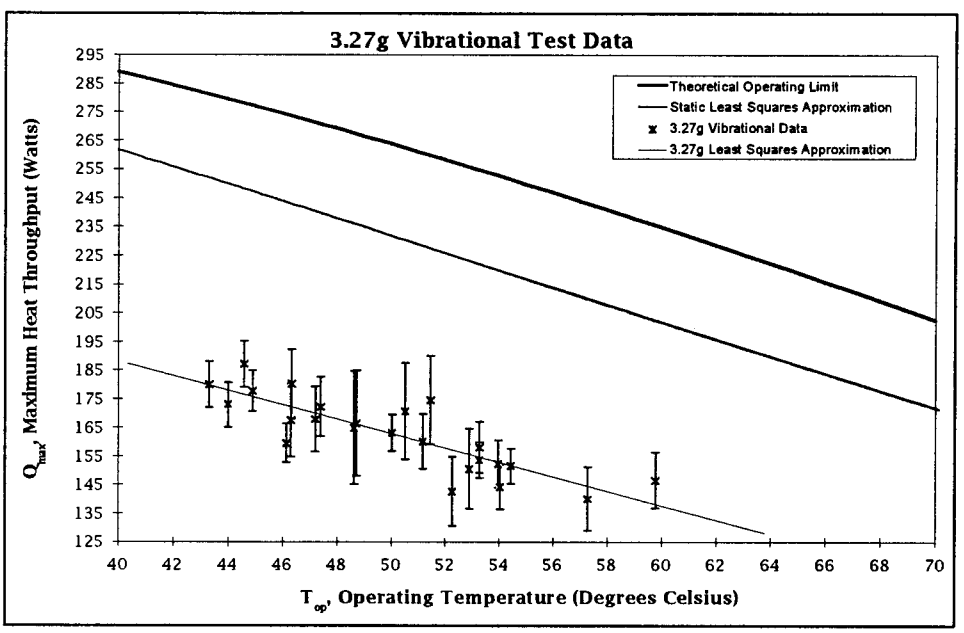

Figure 4.4 Q_{max} versus T_{op}: 3.27g Vibrational Test Case

correspondence is demonstrated by the two least squares approximation lines. These lines run almost parallel, indicating the 3.27g data represents a pure shifting of the heat pipe operating limit. This shifting is a direct result of the 3.27g acceleration experienced by the heat pipe.

Analysis

Observational Analysis. One particular point needs to be addressed regarding all three vibrational test cases. In Chapter 2, the idea of critical accelerations and critical temperatures was discussed. The vibrational test frequencies were selected based on the idea that for a fixed vibrational frequency and vibrational amplitude, a specific peak acceleration amplitude resulted. Further, for a specified peak acceleration amplitude there was a critical heat pipe operating temperature. Operating the heat pipe at temperatures above the critical temperature would result in degraded heat pipe performance. This performance decrease was hypothesized to be due to the working fluid being shaken out of the upper capillary grooves.

Fig. 4.5 shows the critical acceleration-critical temperature graph of Chapter 2, but superimposed on this graph are the operating temperature ranges for the three vibrational test cases. An examination of this figure reveals that for the 1.84g and 2.50g test cases, the resulting operating temperature ranges are entirely below the critical acceleration-

critical temperature line. Only the 3.27g test case had an operating temperature range that intersected the critical acceleration-critical temperature line, and then only at the upper end of the range. And yet, all three test cases demonstrated significant degradation in heat pipe performance. The performance degradation was evident over the entire operating temperature range of each vibrational case. In the 3.27g case, the expected change in the performance did not occur as the operating temperature crossed from one side of critical acceleration-critical temperature line to the other. What is the explanation for this disparity between theory and experimental results?

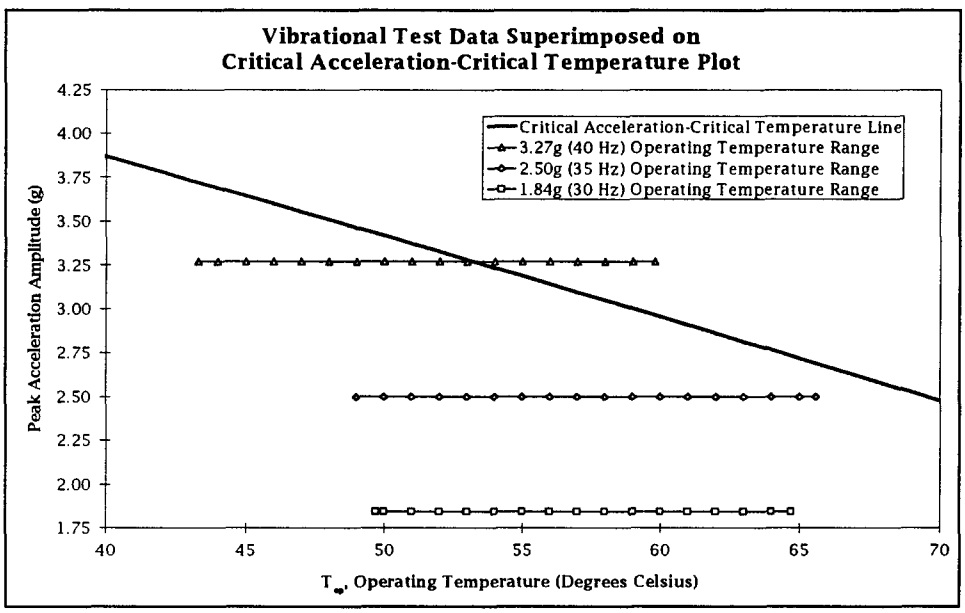

Figure 4.5 Vibrational Test Data Superimposed on Critical Acceleration-Critical Temperature Graph

The first step is to look at the assumptions used in the derivation of the critical acceleration graph. There are four major assumptions made in the derivation shown in Chapter 2. The first of these is the assumption of a full capillary wick. As a heat pipe approaches its capillary limit, this assumption breaks down (2:21-38). As the fluid volume decreases, the acceleration needed to free the droplets increases. The second assumption involved the choice of a control volume. The entire fluid volume inside the capillary groove was assumed to be the control volume. In a vibrational case, it is possible for droplets to form from only a portion of the fluid in the capillary groove. The third assumption dealt with the fluid pressures and vapor pressures. These were assumed to be of the same order. However, pressure imbalances due to pressure gradients or rapid working fluid vaporization (boiling), could result in changes of the critical acceleration-critical temperature line. The final assumption ignored the end effects on individual control volumes. The shear effects between adjacent fluid elements could adversely affect the theoretical analysis.

Any or all of these assumptions and their limitations could have combined to result in the disparity between the theory and the experimental results regarding critical frequencies. The important point in this case is how the information resulting from the theoretical derivation was used. The theory was used, not to give a precise representation of

the actual critical frequencies, but rather, as a rough order of magnitude for the experimental investigations. The theoretical critical frequencies were used to scope the experiment, not to exactly predict it. The purpose of this investigation was to gather information to be used to further refine the theoretical explanation for the performance of heat pipes subjected to vibrations

Statistical Analysis. To more readily see the correlation between vibrational frequency the resulting induced acceleration load and heat pipe performance, a statistical analysis was in order. To do this, the Q_{max} at the various operating temperatures and acceleration levels needed to be quantified. This quantification could only be accomplished by eliminating one of the parameters, either peak acceleration amplitude or operating temperature. Since peak acceleration amplitude was the parameter of interest, operating temperature was eliminated. Operating temperature was eliminated as a parameter by defining a new parameter, $DelQ_{max}$. $DelQ_{max}$ is the difference between Q_{max} for a given data point and the value of the static least squares approximation (Eq. 4-1) at the same operating temperature. $DelQ_{max}$ then became a function of only peak acceleration amplitude. A positive difference ($DelQ_{max}$) indicated a heat pipe performance enhancement. A negative difference indicated a degradation in heat pipe performance. It was then possible to establish a

mean and standard deviation for each vibrational test case. These results are displayed in Fig. 4.6. This figure displays peak acceleration amplitude along the abscissa, with $DelQ_{max}$ along the ordinate. In Fig. 4.6, the symbols represent the mean difference at the various acceleration amplitudes. The vertical bars represent the standard deviation of the difference.

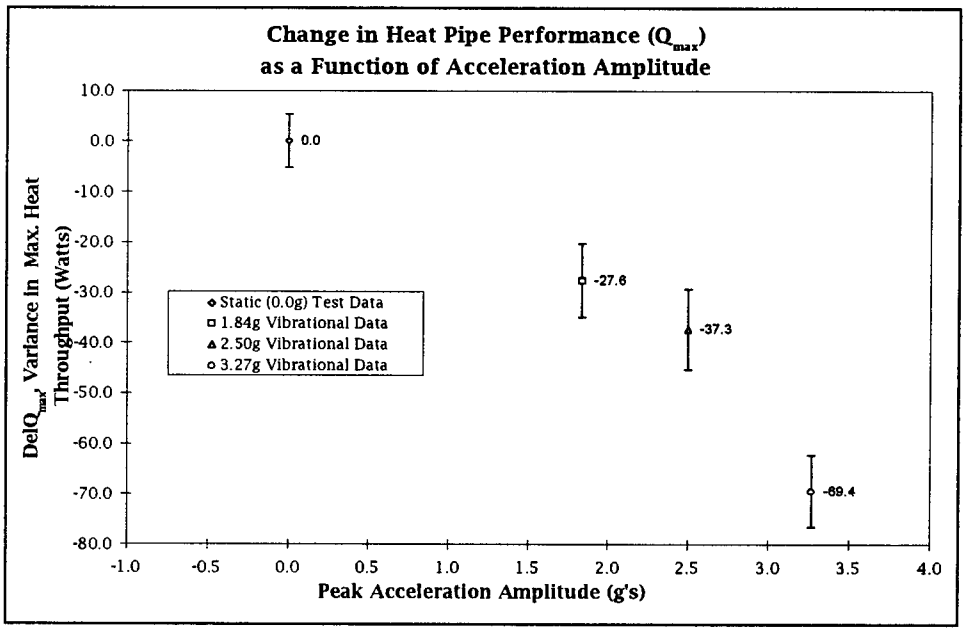

Figure 4.6 Change in Q_{max} as a Function of Peak Acceleration Amplitude

An examination of Fig. 4.6 demonstrates that as the peak acceleration amplitude increases, the magnitude of $DelQ_{max}$ increases as well. The negative signs indicate the difference represents a degradation in heat pipe performance. At an acceleration amplitude of 1.84g, the magnitude of $DelQ_{max}$ increased from a mean value of 0.0 Watts at static con-

ditions, to 27.6 Watts. This represented an average degradation of 12.9 percent from static heat pipe performance. The standard deviation increased, from 5.3 Watts for the static case, to 7.3 Watts for the 1.84g case. As the acceleration amplitude was increased, so did the magnitude of $DelQ_{max}$. For the peak acceleration amplitude of 2.50g, the magnitude of $DelQ_{max}$ increased to 37.3 Watts, representing an average decrease of 14.8 percent from static heat pipe performance. The standard deviation increased to 8.0 Watts. A dramatic increase in the magnitude of $DelQ_{max}$ is seen for 3.27g. At this peak acceleration amplitude, $DelQ_{max}$ jumps to 69.4 Watts, while the standard deviation declines slightly, to 7.3 Watts. This represents an average performance decrease of 28.1 percent from the static test case.

Further examination of Fig. 4.6 reveals the standard deviation bars associated with the static test condition do not overlap the standard deviation bars associated with any of the three test conditions. This indicates the degradation in heat pipe performance demonstrated in this data is conclusive. Transverse vibration has a detrimental impact on heat pipe maximum heat throughput. Further, this degradation increases as the peak acceleration amplitude of the vibration is increased.

V. Conclusions and Recommendations

Conclusions

An analysis of the data collected as part of this investigation revealed that transverse, sinusoidal vibrations affect the performance of an ammonia/aluminum axial groove wick heat pipe. This effect is manifested as a degradation in the maximum heat throughput, Q_{max}, of the heat pipe at wick dryout. Further, the magnitude of this degradation increases as the peak acceleration amplitude of the vibrations are increased. These results agree with the trends identified by Charlton in his 1992 study.

A vibration with peak acceleration amplitude of 1.84g, resulted in a mean decrease of 27.6 Watts in Q_{max}, from the static baseline established. This degradation represents an average decrease of 12.9 percent in Q_{max}, over the tested range of operating temperatures. This departure from the static baseline grew to a mean difference of 37.3 Watts for a peak acceleration amplitude of 2.50g. At 2.50g, the mean degradation in Q_{max} represented an average decrease of 14.8 percent in heat pipe performance over the tested range of operating temperatures. The performance degradation was particularly evident at a peak acceleration amplitude of 3.27g. At this vibrational load, Q_{max} was decreased by a

mean value of 69.3 Watts. This represented a mean performance decrease of 28.1 percent over the range of tested operating temperatures.

The data collected, with one exception showed clear and conclusive evidence of degradation in heat pipe performance as a result of transverse vibration. The single exception was a data point collected at the 1.84g peak acceleration amplitude. The uncertainty of this one point overlapped the static baseline being used. However, the other twenty-three data points collected at the same acceleration amplitude showed definite performance degradation. Therefore, assuming heat pipe performance degradation across the entire range of operating temperatures at the 1.84g acceleration level is justified.

Recommendations

The data collected as part of this investigation demonstrated a definite degradation in heat pipe performance due to transverse vibration. However, the data covered only a small fraction of the operating range of the tested heat pipe. In particular, due to coolant system constraints, the designed operating temperature of the heat pipe could not be tested.

The following are areas for improvements to this investigation, and some possibilities for follow-on work.

1. Modify the coolant system to use cryogens in order to test the heat pipe at the designed operating temperature.

2. Improve the data collection system (DAS). The greatest degree of uncertainty in this investigation arose from the coolant manifold outlet temperature. The error in this temperature was the largest contributor to the uncertainty of this experiment. Follow-on work should include more precise temperature measurement apparatus, perhaps shielded thermocouples to prevent stray voltages from impacting the data system.

3. This was the first investigation of vibrational effects on the performance of an axial groove heat pipe. Further work remains to investigate the effects of other vibrational modes, vibration orientation, and heat pipe orientation on the axial groove heat pipe. Investigations should include the effects of longitudinally orientated vibration, and the effects of square and impulsive vibration waveforms.

4. Additional work with transverse vibrations should be done to find the peak acceleration amplitude below which there is no performance degradation.

5. It is theoretically possible, at certain peak acceleration amplitudes, droplets can be shaken free from the lower capillary grooves with sufficient momentum to impact on the upper capillary grooves. It is possible that this condition would result in rewetting of the upper capillary grooves. An investigation to determine the existence of this condition would be valuable.

6. Additional work needs to be accomplished in the development of the theoretical understanding of the fluid dynamics at wick dryout, particularly in a dynamic environment.

7. This investigation was governed by the capillary limit of the test heat pipe. Additional work should be done to discover the effect of vibrations on heat pipes limited by the other three heat transport limits. The entrainment limit and the boiling limit, which are fluid limited cases, like the capillary limit, should be evaluated for similarity to the work already accomplished with capillary limited heat pipes.

Appendix A: Heat Transport Limits

Heat pipes are subject to four different heat transport limits, depending upon the portion of the operational range in which they are being used. These limits are, from the lowest operating temperature to the highest: sonic limit, entrainment limit, capillary limit and boiling limit.

Sonic Limit

The sonic limit is reached when the vapor flow leaving the evaporator section, (or the adiabatic section if present), has attained sonic velocity (5:84). Once the vapor flow reaches sonic speed, the flow is choked and maximum mass flow and heat transport rate are achieved (19:126).

The equation for the sonic heat transport limit was first derived by Levy and is known as the Levy Equation. Chi has reproduced the derivation of this equation (5:83-84).

$$Q_{s,max} = A_v \rho_o \lambda \left[\frac{\gamma_o R_v T_o}{2(\gamma_o + 1)} \right]^{1/2} \qquad \text{(A-1)}$$

where $Q_{s,max}$ = sonic heat transport limit (Watts)
A_v = vapor core cross-sectional area (m^2)
ρ_o = vapor density at stagnation temperature (kg/m^3)
λ = latent heat of vaporization (J/kg)
γ_o = specific gas constant
R_v = vapor gas constant (J/kg-K)
T_o = stagnation temperature (K)

The sonic heat transport limit for the heat pipe used in this experiment is represented in Fig. A.1.

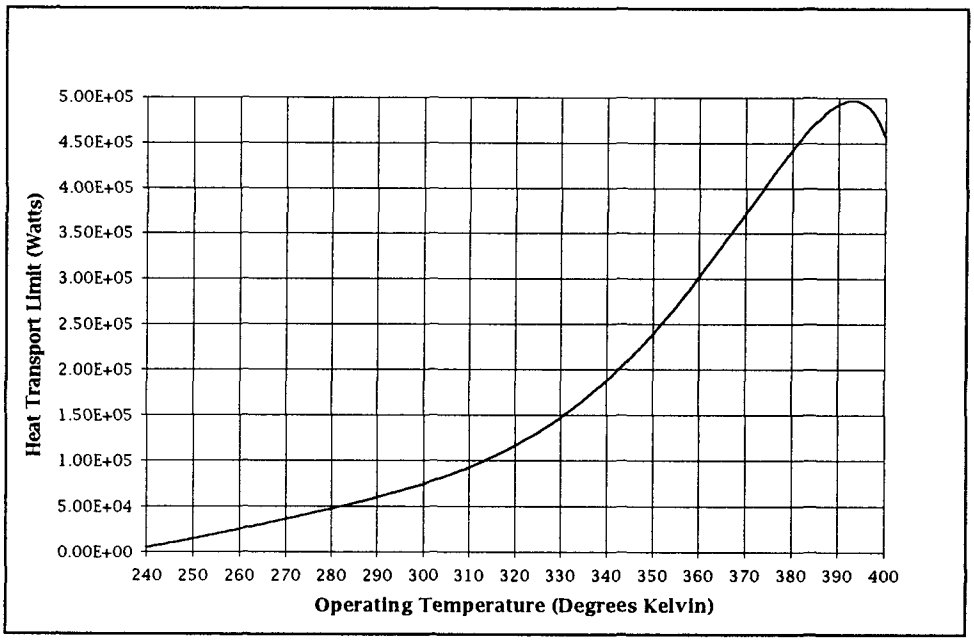

Figure A.1 Sonic Heat Transport Limit

Entrainment Limit

The entrainment limit is a result of the interactions of the vapor stream and the liquid stream. The interface between these opposite flowing streams is a mutual shear layer. If the relative velocity between the two streams is great enough, liquid droplets will be torn from the liquid stream and become entrained in the vapor stream (2:41). When this occurs, evaporator wick dryout follows rapidly (5:86).

Chi derives the equation for computing the entrainment heat transport limit (5:87).

$$Q_{e,max} = A_v \lambda \left[\frac{\sigma \rho_v}{2 r_{h,s}} \right]^{1/2} \qquad \text{(A-2)}$$

where $Q_{e,max}$ = entrainment heat transport limit (Watts)
A_v = vapor core cross-sectional area (m^2)
λ = latent heat of vaporization (J/kg)
σ = surface tension coefficient (N/m)
ρ_v = vapor density (kg/m^3)
$r_{h,s}$ = hydraulic radius of wick at vapor/wick interface (m)

The entrainment heat transport limit for the heat pipe used in this experiment is represented in Fig. A.2.

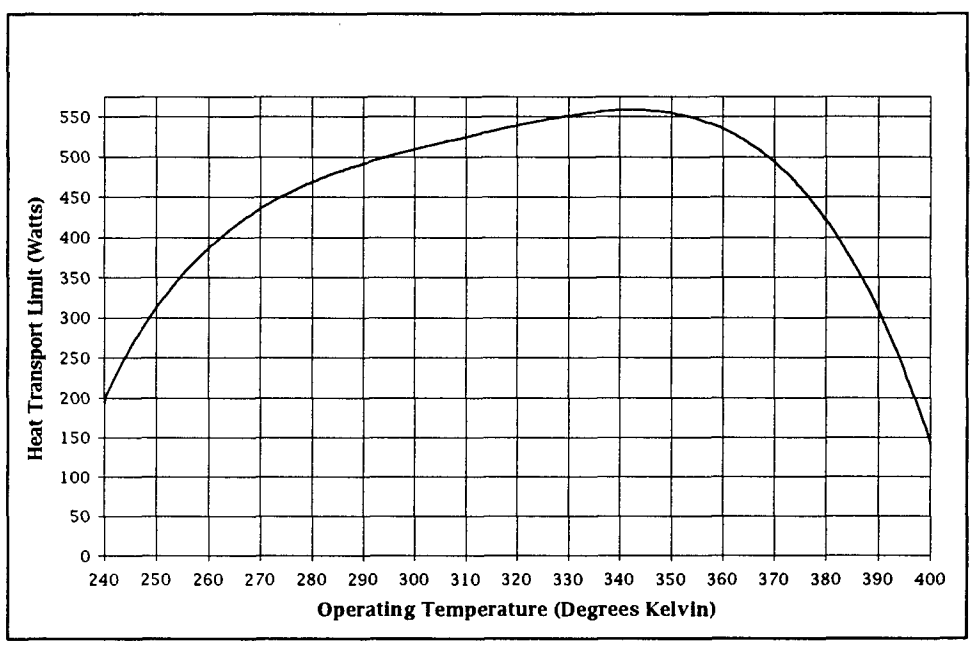

Figure A.2 Entrainment Heat Transport Limit

Capillary Limit

The capillary limit occurs when liquid is evaporating more rapidly than capillary forces can replenish the liquid. This condition results in local wick dryout and increased wall temperatures (2:27).

Chi has derived the equations for determining the capillary heat transport limit (5:51-55).

$$Q_{c,max} = \frac{(QL)_{c,max}}{\left(\frac{1}{2}L_c + L_a + \frac{1}{2}L_e\right)} \tag{A-3}$$

with

$$(QL)_{c,max} = \left(\frac{2\sigma}{r_c} - \Delta P_\perp - \rho_l g L_t \sin\Phi\right) \Big/ (F_l + F_v) \tag{A-4}$$

$$F_l = \mu_l / KA_w\rho_l\lambda \tag{A-5}$$

and

$$F_v = (f_v Re_v)\mu_v / \left(2r_{h,v}^2 A_v \rho_v \lambda\right) \tag{A-6}$$

where $Q_{c,max}$ = capillary heat transport limit (Watts)
$(QL)_{c,max}$ = capillary limit on heat transport factor (W-m)
L_c = length of condenser section (m)
L_a = Length of adiabatic section (m)

L_e = length of evaporator section (m)
L_t = total length of the heat pipe (m)
σ = surface tension coefficient (N/m)
r_c = effective pore radius (m)
$\Delta P_\perp$ = hydrostatic pressure perpendicular to pipe axis (N/m^2)
ρ_l = liquid density (kg/m^3)
ρ_v = vapor density (kg/m^3)
λ = heat of vaporization (J/kg)
Φ = heat pipe inclination (radians)
g = gravitational forces (9.81 m/sec^2)
F_l = liquid frictional coefficient
F_v = vapor frictional coefficient
μ_l = liquid viscosity (kg/m-sec)
μ_v = vapor viscosity (kg/m-sec)
K = effective wick permeability (m^{-2})
f_vRe_v = vapor drag coefficient/Reynolds number
A_w = wick cross-sectional area (m^2)

For this experiment, some simplifications can be made to Eq. A-4. Since there is no connection between the grooves in the tested heat pipe, the hydrostatic pressure term, $\Delta P_\perp$, is zero. The heat pipe was maintained in a nearly horizontal position throughout the test, therefore the pipe inclination angle, Φ, is zero. These simplifications reduce Eq. A-4 to:

$$(QL)_{c,max} = \left(2\sigma/r_c\right) \Big/ (F_l + F_v) \qquad \text{(A-7)}$$

The effective wick permeability used in Eq. A-5 is a function of the wick geometry. For the axial groove wick used in this study, the equa-

tion for the effective wick permeability of the trapezoidal shaped groove is provided by Brennan and Kroliczek (2:118).

$$K = 0.435\left\{\frac{\left(w\delta + \delta^2 \tan\alpha\right)^{2.1}}{w^{0.2}\left[2\delta/\cos\alpha\,(1+\sin\alpha) + w\right]^2}\right\} \qquad \text{(A-8)}$$

where K = effective wick permeability (m^{-2})
w = groove width at the inner radius (m)
δ = groove depth (m)
α = groove angle (degrees)

The capillary heat transport limit for the heat pipe used in this experiment is shown in Fig. A.3.

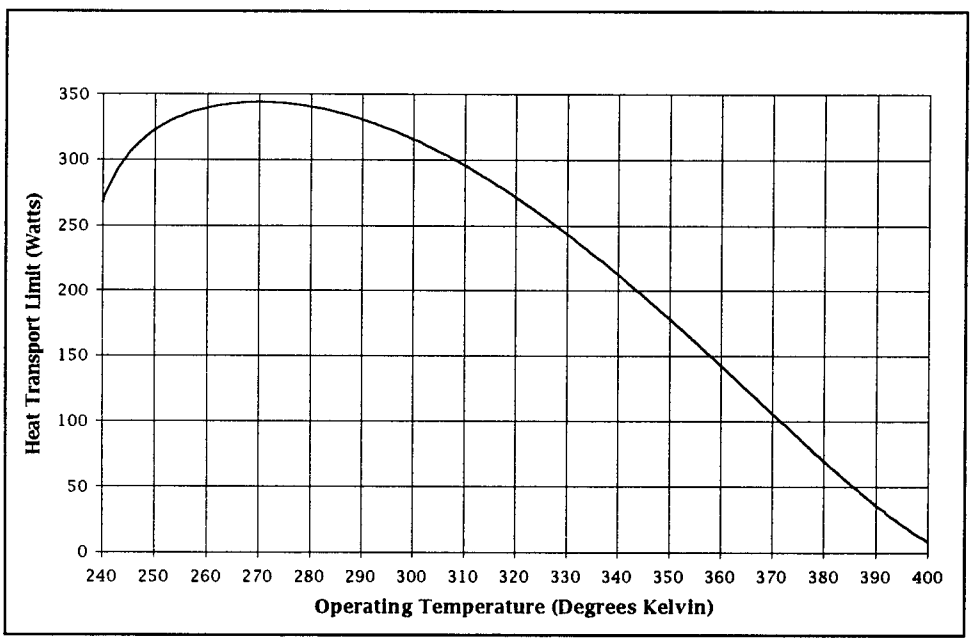

Figure A.3 Capillary Heat Transport Limit

Boiling Limit

The boiling limit results when the heat flux density is great enough to cause the saturation vapor pressure at the interface between the wick and the wall to exceed the liquid pressure at the same point (5:89-90). When this occurs, vapor bubbles form in the liquid stream. These bubbles cause hot spots and restrict liquid circulation, leading to wick dryout (5:90). The heat transport limit at which this occurs is known as the boiling limit.

Chi derives the equation for computing the boiling heat transport limit (5:91).

$$Q_{b,max} = \frac{2\pi L_e k_e T_v}{\lambda \rho_v \ln(r_i/r_v)}\left(\frac{2\sigma}{r_n} - P_c\right) \qquad \text{(A-9)}$$

where $Q_{b,max}$ = boiling heat transport limit (Watts)
L_e = evaporator section length (m)
k_e = effective thermal conductivity of the liquid/saturated wick matrix (W/m-K)
T_v = vapor temperature (K)
λ = latent heat of vaporization (J/kg)
ρ_v = vapor density (kg/m^3)
r_i = inside radius of pipe (m)
r_v = vapor core radius (m)
σ = surface tension coefficient (N/m)
r_n = boiling nucleation radius (m)
P_c = capillary pressure (N/m^2)

The effective thermal conductivity, k_e, used in Eq. A-9, is highly dependent upon the wick geometry (5:47-48). Chi gives the equation for

finding the effective thermal conductivity of an axially grooved heat pipe (5:50).

$$k_e = \frac{wk_l(0.185w_f k_w + \delta k_l) + (w_f k_l k_w \delta)}{(w + w_f)(0.185w_f k_w + \delta k_l)} \qquad \text{(A-10)}$$

where w_f = groove fin thickness (m)
w = groove width (m)
δ = groove depth (m)
k_l = liquid thermal conductivity (W/m-K)
k_w = wall thermal conductivity (W/m-K)

The radius of nucleation, r_n, used in Eq. A-9 is also a function of the boiling surface (2:43). A wide range of values for r_n have been reported. Chi gives typical nucleation radii of 254 to 2540 nanometers (5:92) while Silverstein reports values ranging from 1 to 7 micrometers (19:162). A third source, Brennan and Kroliczek, give typical nucleation radii of 1 to 10 micrometers (2:53). Brennan and Kroliczek also point out that the boiling limit model is very conservative. Even using their lower limit for nucleation radius, they've found the model boiling limit can easily be an order of magnitude lower than the actual measured boiling limit (2:44).

The boiling limit for the heat pipe used in this experiment, using Chi's lower limit of 254 nanometers, is represented in Fig. A.4.

Evaluation

The heat transport limit for this investigation was based on an anticipated heat pipe operating temperature of 313 to 353 Kelvin (40 to 80 degrees Celsius. Based on the theoretical curves shown in Fig. A.1, Fig. A.2, Fig. A.3, and Fig. A.4, the boiling heat transport limit is expected to be the performance limiting condition for the tested heat pipe. This is based on the boiling limit having the lowest heat transport capability over the expected operating temperature range.

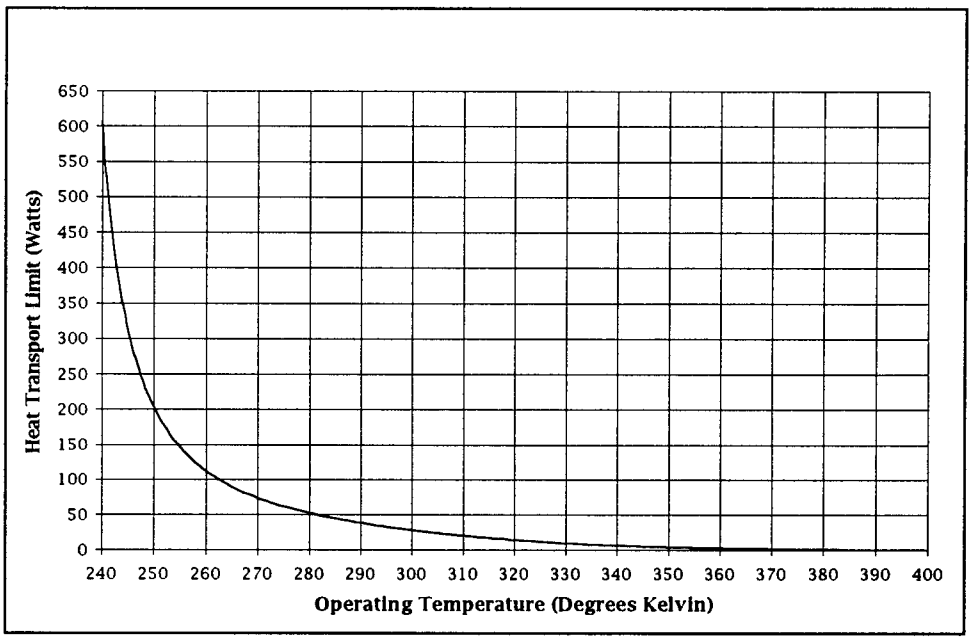

Figure A.4 Boiling Heat Transport Limit

APPENDIX B: Experimental Equipment

In addition to the heat pipe itself, the equipment for this experiment consisted of five major subsystems. These included the Coolant System, the Heater System, the Vibration System, the Data Acquisition System, and the Support System. The equipment arrangement is shown in Fig. B.1. The basic approach for the experiment was to use the vibration system to apply a controlled, constant, sinusoidal vibration to the heat pipe while the heater system was used to slowly increment the thermal load experienced by the heat pipe. Heat pipe surface temperatures were measured continuously, using thermocouples mounted at various points along the heat pipe. Additional thermocouples in the coolant system provided the inlet and outlet temperatures of the coolant water. These temperatures were later used to compute heat pipe performance characteristics. The individual subsystems will be explored in greater detail.

Coolant System

The coolant system was used as the heat sink to maintain the temperature of the condenser end of the heat pipe. Additionally, by adjusting the coolant temperature and flow rate, the operating temperature of the heat pipe was controlled. The primary component of the coolant

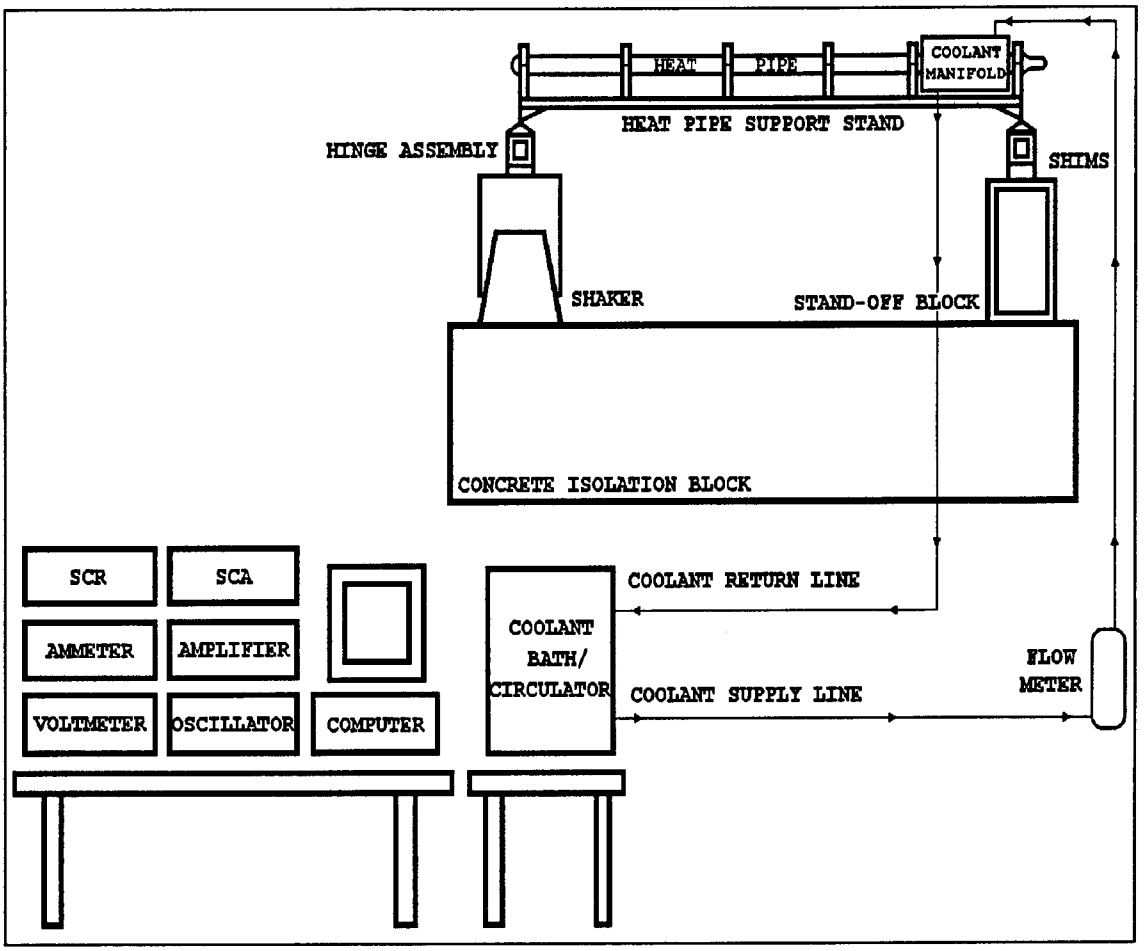

Figure B.1 Experimental Equipment Configuration

system was the NESLAB RTE-100 Refrigerated Bath/Circulator. This device maintained the coolant water at a constant temperature, with an accuracy of ± 0.1°C, and provided the coolant flow. The actual flow of the coolant was controlled by a needle valve and measured using an FTB-601 Ultra-Low Flow Sensor and a DPF78 Ratemeter, both of which are manufactured by Omega. These components allowed a flow rate measurement from 0.1 to 2.0 liters per minute with a 1 percent readout error. The

coolant water interacted with the condenser end of the heat pipe inside the coolant manifold. This manifold was constructed of 25.4 mm ID copper tubing, to which copper endplates and 6.35 mm ID inlet and outlet tubes were attached. Tygon tubing was used as the coolant piping. To prevent heat intrusion from the environment, the coolant manifold and the entire coolant loop were insulated with 9.52 millimeters of polystyrene foam insulation to isolate the coolant lines from the outside temperature.

Heater System

The heater system was used to incrementally increase the thermal heat load experienced by the evaporator section of the heat pipe. This heat was supplied by controlling both the voltage and the current flowing through a nichrome wire heater. The heater consisted of 95.25 millimeters of nichrome wire, sheathed in Inconel 600, wrapped in a helical shape about a 22.25 mm diameter aluminum heater block. This block was designed to fit the square profile of the heat pipe, and to allow a uniform heat flux into the circular wick area of the heat pipe. The power supplied to the heater was controlled using an SCA Power Controller and a Signal Conditioning Rectifier (SCR). Both a voltmeter and an ammeter were used to measure the incoming voltage and current, respectively. The SCR was adjusted so a one-tenth incremental increase on the SCR led

to an increase of about 5 watts in supplied power. The heater system was designed to provide a peak input power of 500 watts to the heat pipe. To prevent heat loss to the environment, the heater was wrapped with three layers of insulation. The inner two layers consisted of a 6.35 mm layer of RPC-X-AQ Ceramic Fiber Insulation covered with Aluminum Refractory Tape. The outer insulation layer consisted of 9.52 mm polystyrene foam insulation covered with Aluminum Refractory Tape. These measures did not completely eliminate heat loss at the evaporator. However, this was not overly important because heat pipe power throughput was computed based on measurements made at the condenser.

Vibration System

The vibration system provided the controlled, sinusoidal vibrations which were the heart of this experiment. These vibrations were generated by a Model 5PM benchtop shaker, manufactured by Unholtz-Dickie Corporation (UDC). The control mechanisms for the shaker, also manufactured by UDC, included a Model TA30 Power Amplifier and an OSP-4 Oscillator-Servo-Programmer, as well as a Kistler feedback/controller accelerometer mounted on the heat pipe support bracket.

Together, the vibration system allowed control of the vibration frequency from 5 to 5000 Hertz and a peak-to-peak displacement ampli-

tude of up to 12.70 mm. The operational frequency was controllable to the nearest 1 Hertz, while the displacement was controlled to the nearest 0.1 percent of selected scale. For this experiment, a constant peak-to-peak displacement amplitude of 0.4 inches (10.16 mm) was used along with three test frequencies; 30 Hertz, 35 Hertz, and 40 Hertz.

Data Acquisition System

The data acquisition system was used to display and record pertinent experimental data during each test run. This data included:

1. vibrational frequency
2. vibrational peak amplitude
3. heat pipe surface temperature
4. coolant water inlet/outlet temperature
5. heater voltage
6. heater current
7. coolant water flow rate
8. coolant water bath temperature

With the exception of items 3 and 4, the data was recorded manually from previously described display devices.

The temperatures in items 3 and 4 were taken using T-type, Copper-Constantan thermocouples (TCs). The TCs were manufactured by Omega Corporation and had an operating range of -160 to 400°C with an error rating of ± 0.5°C. For the heat pipe surface temperature measurements, these TCs were mounted into the groove on the outside of the heat pipe and covered with silicone heat sink compound. For the coolant water inlet and outlet temperature measurements, the TCs were

mounted in the coolant flow loop using T-adapters. The location of the twelve TCs used in this experiment were shown in Fig. 3.1.

The signals from the TCs were fed into a Keithley MetraByte EXP-16 Expansion Multiplexer/Amplifier System. This multiplexed signal was then sent to a PC workstation for processing and recording, by means of a Keithley MetraByte DAS-8 Analog and Digital Input/Output Board. In the PC, the signals were converted from voltages into temperatures, and the temperature at each TC was recorded every 5 seconds of the test run.

Support System

The final subsystem, the support system, was used to hold the other systems together and to isolate the experiment from outside influences to the greatest degree possible.

The heat pipe support stand was manufactured by the Air Force Institute of Technology (AFIT) Model Fabrication Center. It was designed to hold the heat pipe in a fixed configuration and to provide support to the heat pipe during vibrational testing. The interface between the heat pipe and the support stand consists of phenolic mounting blocks. These blocks serve to mechanically, thermally, and electrically isolate the heat pipe from its' environment.

Two hinge assemblies were designed to interface between the heat pipe support stand and the shaker, on one end, and the stand-off block,

on the other end. These hinge assemblies constrained the movement of the heat pipe to a single direction, minimizing off-axis vibrations. Both the shaker and the stand-off block were mounted to the concrete isolation block.

The concrete isolation block served as a uniform frame of reference for the other components of the experiment and was used to isolate the experiment for external vibrations.

Appendix C: Example Test Run Data

This appendix contains the raw experimental data from a single test run. This test run was used to validate the wick dryout criteria selected for this investigation, as described in Chapter 3.

The test data collected by the data acquisition system has the following format:

Line 1: file description (user designated)
Line 2: date and time test run began
Line 3: column designator for time index and multiplexer channel
Line 4: first line of actual test data

It is important to recall the discussions of Chapter 3 when reviewing the data contained in this appendix. In Chapter 3, the discovery of the multiplexer channel bias was discussed. The effects of this bias on the test data were minimized by matching the accuracy of a given multiplexer channel to the criticality of the data for a specific thermocouple. For this reason, the multiplexer channel assignments listed in the data file do not represent the correspondingly numbered thermocouples. Table C.1 gives the multiplexer channel assignments resulting from the thermocouple/multiplexer channel matching. Column 1 lists the multiplexer channels. Columns 2 and 3 give the assigned thermocouple by number and name, respectively. The physical location of the various thermocouples were shown in Fig. 3.1. The differences between multi-

plexer channel and thermocouple number must be considered while reviewing the test data.

Table C.1 Multiplexer Channel/Thermocouple Assignment

Multiplexer Chan.	Thermocouple	Description
T1	TC10	Last TC in Condenser Section
T2	TC12	Coolant Manifold Outlet
T3	TC2	First TC in Evaporator Section (Bottom)
T4	TC11	Coolant Manifold Inlet
T5	TC4	Last TC in Evaporator Section
T6	TC7	Third TC in Adiabatic Section
T7	TC1	First TC in Evaporator Section (Top)
T8	TC5	First TC in Adiabatic Section
T9	TC8	First TC in Condenser Section
T10	TC6	Second TC in Adiabatic Section
T11	TC3	Center TC in Evaporator Section
T12	TC9	Center TC in Condenser Section

In the example test run, wick dryout, using the criteria defined for this investigation, occurs at time index 2060. This is determined by reading the temperature difference between column T3 and column T7, beginning at this time index. The temperature difference meets the first criteria for wick dryout, namely a difference of 1.1°C or more. This temperature difference lasts for 10 or more time indices, meeting the second wick dryout criteria.

For a normal static test run, the test would be complete at this point. However, this test run was also being used to validate the wick dryout criteria defined in this investigation. Once wick dryout had been

confirmed, based on the defined criteria, additional power was supplied to the heater. The purpose was to drive the heat pipe to the true wick dryout condition more commonly used. This occurs at time index 3500.

An examination of the data in column T7 of the test run just prior to time index 3500 reveals the temperature measured by TC1 to be increasing by 0.3 to 0.5°C per time index. Suddenly, at time index 3500, this temperature increase jumps to 0.8°C or more per time index. This sudden change in heat pipe wall temperature is generally referred to as wick dryout in the literature (3:2.19) The example test data proves the validity of the wick dryout criteria selected for this investigation. The addition of more power to the heater, once the selected dryout criteria is met, led to true wick dryout without any signs of thermocouple temperature regression.

Another item of note in the example data set is the recovery of the heat pipe once the heat input has been terminated. At time index 3600, the heat pipe is still at full wick dryout, when the heat input is stopped. An examination of columns T3 and T7, demonstrate that wick dryout recovery occurs within seven time increments. This is evidenced by these two thermocouple temperatures returning to a difference of less than 1.1°C at time index 3635.

Throughout the data set, there are anomalous temperature readings. They are typically several degrees different from the readings both

prior to, and immediately following, the anomalous data reading. An example of this anomaly occurs at time index 175, in column T1. These digressions are most likely due to noise in the DAS. Unless these anomalies occur at the time of wick dryout, they are ignored because the readings immediately return to normal and the corrupted data has no bearing on the remainder of the test. In the event an anomaly occurs in one of the critical TCs at the time of wick dryout, the data values immediately prior to and after the corrupted data are used to interpolate the correct data point. This interpolation has minimal impact on the outcome of the test run. Investigations were performed to verify this assessment. In this investigation, good data was assumed to be corrupted and the interpolation method was used to obtain a value for the "corrupted data point". The result using the interpolation method was a data value that was within the systems margin of error with regards to the data point assumed to be corrupted. This method allowed the anomalous data points to be interpolated without any loss in data accuracy.

Example Test Run Data

Static Validation Run #2

DATE: 25 August 1994 TIME: 11:30:24

TIME	T1	T2	T3	T4	T5	T6	T7	T8	T9	T10	T11	T12
0	21.6	3.4	22.8	0.9	21.6	21.6	22.8	22.2	14.6	22.8	24.0	22.5
5	21.6	3.4	22.8	1.2	21.6	21.9	22.8	22.2	14.9	23.1	24.0	22.5
10	21.6	3.7	22.8	1.2	21.6	21.6	22.8	22.2	14.6	23.1	24.0	22.8
15	21.6	3.7	22.8	1.2	21.6	21.9	22.8	22.2	14.3	23.1	24.3	22.5
20	21.5	3.6	22.7	1.1	21.5	21.8	22.7	22.1	14.5	23.0	24.2	22.7
25	21.6	4.0	22.8	1.2	21.9	21.9	22.8	22.2	14.0	22.8	24.0	22.5
30	21.6	3.7	22.8	1.2	21.6	21.6	22.8	22.2	14.0	23.1	24.3	22.5
35	21.6	3.7	22.8	1.2	21.6	21.6	22.8	22.2	14.0	23.1	24.3	22.8
40	21.6	3.7	22.8	1.2	21.6	21.9	22.8	22.2	14.0	23.1	24.3	22.5
45	21.6	3.7	22.8	1.2	21.9	21.9	22.8	22.2	11.5	23.1	24.6	22.8
50	23.1	3.7	23.1	1.2	22.2	21.9	23.1	22.5	11.5	23.1	24.6	22.8
55	21.9	3.7	23.1	1.2	22.2	21.9	23.1	22.5	12.1	23.4	24.9	22.8
60	21.9	3.7	23.1	1.2	22.2	22.2	23.1	22.5	11.8	23.4	24.9	23.1
65	22.1	3.6	23.3	1.1	22.4	22.1	23.3	22.4	11.4	23.3	24.8	23.0
70	22.2	3.7	23.4	1.2	22.5	22.5	23.4	22.8	11.8	23.4	25.2	23.1
75	22.5	4.0	23.7	1.2	23.4	22.5	23.7	22.8	12.1	23.7	25.2	23.1
80	22.5	4.0	23.7	1.2	22.8	22.5	23.7	23.1	12.1	23.7	25.5	23.4
85	22.5	4.0	23.7	1.2	22.8	22.8	23.7	23.1	12.4	24.0	25.5	21.6
90	22.8	4.0	24.0	1.2	23.1	14.6	24.0	23.1	12.7	24.0	25.8	23.4
95	22.8	4.0	24.0	1.2	23.1	23.1	24.0	23.4	13.1	24.3	25.8	23.7
100	23.1	3.7	24.0	1.2	23.4	23.1	24.3	23.4	13.4	24.3	26.1	23.7
105	23.1	4.0	24.6	1.2	23.4	23.1	24.3	23.7	13.4	24.3	26.1	24.0
110	23.1	4.0	24.3	1.2	23.4	23.4	24.6	23.7	13.4	24.3	26.4	24.0
115	23.4	4.0	24.6	1.2	23.4	23.4	24.3	24.3	14.0	24.6	26.4	24.3
120	23.4	4.0	24.9	1.2	23.7	23.4	24.6	24.3	13.1	24.6	26.7	24.3
125	23.4	4.0	24.9	1.2	23.7	23.7	24.9	24.3	14.0	25.2	26.7	24.3
130	23.7	4.0	24.9	1.2	23.7	23.4	24.9	24.3	14.0	24.9	27.0	24.6
135	23.7	4.0	24.9	1.2	24.0	23.7	25.2	24.6	13.7	24.6	27.0	24.6
140	23.7	4.0	25.2	1.2	24.0	23.7	25.2	24.6	14.6	24.9	27.3	24.6
145	23.7	4.0	25.2	1.2	24.0	24.0	25.2	24.6	14.9	24.9	27.3	24.9
150	23.7	4.0	25.2	1.2	24.3	24.0	25.2	24.6	15.2	25.2	20.4	24.9
155	24.0	4.0	25.5	1.2	24.3	24.0	26.1	24.9	15.2	25.2	27.3	24.9
160	24.0	4.0	25.5	1.2	24.3	24.3	25.5	25.2	16.1	25.2	27.6	24.9
165	24.0	4.0	25.5	1.2	24.3	24.0	25.5	25.2	15.8	25.2	27.6	25.2
170	24.0	4.0	25.5	1.2	24.6	24.3	25.5	25.2	15.5	25.5	27.6	25.2
175	26.1	4.0	25.8	1.2	24.6	24.3	25.8	25.5	15.8	25.5	27.6	25.2
180	24.3	4.0	25.8	1.2	24.6	21.3	25.8	25.5	15.8	25.5	27.9	25.2
185	24.6	4.0	25.8	1.2	24.6	24.6	25.8	25.5	16.5	25.8	27.9	25.5
190	24.6	4.0	26.1	1.2	24.9	24.6	25.8	25.8	16.5	25.8	27.9	25.5
195	24.6	4.0	26.1	1.2	24.9	24.6	25.8	25.8	16.5	26.7	28.2	25.5
200	24.6	4.0	26.1	1.2	24.9	24.6	26.1	25.8	16.8	25.8	28.2	25.5

205	24.6	4.0	26.1	1.2	25.2	24.9	26.1	25.8	14.6	26.1	28.2	25.8
210	24.9	4.0	26.1	1.2	25.2	24.6	26.1	25.8	14.0	26.1	28.2	25.8
215	24.9	4.0	26.1	1.2	25.2	24.9	26.4	25.8	14.3	26.1	28.5	25.8
220	24.9	4.0	26.4	0.3	25.2	25.2	26.4	26.1	13.7	26.4	28.5	25.8
225	24.9	4.0	24.0	1.2	25.2	25.2	26.4	26.1	14.6	26.4	28.5	25.8
230	24.9	4.0	26.4	1.2	25.2	24.9	26.4	26.1	14.0	26.4	28.5	25.8
235	24.9	4.0	26.4	1.2	25.2	24.9	26.4	26.1	14.3	26.4	28.5	25.8
240	24.9	4.3	26.4	1.2	25.8	25.2	26.4	26.1	14.6	26.4	28.5	25.8
245	24.9	4.0	26.4	1.2	25.2	24.9	26.4	26.1	14.9	26.4	28.5	25.8
250	24.9	4.0	26.4	1.2	25.2	25.2	26.4	26.1	15.5	26.4	28.5	12.7
255	24.9	4.3	26.4	1.2	25.2	25.2	26.4	26.1	14.9	26.4	28.5	25.8
260	24.9	4.3	26.4	1.2	25.2	24.9	26.4	26.1	14.9	26.4	28.5	25.8
265	24.9	4.0	26.4	1.2	25.2	25.2	26.4	26.1	14.9	26.4	28.5	25.8
270	25.2	4.3	26.4	1.2	25.2	25.2	26.4	26.1	14.9	26.4	28.5	19.5
275	24.9	4.0	26.4	1.2	25.5	25.2	26.4	27.3	14.9	26.4	28.5	26.1
280	25.2	4.0	26.7	1.2	25.5	25.2	26.4	26.1	15.5	26.4	28.5	26.1
285	25.2	4.3	26.7	1.2	25.5	25.2	26.4	26.1	15.5	26.4	28.5	26.1
290	25.2	4.0	26.7	1.2	25.5	25.2	26.4	26.4	15.5	26.4	28.8	26.1
295	25.2	4.0	26.7	1.2	25.5	25.2	26.7	26.4	15.5	26.4	28.8	26.1
300	25.2	4.0	26.7	1.2	25.8	25.5	26.7	26.4	16.1	26.7	28.8	26.1
305	25.5	4.0	27.0	1.2	25.8	25.5	27.0	26.7	16.1	26.7	29.1	26.4
310	25.5	4.3	27.3	1.2	26.1	25.8	27.0	26.7	15.8	27.0	29.1	13.7
315	25.5	4.3	27.3	1.2	26.1	25.8	27.0	26.7	16.1	27.0	29.4	26.4
320	25.8	4.3	27.3	1.2	26.4	25.8	27.3	26.7	16.8	27.3	25.5	26.7
325	25.8	4.3	27.6	1.2	26.4	26.1	27.6	27.6	16.8	27.3	29.7	26.7
330	25.8	4.3	27.6	1.2	26.4	26.1	27.6	27.0	17.4	27.3	30.0	26.7
335	26.1	4.3	27.9	1.2	26.4	26.1	27.9	27.0	17.4	27.6	30.0	27.0
340	26.4	4.3	27.9	1.2	26.7	26.4	27.9	27.3	17.4	27.6	30.3	27.0
345	26.0	4.2	28.1	1.1	26.6	26.3	27.8	27.2	13.6	27.5	30.2	27.2
350	26.4	4.3	28.2	1.2	27.0	26.4	28.2	27.3	14.6	27.9	30.3	27.3
355	26.7	4.3	28.2	1.2	27.0	26.7	28.2	27.6	14.6	27.9	30.6	27.6
360	26.7	4.3	28.5	1.2	27.0	27.0	28.5	27.6	15.5	28.2	30.6	27.6
365	27.0	4.3	28.5	1.2	27.3	27.0	28.5	27.9	14.9	28.2	30.9	27.6
370	27.0	4.3	28.5	1.2	27.3	26.7	28.8	28.2	15.2	28.2	30.9	27.9
375	27.0	4.3	28.8	1.2	27.6	27.0	28.8	28.2	15.8	28.5	30.9	27.9
380	27.0	4.3	28.8	1.2	27.6	27.0	28.8	28.2	16.1	28.5	31.2	27.9
385	27.2	4.2	29.0	1.1	27.5	27.2	28.7	28.1	16.7	28.4	31.1	28.1
390	27.6	4.6	29.4	1.2	27.9	27.9	29.1	28.5	16.5	28.8	30.0	28.2
395	27.9	4.6	29.4	1.2	28.2	28.2	29.1	28.5	16.5	29.1	29.4	28.8
400	27.9	4.6	29.4	1.2	28.2	28.2	29.1	28.5	16.5	29.4	29.4	28.8
405	28.2	4.6	29.4	1.2	28.2	28.2	29.4	28.8	16.8	29.4	29.4	28.8
410	28.2	4.6	29.4	1.2	28.2	28.2	30.0	28.8	18.0	29.4	29.4	28.8
415	28.2	4.6	29.7	1.2	28.2	28.2	30.0	28.8	18.0	29.4	29.7	28.8
420	28.2	4.6	29.4	1.2	30.3	28.5	30.0	28.8	18.3	29.4	29.4	28.2
425	28.2	4.6	29.7	1.2	28.5	28.2	30.0	28.8	18.3	29.4	29.4	29.1
430	28.2	4.6	29.7	1.2	28.5	28.2	30.0	28.8	18.0	29.4	29.7	29.1
435	28.2	4.6	29.7	1.2	28.5	28.2	30.0	28.8	18.3	30.6	29.4	29.1
440	28.2	4.6	29.7	1.2	28.5	28.2	29.7	28.8	14.6	29.4	29.7	29.1
445	28.2	4.6	29.7	1.2	28.5	28.5	29.7	28.8	14.3	29.4	29.7	29.1
450	28.2	4.6	29.7	1.2	28.5	28.5	29.7	28.8	14.3	29.4	29.7	29.1

455	28.2	4.6	29.7	1.2	28.5	28.2	29.7	28.8	14.3	29.4	29.7	29.1
460	28.2	4.6	29.7	1.2	28.5	28.2	30.0	28.8	15.2	29.4	29.7	29.1
465	28.2	4.6	29.7	1.2	28.2	28.5	30.0	28.8	15.5	29.4	29.7	29.1
470	28.2	4.6	29.7	1.2	28.5	28.5	30.0	28.8	15.5	29.4	29.7	29.1
475	28.2	4.6	29.7	1.2	28.5	28.5	29.7	28.8	15.8	29.4	29.7	29.1
480	28.2	4.6	29.7	1.2	28.5	28.2	30.0	28.8	15.8	29.4	29.7	29.1
485	28.2	4.6	29.7	1.2	28.5	28.5	29.7	28.8	17.4	29.4	29.7	29.1
490	28.2	4.6	29.7	1.2	28.2	28.5	30.0	28.8	17.4	29.4	29.7	29.1
495	28.2	4.6	29.7	1.2	28.5	28.5	30.0	28.8	17.7	29.4	29.7	29.1
500	28.2	4.6	29.7	1.2	28.5	28.5	30.0	28.8	17.1	29.4	29.7	29.1
505	28.2	4.6	29.7	1.2	28.5	28.5	30.3	28.8	17.4	29.4	29.7	29.1
510	28.2	4.6	29.7	1.2	28.5	28.5	30.0	28.8	17.1	29.7	29.7	29.1
515	28.2	4.6	29.7	1.2	28.5	28.5	30.0	28.8	18.3	29.7	29.7	29.1
520	28.2	4.6	29.7	1.2	28.5	28.5	32.0	29.1	18.3	29.4	29.7	29.1
525	28.2	4.6	29.7	1.2	28.5	28.5	30.0	28.8	18.6	29.4	29.7	29.1
530	28.2	4.6	30.0	1.2	28.5	28.5	30.3	28.8	18.3	29.4	29.7	29.1
535	28.2	4.6	30.0	1.2	28.5	28.5	30.3	28.8	18.6	29.4	30.0	29.1
540	28.5	4.6	30.0	1.2	28.5	28.5	30.3	28.8	18.3	29.7	30.0	28.2
545	28.5	4.6	30.0	1.2	28.8	28.5	30.0	29.1	18.6	29.7	30.0	29.4
550	28.5	4.6	30.0	1.2	28.8	28.8	30.3	29.1	18.6	29.7	30.0	29.4
555	28.5	4.6	30.3	1.2	28.8	17.7	30.0	29.4	18.9	29.7	30.3	29.4
560	28.8	4.6	30.3	1.2	29.1	29.1	30.9	29.4	19.5	30.0	30.3	29.7
565	30.6	4.6	30.6	1.2	29.1	29.1	30.9	30.0	19.5	30.3	30.6	30.0
570	29.1	4.6	29.7	1.2	29.4	29.4	30.6	30.0	18.9	30.3	30.6	30.0
575	29.0	4.5	30.8	1.1	29.6	29.3	30.5	30.2	14.8	30.2	30.5	29.9
580	29.4	4.6	30.9	1.2	29.4	29.4	31.2	30.0	15.2	30.6	30.9	30.3
585	29.4	4.6	30.9	1.2	29.7	29.7	30.9	30.3	15.2	30.6	30.9	30.3
590	30.3	4.6	30.9	1.2	29.7	29.7	30.6	30.6	15.8	30.6	30.9	30.3
595	29.5	4.8	31.0	1.3	29.8	29.8	31.3	30.7	16.3	31.0	31.3	30.7
600	29.7	4.6	31.2	1.2	30.0	30.0	31.7	30.6	15.5	30.9	31.2	30.6
605	29.7	4.6	31.2	1.2	30.0	30.0	31.2	30.6	16.5	30.9	31.2	30.6
610	29.7	4.6	31.5	1.2	30.0	27.6	31.2	30.6	16.5	30.9	31.2	30.6
615	30.0	4.6	31.5	1.2	30.3	30.0	31.5	30.6	17.1	31.2	31.5	30.6
620	30.0	5.0	31.5	1.2	30.3	30.0	31.5	30.6	17.4	31.2	31.5	29.4
625	30.0	4.6	31.5	1.2	30.3	30.3	31.5	30.9	18.0	31.5	31.5	30.9
630	30.0	4.6	31.5	1.2	30.3	30.3	31.7	30.9	17.7	31.5	31.5	30.9
635	30.0	5.0	31.7	1.2	30.6	30.3	31.7	30.9	18.6	31.5	31.5	30.9
640	30.3	4.6	31.7	1.2	30.6	30.3	31.7	30.9	18.6	31.5	31.7	30.9
645	30.3	4.6	31.7	1.2	30.6	30.6	31.7	31.2	18.6	31.5	31.7	31.2
650	30.3	4.6	31.7	1.2	30.6	30.6	32.0	31.2	18.9	31.7	31.7	30.9
655	30.3	5.0	31.7	1.2	30.6	30.6	32.0	31.2	19.5	31.7	31.7	31.2
660	30.3	4.6	32.0	1.2	30.6	30.6	32.3	31.2	19.5	31.7	32.0	31.2
665	30.6	4.6	32.0	1.2	30.9	30.6	32.0	31.2	19.8	31.7	32.0	31.2
670	30.6	5.0	32.3	1.2	30.9	30.9	32.6	31.5	19.5	32.0	32.0	31.5
675	30.6	4.6	31.7	1.2	30.9	30.9	32.3	31.5	19.8	32.0	32.0	31.5
680	30.6	4.6	32.0	1.2	30.9	30.9	32.3	31.5	20.4	32.0	32.0	31.7
685	30.6	5.0	32.3	1.2	31.2	30.9	32.3	31.7	17.4	32.0	32.3	31.5
690	30.6	5.0	32.6	1.2	31.2	31.2	32.6	31.7	16.1	32.3	32.3	31.5
695	30.6	5.0	32.6	1.2	31.2	31.2	32.3	31.7	16.1	32.3	32.3	31.7
700	30.9	5.0	32.6	1.2	31.2	31.2	32.6	32.0	17.1	32.3	32.3	31.7

705	30.9	5.0	32.6	1.2	31.2	31.2	32.6	32.0	16.5	32.3	32.3	31.7
710	30.6	3.1	32.6	1.2	31.2	31.2	32.6	32.0	16.8	32.6	32.3	31.7
715	30.9	5.0	32.6	1.2	31.2	31.2	32.6	32.3	18.3	32.6	32.6	31.7
720	30.9	5.0	32.6	1.2	31.2	31.2	32.9	32.3	18.3	32.6	32.6	31.7
725	30.9	5.0	32.6	1.2	31.2	31.2	33.8	32.3	17.7	32.6	32.6	31.7
730	30.9	5.0	32.6	1.2	31.2	31.2	32.6	32.3	18.0	32.6	32.6	31.7
735	30.9	5.0	32.6	1.2	31.2	31.5	33.2	32.3	18.3	32.3	32.6	31.7
740	30.9	5.0	32.6	1.2	31.5	31.5	32.6	32.3	18.0	32.6	32.6	31.7
745	30.9	5.0	32.6	1.2	31.5	31.5	32.6	32.3	18.6	32.6	32.6	31.7
750	30.9	5.0	32.6	1.2	31.5	31.5	32.6	32.6	18.3	32.3	32.6	32.0
755	30.9	5.0	30.0	1.2	31.5	31.5	32.6	32.3	20.1	32.3	32.6	32.0
760	30.9	5.0	32.6	1.2	31.5	31.5	32.6	32.3	19.8	32.3	32.6	32.0
765	30.9	5.0	32.6	1.2	31.5	31.5	32.9	32.6	15.8	32.3	32.6	32.0
770	30.9	5.0	32.6	1.2	31.5	31.5	32.9	32.6	16.5	32.3	32.6	32.0
775	29.1	5.0	32.6	1.2	31.5	31.2	32.6	32.6	15.8	32.3	32.9	32.0
780	30.9	5.0	32.6	1.2	31.5	31.5	32.9	32.6	16.1	32.3	32.6	32.0
785	30.9	5.0	32.9	1.2	31.5	31.5	32.6	32.6	17.1	32.3	32.6	32.0
790	30.9	5.0	32.6	1.2	31.5	31.5	32.9	32.3	17.1	32.3	32.6	32.0
795	30.9	5.0	32.6	1.2	31.5	31.5	32.6	32.6	18.3	32.3	32.6	32.0
800	31.3	5.1	33.0	1.3	31.6	31.6	33.0	32.7	18.4	32.4	33.0	31.8
805	31.2	5.0	32.9	1.2	31.5	31.5	32.9	32.6	18.3	32.6	32.9	32.0
810	31.2	5.0	33.2	1.2	31.7	31.7	32.9	32.9	18.9	32.6	32.9	32.3
815	31.5	5.0	33.2	1.2	31.7	31.7	32.9	32.9	18.0	32.9	33.2	32.3
820	31.5	5.3	33.2	1.2	32.0	32.0	33.2	33.2	18.9	32.9	33.2	32.6
825	31.7	5.0	33.5	1.2	32.0	32.0	33.5	33.5	19.2	33.2	33.2	32.6
830	31.7	5.3	33.5	1.2	32.0	32.3	33.5	33.2	20.1	32.3	33.5	32.9
835	31.7	5.3	33.8	1.2	32.3	32.3	33.5	33.2	20.1	32.3	33.8	32.9
840	32.0	5.0	33.8	1.2	32.6	32.6	33.5	33.5	18.9	32.6	31.5	32.9
845	32.0	5.0	34.1	1.2	32.6	32.6	33.5	33.5	18.9	32.3	33.8	33.2
850	32.3	5.0	34.1	1.2	32.6	32.6	33.8	33.8	18.0	32.6	34.1	33.2
855	32.3	5.0	34.4	1.2	32.6	32.9	34.1	33.8	17.7	32.6	34.1	33.2
860	32.6	5.0	34.4	1.2	32.9	32.9	34.4	33.8	17.1	32.9	34.4	33.5
865	32.6	5.3	34.4	1.2	33.2	33.2	34.1	34.1	17.7	33.2	34.4	33.5
870	32.9	5.0	34.7	1.2	33.2	33.2	34.4	34.4	18.6	34.4	34.7	33.8
875	33.0	5.4	35.1	1.3	33.6	33.6	34.8	34.5	18.7	34.5	34.8	33.9
880	33.3	5.4	35.1	1.3	33.6	33.6	34.8	34.8	19.9	34.2	35.1	34.2
885	33.3	5.4	35.1	1.3	33.9	33.9	35.1	34.8	18.7	33.6	35.1	34.2
890	33.2	5.3	35.0	1.2	33.8	32.3	34.7	34.7	18.6	33.8	35.0	34.1
895	33.2	5.3	35.3	1.2	33.8	33.8	35.0	34.7	19.2	34.1	35.0	34.4
900	33.2	5.3	35.3	1.2	33.8	33.8	35.0	35.0	19.8	34.7	35.3	34.4
905	33.3	5.4	35.4	1.3	34.2	34.2	35.4	35.1	20.2	34.8	35.4	34.5
910	33.5	5.3	35.6	1.2	34.1	34.1	35.3	35.3	20.4	34.7	35.3	34.4
915	33.5	5.3	35.6	1.2	34.1	34.1	35.6	35.3	20.4	35.0	35.3	34.7
920	33.5	5.3	35.6	1.2	34.1	34.1	35.6	35.3	19.2	35.0	35.3	34.7
925	33.5	5.3	35.6	1.2	34.4	34.1	35.3	35.3	19.2	35.3	35.3	34.7
930	33.8	5.3	35.6	1.3	34.4	34.1	35.6	35.3	19.8	35.0	35.3	34.7
935	33.9	5.4	35.7	1.3	34.5	34.5	35.4	35.4	20.8	35.4	35.7	34.8
940	33.8	5.3	35.6	1.2	34.4	34.4	35.6	35.6	21.0	34.1	35.9	34.7
945	33.8	5.3	35.9	1.2	34.4	34.4	35.6	35.6	20.7	34.7	35.6	35.0
950	34.2	5.4	35.9	1.3	34.5	34.5	35.9	35.7	21.4	34.8	35.7	35.1

955	34.1	5.3	35.9	1.2	34.7	34.4	35.6	35.9	21.3	34.7	35.6	35.0
960	34.1	5.3	35.9	1.2	34.7	34.7	35.9	35.9	21.0	35.0	35.9	35.0
965	34.1	5.3	36.1	1.2	34.7	34.7	35.9	35.9	18.0	34.7	35.9	35.0
970	34.1	5.3	36.1	1.2	34.7	34.1	36.1	35.9	18.3	34.4	36.1	35.0
975	34.4	5.3	36.1	1.2	34.7	34.7	36.1	35.9	18.6	35.0	36.1	35.3
980	34.5	5.4	36.2	1.3	35.1	35.1	36.2	36.2	18.4	35.4	36.2	35.4
985	34.4	5.3	36.1	1.2	35.0	35.0	36.1	36.1	18.9	35.0	36.1	35.3
990	34.4	5.3	36.1	1.2	35.0	35.0	35.9	35.9	19.8	34.7	36.1	35.3
995	34.4	5.3	36.4	1.2	35.3	35.0	36.1	36.1	21.0	34.4	36.4	35.6
1000	34.8	5.4	36.5	1.3	35.4	35.4	36.5	36.2	20.2	34.8	36.5	35.7
1005	34.7	5.6	36.4	1.2	35.0	35.3	36.4	36.1	19.8	35.0	36.4	35.6
1010	34.7	5.3	36.4	1.2	35.3	35.3	36.1	36.1	20.4	35.0	36.4	35.6
1015	34.7	5.3	36.7	1.2	35.3	35.3	36.7	36.1	21.3	35.3	36.4	35.6
1020	34.4	5.3	36.7	1.2	35.3	35.3	36.1	36.1	22.2	35.3	36.7	35.6
1025	34.7	5.3	36.7	1.2	35.3	35.6	36.4	36.4	23.7	35.0	36.7	35.9
1030	34.8	5.4	36.8	1.3	35.4	35.4	36.8	36.5	22.3	35.4	36.8	35.9
1035	35.0	5.6	36.7	1.2	35.3	35.6	36.7	36.4	22.5	35.3	36.7	35.9
1040	35.0	5.3	37.0	0.7	35.6	35.6	37.0	36.4	22.8	35.3	36.7	35.9
1045	35.1	5.4	36.8	1.3	38.6	35.7	36.5	36.5	22.3	35.7	37.1	35.9
1050	35.0	5.3	37.0	1.2	35.6	35.6	36.4	36.7	18.9	35.6	36.7	36.1
1055	35.1	5.4	37.1	1.3	35.7	35.7	37.1	36.8	19.0	35.7	37.1	36.2
1060	35.3	5.3	37.0	1.2	35.9	35.9	36.7	36.7	18.6	35.9	37.0	30.0
1065	35.3	5.3	37.3	1.2	35.9	35.9	37.0	37.0	18.3	37.9	37.3	36.4
1070	35.7	5.7	37.4	1.3	36.2	36.2	37.4	37.1	19.0	35.9	37.4	36.2
1075	35.6	5.6	37.3	1.2	36.4	36.1	37.6	37.0	19.5	36.1	37.6	36.4
1080	35.6	5.6	37.6	1.2	36.1	36.1	37.6	37.0	20.1	36.4	31.2	36.4
1085	35.6	5.6	37.6	1.2	36.4	34.4	37.6	37.3	20.7	37.0	37.6	36.4
1090	35.9	5.7	37.7	1.3	36.5	36.5	37.4	37.4	21.4	37.1	37.7	36.8
1095	35.9	5.7	38.0	1.3	36.5	36.5	38.0	37.7	21.7	37.4	37.7	37.1
1100	36.1	5.6	37.9	1.2	41.4	36.7	37.9	37.6	23.1	37.6	37.9	37.0
1105	35.7	5.7	38.0	1.3	36.8	36.8	37.7	37.7	22.6	37.7	38.0	37.1
1110	36.5	5.7	38.0	1.3	36.8	36.8	38.6	38.0	23.5	38.0	38.3	37.4
1115	36.7	.5.6	38.2	1.5	37.0	37.0	38.5	37.9	23.1	37.9	38.2	37.3
1120	36.5	6.0	38.3	1.3	37.1	37.1	38.3	38.3	23.8	38.0	38.6	37.7
1125	36.8	5.7	38.6	1.3	37.4	37.4	38.6	38.3	19.3	38.3	38.6	37.7
1130	36.8	5.7	38.9	1.3	37.4	37.4	38.9	38.6	19.3	38.3	38.6	37.7
1135	36.8	5.7	38.9	1.3	37.7	37.7	39.2	38.6	19.6	38.3	38.9	38.0
1140	37.1	5.7	38.9	1.3	37.7	37.7	39.2	38.6	19.6	38.3	38.9	38.0
1145	37.1	5.7	38.9	1.6	37.7	37.7	38.9	38.6	21.1	38.3	38.9	38.0
1150	37.0	5.6	38.8	1.2	37.6	37.6	38.8	38.8	19.8	37.9	39.1	37.9
1155	36.7	5.6	39.1	1.2	37.9	37.6	39.1	38.8	20.7	38.2	39.1	37.9
1160	37.3	5.6	39.1	1.2	37.9	37.9	38.8	38.8	21.6	37.9	39.1	38.2
1165	37.4	5.7	39.5	1.3	38.0	37.1	39.5	39.2	22.0	38.0	39.5	38.3
1170	37.3	5.6	39.4	1.2	38.2	37.9	39.4	39.1	22.5	37.9	39.4	38.2
1175	37.6	5.6	39.7	1.5	38.2	38.2	39.4	39.4	22.8	37.9	39.7	38.5
1180	37.3	5.6	39.7	1.2	38.5	38.2	40.0	39.4	22.5	38.2	39.7	38.5
1185	38.0	5.7	39.8	1.3	38.6	38.6	40.0	39.5	23.2	38.3	39.8	38.9
1190	37.9	5.6	39.7	1.2	38.5	38.2	40.0	39.7	23.1	37.9	39.7	38.8
1195	38.0	5.7	40.0	1.3	38.6	38.6	40.0	39.8	22.9	38.3	40.0	38.9
1200	37.9	5.6	40.0	1.2	38.5	38.5	40.0	39.7	21.9	38.2	40.0	38.8

1205	38.0	6.0	40.0	1.3	38.9	38.9	40.0	39.8	22.6	38.3	40.0	38.9
1210	38.0	5.7	40.0	1.3	38.9	38.9	40.3	40.6	23.2	38.6	40.3	39.2
1215	38.2	5.9	40.0	1.2	38.8	38.8	40.2	40.0	23.1	38.5	40.0	39.1
1220	38.2	5.9	40.2	1.2	38.8	38.8	40.0	40.0	23.1	38.5	40.2	39.1
1225	38.2	5.9	40.2	1.2	42.3	39.1	40.2	40.0	23.7	38.5	40.2	38.5
1230	38.2	5.9	40.2	1.2	39.4	38.8	40.2	40.0	18.6	38.5	40.2	39.4
1235	38.3	5.7	40.3	1.3	38.9	39.2	40.0	40.0	19.9	38.6	40.3	39.2
1240	38.5	5.6	40.2	1.2	39.1	39.1	40.0	40.0	20.4	38.8	40.2	39.4
1245	38.3	6.0	40.3	1.3	39.2	38.9	40.6	40.0	20.2	38.9	40.3	39.5
1250	38.6	5.7	40.3	1.3	39.2	39.2	40.6	40.0	21.4	38.9	40.3	39.5
1255	38.6	6.0	40.3	1.3	39.2	39.2	40.3	40.0	22.3	39.2	40.6	39.5
1260	38.6	6.0	40.6	0.4	39.2	39.5	40.6	40.3	22.6	38.9	40.3	39.5
1265	38.6	4.1	40.6	1.3	39.5	39.5	40.6	40.3	23.2	39.2	40.6	39.5
1270	38.6	6.0	40.6	1.3	39.2	39.5	40.9	40.6	23.5	39.5	40.6	39.8
1275	38.6	6.0	40.6	1.3	39.5	39.5	40.9	40.3	23.5	39.2	40.6	39.8
1280	38.9	5.7	40.6	1.3	39.5	39.5	40.6	40.3	23.8	39.2	40.6	39.8
1285	38.9	5.7	40.6	1.3	39.5	39.5	40.9	40.6	23.8	39.2	40.6	39.8
1290	38.9	5.7	40.6	1.3	39.5	39.5	40.9	40.3	25.0	39.5	40.6	39.8
1295	38.9	6.0	40.6	1.3	39.5	39.5	40.6	40.6	24.4	39.5	40.9	39.8
1300	38.9	6.0	40.6	1.3	39.5	39.5	40.9	40.6	19.3	39.8	40.6	39.8
1305	38.8	3.7	40.8	1.2	39.7	39.4	40.8	40.5	20.4	39.7	40.8	39.7
1310	38.9	6.0	40.9	1.3	39.5	39.8	41.2	40.6	19.6	40.0	40.9	39.8
1315	39.2	6.0	40.9	1.3	39.8	39.8	40.9	40.6	21.7	40.0	40.9	39.8
1320	39.1	5.9	41.1	1.2	40.0	40.0	41.1	40.8	22.2	40.0	41.1	38.2
1325	39.2	6.0	41.2	1.3	40.0	40.0	41.2	40.9	23.2	40.3	41.2	40.3
1330	39.5	6.0	41.5	1.3	40.3	40.0	41.8	41.2	22.3	40.3	41.5	40.3
1335	39.8	6.0	41.5	1.3	40.3	40.3	41.8	41.5	23.2	40.9	41.5	40.3
1340	39.8	6.0	41.8	1.3	40.3	40.6	42.1	41.5	23.8	41.2	41.8	40.6
1345	40.0	6.0	41.8	1.3	40.6	40.6	42.1	41.5	23.2	41.8	41.8	40.9
1350	40.0	6.0	42.1	1.3	40.9	40.9	42.4	41.8	23.2	41.8	42.1	40.9
1355	40.2	5.9	42.0	1.2	40.8	40.8	42.3	42.0	23.7	42.0	42.0	40.8
1360	40.3	6.3	42.4	1.3	41.2	41.2	42.7	42.1	24.1	42.1	42.4	41.2
1365	40.5	5.9	42.3	1.2	41.7	41.1	42.6	42.3	24.9	42.0	42.3	30.6
1370	40.6	6.0	42.7	1.3	41.5	41.5	43.0	42.4	25.3	41.8	42.7	41.5
1375	40.6	6.0	42.7	1.3	41.5	41.5	43.0	42.4	22.6	41.8	42.7	41.5
1380	40.9	6.3	42.7	1.3	41.5	41.8	43.3	42.7	21.4	43.6	43.0	41.8
1385	40.9	6.0	43.0	1.3	41.5	41.8	43.3	42.7	22.6	41.8	43.3	41.8
1390	41.2	6.0	43.0	1.3	41.8	41.8	43.6	43.0	22.3	41.8	43.3	42.1
1395	41.5	6.0	43.3	1.3	41.8	42.1	43.6	45.3	23.8	41.8	43.3	42.1
1400	41.5	6.0	43.3	1.3	41.8	42.1	43.6	43.0	23.8	42.1	43.6	42.1
1405	41.5	6.0	43.6	1.3	42.1	42.4	43.9	43.3	24.4	42.4	43.6	42.4
1410	41.4	5.9	43.5	1.2	42.0	42.3	44.1	43.2	24.0	42.9	43.5	42.3
1415	41.5	6.0	43.6	1.6	42.4	42.4	44.2	43.6	25.0	43.0	43.6	42.4
1420	41.8	6.3	43.9	1.3	42.4	42.4	44.2	43.6	25.0	43.3	43.9	42.4
1425	41.8	6.0	43.9	1.3	42.4	42.7	44.4	43.6	23.8	43.6	43.9	42.7
1430	41.8	6.3	43.9	0.4	42.7	42.7	44.4	43.9	20.8	43.6	43.6	42.7
1435	41.5	6.0	43.9	1.3	42.4	42.7	44.4	43.9	19.9	43.6	44.2	42.7
1440	42.1	6.3	44.2	1.3	42.7	43.0	44.4	43.9	22.3	43.6	44.2	42.7
1445	41.8	6.3	44.2	1.3	42.7	43.0	44.7	43.9	21.4	43.6	44.2	43.0
1450	46.7	6.3	44.2	1.3	42.7	43.0	44.4	44.4	23.2	43.6	44.2	43.0

1455	42.3	5.9	44.1	1.5	42.6	42.9	44.6	44.1	22.5	43.5	44.3	42.9
1460	42.4	6.3	44.4	1.3	43.0	43.3	44.7	44.2	23.5	43.3	44.4	43.0
1465	42.4	6.3	44.4	1.6	43.0	43.3	44.7	44.2	23.8	43.3	44.4	40.3
1470	42.4	6.3	44.4	1.3	43.0	43.3	44.7	44.2	24.7	43.6	44.4	43.3
1475	42.4	6.3	44.4	1.3	43.3	43.3	44.7	44.2	22.3	43.6	44.4	43.3
1480	42.6	6.2	44.3	1.2	43.2	43.2	44.6	44.1	20.4	43.5	44.3	42.9
1485	42.4	6.3	44.4	1.3	43.0	43.3	44.7	44.4	21.1	43.9	44.4	43.0
1490	42.4	6.3	44.4	1.6	43.0	43.3	45.0	44.4	22.9	43.6	44.4	43.0
1495	42.4	6.3	44.4	1.3	43.0	43.3	44.7	44.2	23.2	43.9	44.4	43.0
1500	42.4	6.3	44.4	1.3	43.0	43.3	44.7	44.2	24.1	43.6	44.4	43.3
1505	42.7	6.3	44.4	1.6	43.0	43.3	45.0	44.4	23.8	43.6	44.7	43.3
1510	42.7	6.3	44.4	1.6	43.0	43.3	45.0	44.4	24.4	44.2	44.7	43.3
1515	42.7	6.3	44.7	1.3	43.3	43.6	45.0	44.4	25.3	44.2	44.7	43.3
1520	42.4	6.3	44.7	1.6	43.3	43.6	45.0	44.4	24.1	44.2	44.7	43.6
1525	42.7	6.3	44.7	1.6	43.3	43.6	45.3	44.4	25.0	44.4	44.7	43.6
1530	42.7	6.6	44.7	1.6	43.3	43.6	45.9	44.7	24.7	44.4	44.7	43.6
1535	42.7	6.3	44.7	1.6	43.6	43.6	45.0	44.4	25.6	43.0	44.7	43.6
1540	43.0	6.3	45.0	1.3	43.6	43.6	45.3	44.7	25.9	44.4	45.0	43.6
1545	43.0	6.3	45.0	1.6	43.6	43.9	45.3	44.7	26.2	44.4	45.0	43.6
1550	43.0	6.3	45.0	1.6	43.6	43.9	45.3	44.7	24.7	44.7	45.0	43.6
1555	43.0	6.3	45.0	1.6	43.6	43.9	45.6	44.7	21.1	44.7	45.0	43.9
1560	43.2	6.2	44.9	0.7	43.5	43.8	45.5	44.6	21.3	44.6	44.9	43.8
1565	43.3	6.3	45.3	1.6	43.6	43.9	45.3	44.7	21.1	44.7	45.0	43.9
1570	43.3	6.3	45.0	1.6	43.6	43.9	45.3	45.0	22.6	44.7	45.0	43.9
1575	43.0	6.3	45.0	1.3	43.6	43.9	45.6	44.7	23.2	44.7	45.0	43.9
1580	43.0	6.3	45.0	1.6	43.6	43.9	45.6	44.7	23.5	44.7	45.0	43.6
1585	43.0	6.3	45.0	1.6	46.7	43.9	45.6	44.7	22.9	44.7	45.0	43.9
1590	43.3	6.3	45.0	1.6	43.6	43.9	45.3	44.7	23.8	44.7	45.0	43.9
1595	43.3	6.3	45.0	1.3	43.6	43.9	45.3	44.7	25.6	44.7	45.3	43.9
1600	43.0	6.3	45.0	1.3	43.6	43.9	45.6	45.0	25.0	44.7	45.0	43.9
1605	43.3	6.3	45.0	1.6	43.9	44.2	45.6	45.0	25.9	44.7	45.3	43.9
1610	43.3	6.3	45.0	1.6	43.9	44.2	45.6	45.0	25.9	44.7	44.4	43.9
1615	43.3	6.0	45.3	1.3	43.9	44.2	45.9	45.0	25.3	44.7	45.3	31.3
1620	43.3	6.3	45.3	1.3	44.2	44.2	45.9	45.0	21.1	45.0	45.3	44.2
1625	43.6	6.3	45.6	1.3	44.2	44.4	45.9	45.3	21.7	45.3	45.6	44.2
1630	43.7	6.4	45.7	1.7	44.2	44.5	46.0	45.7	23.6	45.4	45.7	44.5
1635	43.9	6.3	45.6	1.6	44.4	44.7	46.2	45.6	24.1	45.6	45.9	44.4
1640	43.9	6.3	45.9	1.6	47.3	44.7	46.5	45.6	24.7	45.9	45.9	44.4
1645	44.2	6.3	45.9	1.3	44.7	45.0	46.5	45.9	25.0	45.9	45.9	44.7
1650	44.2	6.3	46.2	1.6	44.7	45.0	46.7	45.9	25.3	45.9	46.2	44.7
1655	44.2	6.3	46.2	1.6	44.7	45.0	46.7	45.9	25.9	46.2	46.2	45.0
1660	44.4	6.3	46.2	1.3	45.0	45.3	46.7	46.2	25.9	46.5	44.2	45.0
1665	44.4	6.3	46.5	1.6	47.3	45.3	47.0	46.2	26.2	46.5	46.5	45.0
1670	44.4	6.3	46.7	1.3	45.0	45.3	47.3	46.5	26.8	46.5	46.5	45.0
1675	44.7	6.6	46.7	1.3	45.3	45.6	47.3	46.5	25.6	46.7	46.7	45.3
1680	44.7	6.6	46.7	1.3	45.3	45.6	47.3	46.7	24.1	46.7	46.7	45.3
1685	44.7	6.6	46.7	1.3	45.3	45.6	47.3	46.7	22.9	46.7	46.7	45.3
1690	44.7	6.6	46.7	1.6	45.3	45.6	47.3	46.7	22.6	46.7	46.7	45.3
1695	44.7	6.6	46.7	1.3	45.6	45.9	47.9	46.7	23.8	46.7	46.7	45.3
1700	44.7	6.6	46.7	1.6	45.6	45.6	47.6	46.7	23.2	46.7	45.0	45.3

1705	44.7	6.6	46.7	1.3	45.3	45.6	47.6	46.5	24.7	46.7	47.0	45.3
1710	44.7	6.6	46.7	1.3	45.3	45.9	47.6	46.7	25.6	46.7	47.0	45.3
1715	45.0	6.6	46.7	1.6	45.6	45.9	47.6	46.7	25.6	46.7	47.0	45.6
1720	44.7	6.6	47.0	1.6	45.6	45.9	47.9	46.7	25.9	46.7	47.0	45.6
1725	45.0	6.6	47.0	1.6	45.6	45.9	47.6	47.0	25.9	46.7	47.0	45.6
1730	45.1	5.8	47.1	1.7	45.7	46.0	48.0	47.1	22.1	46.8	47.1	45.7
1735	44.9	6.2	46.9	1.5	45.5	45.8	47.8	46.6	22.2	46.9	46.9	45.5
1740	45.0	6.6	47.0	1.3	45.6	46.2	47.9	47.0	22.9	47.0	47.0	45.6
1745	45.0	6.6	47.0	1.6	45.6	46.2	47.6	47.0	24.1	47.0	47.3	45.9
1750	45.0	6.6	47.3	1.6	45.9	46.2	47.9	47.0	26.8	47.0	47.3	45.9
1755	45.3	6.6	47.3	1.3	45.9	46.2	48.2	47.0	26.8	47.0	47.3	45.9
1760	45.3	6.6	47.3	1.3	45.9	46.2	48.5	47.3	27.1	47.0	47.3	45.9
1765	45.3	6.6	47.3	1.3	46.2	46.5	48.2	47.3	27.4	47.3	47.3	45.9
1770	45.3	6.6	47.3	1.6	46.2	46.5	48.2	47.3	22.0	47.3	47.6	46.2
1775	45.3	6.6	47.3	1.6	46.2	46.5	48.5	47.3	21.7	47.3	47.6	46.2
1780	45.6	6.6	47.6	1.6	46.2	46.7	48.5	47.6	22.9	47.3	47.6	46.2
1785	45.6	6.6	46.2	1.3	46.5	46.7	48.2	47.6	25.0	47.6	47.6	46.2
1790	45.9	6.6	47.6	1.3	46.5	46.7	48.5	47.6	25.6	47.3	47.9	46.5
1795	45.6	6.6	47.6	1.6	46.5	46.7	48.7	47.6	25.0	47.6	47.9	46.5
1800	45.9	6.6	47.9	1.3	46.5	47.0	48.7	47.6	24.4	47.6	47.9	46.5
1805	45.6	6.6	47.9	1.6	46.5	46.7	48.5	47.6	23.8	47.6	47.9	46.5
1810	45.6	6.6	47.6	1.6	46.5	46.7	48.7	47.6	26.2	47.6	43.0	46.5
1815	45.6	6.6	47.6	1.6	46.5	46.7	48.7	47.6	26.5	49.0	47.9	46.5
1820	45.9	6.6	47.9	1.6	46.5	46.7	48.7	47.6	26.5	47.6	47.9	46.5
1825	45.9	6.6	47.9	1.3	46.5	46.7	48.7	47.6	26.8	47.6	47.9	46.5
1830	46.0	6.7	48.0	1.7	46.5	46.8	48.8	47.7	27.2	47.7	43.1	46.5
1835	46.0	6.7	48.0	1.4	46.5	46.8	48.8	47.7	27.2	47.7	48.0	46.5
1840	45.9	6.6	47.9	1.3	46.5	46.7	48.5	47.6	22.9	47.6	47.9	46.5
1845	46.0	1.7	48.0	1.7	46.5	46.8	48.8	48.0	24.5	47.7	48.0	46.5
1850	45.9	6.6	47.9	1.6	46.5	47.0	49.0	47.9	22.9	47.6	48.2	46.5
1855	46.0	6.7	48.0	1.4	46.5	47.1	49.1	47.7	23.9	47.7	48.0	46.5
1860	45.9	6.6	47.9	1.6	46.5	47.0	48.7	47.9	30.4	47.6	48.2	46.5
1865	45.9	6.6	47.9	1.6	46.7	47.0	49.0	47.9	25.6	47.6	47.9	46.5
1870	45.9	6.6	47.9	1.6	46.5	47.0	49.0	47.9	26.8	47.6	48.2	46.7
1875	46.0	6.7	48.0	1.4	46.5	47.1	48.8	48.0	26.3	47.7	48.3	46.5
1880	45.9	6.6	47.9	1.6	46.5	47.0	49.0	47.9	25.9	47.6	48.2	46.5
1885	45.9	6.6	47.9	1.6	46.5	47.0	49.0	47.9	27.4	47.6	48.2	46.5
1890	45.9	6.6	47.9	1.6	46.5	38.0	48.7	47.9	27.7	47.6	48.2	46.5
1895	45.9	6.3	47.9	1.6	46.5	47.0	49.0	47.9	27.1	47.6	48.2	44.4
1900	45.9	6.6	47.9	1.3	46.5	47.0	49.0	47.9	27.4	47.6	48.2	46.7
1905	45.9	6.6	47.9	1.3	46.5	47.0	49.0	47.9	23.2	47.6	48.2	46.7
1910	45.9	6.6	47.9	1.6	46.7	47.0	49.0	48.2	21.7	47.6	48.2	46.7
1915	45.9	6.9	47.9	1.3	46.7	47.0	49.0	47.9	23.2	47.6	48.2	46.7
1920	46.3	6.7	48.3	1.4	46.8	47.1	49.1	48.0	23.6	47.7	48.3	46.8
1925	46.2	6.6	48.2	1.3	46.7	47.3	49.0	48.2	24.7	47.6	48.2	46.7
1930	46.3	6.7	48.3	1.4	46.8	47.4	49.4	48.3	26.3	47.7	48.3	46.8
1935	46.2	6.6	48.2	1.6	46.7	47.3	49.3	48.2	26.2	47.6	48.5	46.7
1940	46.3	6.7	48.3	1.7	47.1	47.1	49.4	48.3	26.3	47.7	48.6	47.1
1945	46.2	6.6	48.5	1.6	47.0	47.3	49.3	48.2	27.1	47.6	48.5	47.0
1950	46.3	6.7	48.6	1.7	47.1	47.4	49.7	48.6	26.9	47.7	48.6	47.1

1955	46.5	4.2	48.6	1.7	47.1	47.4	49.7	48.6	27.8	48.0	48.6	47.1
1960	46.5	6.6	48.5	1.6	47.3	47.6	49.6	48.5	23.2	47.9	48.7	47.0
1965	46.5	6.7	48.6	1.7	47.4	47.7	49.7	48.8	23.6	48.0	48.8	47.4
1970	46.5	6.6	48.7	1.6	47.3	42.1	49.6	48.7	23.5	47.9	48.7	46.2
1975	46.5	6.7	48.8	1.7	47.4	47.7	50.0	48.8	23.3	48.0	49.1	47.4
1980	46.8	6.7	48.8	1.4	47.4	48.0	50.0	48.8	25.7	48.3	49.1	47.4
1985	47.1	6.7	49.1	1.7	47.4	48.0	50.0	48.8	25.7	48.6	49.4	47.4
1990	46.7	6.6	49.0	1.6	47.6	47.9	50.2	49.0	27.1	48.7	49.3	47.6
1995	47.0	6.6	49.0	1.3	47.6	42.1	50.4	49.0	27.1	49.0	49.3	47.6
2000	47.1	5.8	49.1	1.7	48.0	48.3	50.3	49.4	29.9	49.1	49.4	48.0
2005	47.0	6.6	49.3	1.6	47.9	48.2	50.7	49.3	27.4	49.0	49.3	47.9
2010	47.1	6.7	49.4	1.4	48.0	48.6	50.3	49.4	23.0	49.1	49.7	41.3
2015	47.4	6.7	49.4	1.7	48.3	48.3	50.3	49.4	22.1	49.1	49.7	48.0
2020	47.0	6.6	49.3	1.3	47.9	48.5	50.4	49.3	24.1	49.0	49.6	47.9
2025	47.3	6.6	49.3	1.6	48.2	48.5	50.4	49.3	25.0	49.0	49.6	47.9
2030	47.3	6.9	49.3	1.6	48.2	48.5	50.4	49.3	25.6	49.0	49.6	47.9
2035	47.3	6.6	49.3	1.6	47.9	48.5	50.7	51.3	26.8	49.0	49.6	47.9
2040	47.3	6.6	49.3	1.6	48.2	48.5	50.4	49.3	25.0	49.3	49.6	47.9
2045	47.3	6.9	49.3	1.3	48.2	48.5	50.4	49.3	26.5	49.0	49.6	47.9
2050	47.4	6.7	49.7	1.7	48.3	48.6	50.8	49.4	26.6	49.4	49.7	48.3
2055	47.3	6.6	49.6	1.6	48.2	48.5	50.4	49.3	26.8	49.3	49.6	48.2
2060	47.4	6.7	49.7	1.7	48.3	48.8	50.8	49.7	27.8	49.4	50.0	48.3
2065	47.4	6.7	49.7	1.4	48.3	48.8	51.7	49.7	28.1	49.4	50.0	48.3
2070	47.7	6.7	49.7	1.4	48.3	48.8	50.8	49.7	28.1	49.4	50.0	48.3
2075	47.6	6.6	49.6	1.6	48.5	48.7	50.7	49.6	28.6	49.3	49.9	48.2
2080	47.7	6.7	49.7	1.7	48.6	48.8	50.8	49.7	27.8	49.7	50.0	48.3
2085	47.7	7.0	49.7	1.4	48.6	48.8	51.1	49.7	23.3	49.4	50.0	48.6
2090	47.7	7.0	49.7	1.7	48.6	48.8	51.1	49.7	22.4	49.7	50.0	48.6
2095	47.6	6.9	49.6	1.3	48.5	48.7	51.0	49.9	23.5	38.0	50.2	48.5
2100	47.7	7.0	49.7	1.7	48.6	48.8	51.1	49.7	23.3	49.7	50.0	48.3
2105	47.6	6.0	49.6	1.3	48.5	49.0	51.0	49.9	25.6	49.6	49.9	48.2
2110	47.6	6.6	49.6	1.6	48.5	48.7	51.0	49.6	25.0	49.6	50.2	48.5
2115	48.0	7.0	50.0	1.7	48.6	49.1	51.1	50.0	23.6	49.7	50.3	48.6
2120	47.7	6.7	49.7	1.7	48.6	48.8	51.1	49.7	24.5	49.7	50.0	48.6
2125	47.6	6.9	49.6	1.3	48.2	48.7	51.0	49.6	25.6	44.4	50.2	48.2
2130	47.7	6.7	49.7	1.7	48.6	48.8	50.8	49.7	26.3	49.4	50.0	48.6
2135	47.7	6.7	49.7	1.7	48.6	48.8	51.1	50.0	26.6	49.7	50.0	48.6
2140	47.6	6.6	49.9	1.6	48.5	48.7	51.3	49.9	27.4	49.6	49.9	48.5
2145	47.6	6.6	50.2	1.6	48.5	49.0	51.3	49.9	24.7	49.6	50.2	48.5
2150	47.6	6.9	49.9	1.6	48.5	40.6	51.0	49.9	23.8	49.6	50.2	48.5
2155	48.0	7.0	50.0	1.7	48.6	49.1	51.1	50.0	25.1	49.7	50.0	48.6
2160	47.4	7.0	50.0	1.7	48.6	49.1	51.1	50.5	27.2	49.7	50.3	48.6
2165	47.7	7.0	50.0	1.4	48.8	48.3	51.4	50.0	28.1	49.7	50.3	48.6
2170	48.0	7.0	50.0	1.4	48.8	49.1	51.4	50.0	29.9	49.7	50.3	48.6
2175	48.0	7.0	50.0	1.7	48.8	49.1	51.1	50.0	29.9	49.7	50.3	48.8
2180	48.0	7.0	50.0	1.7	48.8	49.1	51.4	50.0	30.5	49.7	50.3	48.8
2185	48.0	6.7	50.3	1.4	48.8	49.1	51.4	50.0	29.6	50.0	50.3	48.6
2190	48.0	7.0	50.3	1.7	48.8	49.1	51.4	56.2	30.2	49.7	50.3	48.8
2195	48.0	7.0	50.5	1.7	48.8	49.4	51.4	50.3	30.5	49.4	50.5	48.6
2200	47.9	6.9	50.2	1.6	48.7	49.3	51.3	49.9	36.2	49.6	50.2	48.7

2205	47.9	6.9	49.9	1.3	48.7	49.0	51.3	50.2	30.7	49.9	50.4	48.7
2210	48.0	6.7	50.3	1.7	48.8	49.4	51.7	50.3	29.9	50.0	50.3	48.8
2215	48.3	7.0	50.3	1.4	48.8	49.4	51.4	50.3	29.9	50.0	50.5	48.8
2220	48.3	6.7	50.3	1.7	49.1	49.4	51.7	50.3	23.6	50.0	50.5	48.8
2225	48.3	7.0	50.5	1.4	49.1	49.4	51.7	50.3	21.2	50.0	50.5	48.8
2230	48.2	6.9	50.2	1.3	49.0	49.3	51.6	50.2	22.6	50.2	50.4	49.0
2235	48.3	6.7	50.5	1.7	49.4	49.7	51.9	50.5	25.7	50.3	50.8	49.1
2240	48.6	6.7	50.5	1.7	49.4	49.7	52.2	50.5	26.3	50.3	50.8	49.1
2245	48.5	7.2	50.7	1.6	49.3	49.6	52.1	50.4	26.2	50.4	51.0	49.0
2250	48.5	6.9	50.7	1.6	49.6	49.9	52.1	50.7	26.5	49.6	51.0	49.3
2255	48.7	6.9	50.7	1.6	49.3	47.9	52.1	50.7	27.4	49.9	51.0	49.3
2260	48.8	7.0	50.5	1.7	49.7	50.0	52.5	50.8	29.6	50.3	51.4	49.4
2265	48.8	7.0	51.1	1.7	49.7	50.0	53.1	51.1	35.8	50.0	51.4	49.4
2270	49.1	7.0	51.1	1.7	50.0	50.3	52.8	51.1	29.6	50.0	47.4	49.7
2275	49.0	6.9	51.3	1.6	49.9	50.2	53.0	51.0	30.7	49.9	51.6	49.6
2280	49.1	7.0	51.4	1.4	50.0	50.3	52.8	52.5	30.5	50.0	51.4	49.7
2285	49.4	7.0	51.4	1.7	50.3	50.5	52.8	51.7	30.8	50.0	51.7	50.0
2290	49.4	7.0	51.4	1.7	51.9	50.5	53.3	51.7	31.4	50.8	51.9	48.8
2295	49.4	7.0	51.7	1.7	50.3	50.8	53.3	51.7	31.4	51.4	51.9	50.0
2300	49.4	7.0	51.7	1.7	50.3	50.8	53.6	51.7	31.7	51.4	51.9	50.3
2305	49.7	7.0	51.7	1.7	50.5	50.8	53.9	51.9	22.1	51.7	52.2	50.3
2310	49.7	7.0	51.9	1.7	50.8	51.1	53.6	51.9	21.8	51.1	51.9	50.3
2315	49.7	7.0	51.9	1.7	50.8	51.1	53.9	51.9	23.0	51.1	52.2	50.3
2320	50.0	7.0	51.9	1.7	53.1	51.1	53.9	52.2	24.2	50.8	52.2	50.3
2325	49.6	6.9	51.8	1.6	50.7	51.0	54.1	51.8	27.7	50.7	52.1	50.4
2330	49.7	7.0	51.9	1.4	50.8	51.1	54.7	51.9	28.1	50.8	52.2	50.5
2335	49.9	6.9	51.8	1.6	50.7	51.0	54.1	51.8	28.0	51.0	52.1	50.4
2340	50.0	7.0	51.9	1.7	50.8	51.4	54.2	52.2	28.4	51.1	52.5	50.5
2345	49.9	6.9	52.1	1.3	50.7	51.3	55.2	52.1	28.6	51.0	52.4	50.4
2350	49.9	6.9	52.1	1.6	51.0	45.0	54.4	52.1	29.8	51.0	52.4	50.4
2355	50.0	7.0	52.2	1.7	50.8	51.4	54.5	52.2	30.5	51.9	52.5	50.5
2360	50.0	7.3	52.2	1.7	50.8	51.4	54.7	52.2	31.1	51.9	52.5	50.8
2365	50.2	6.6	52.1	1.6	51.0	51.3	54.7	52.4	30.7	51.8	52.4	50.7
2370	50.2	6.9	52.4	1.6	51.3	51.6	54.4	52.4	31.0	52.1	52.7	50.7
2375	50.3	7.0	52.5	1.7	51.1	51.7	54.7	52.5	31.7	52.2	52.8	50.8
2380	50.3	7.0	52.5	1.7	51.4	51.7	54.7	52.5	31.9	52.2	52.8	50.8
2385	50.3	7.3	52.5	1.7	51.4	51.7	55.0	52.5	31.1	52.2	52.8	51.1
2390	50.3	7.0	52.5	1.7	51.4	51.7	54.7	52.8	31.7	52.2	52.8	51.1
2395	50.2	6.9	52.4	1.6	51.3	51.6	54.9	52.7	25.9	52.1	52.7	51.0
2400	50.5	7.3	52.5	1.7	51.4	51.7	55.0	52.5	22.7	52.2	52.8	51.1
2405	50.3	7.0	52.5	1.4	51.4	51.7	54.5	52.8	23.9	52.2	52.8	51.1
2410	50.3	7.3	52.5	1.4	51.4	51.7	55.0	52.5	25.1	52.2	52.8	51.1
2415	50.5	7.3	52.5	1.7	51.4	51.7	55.0	52.8	24.8	52.5	52.8	51.1
2420	50.5	7.0	52.5	1.7	51.4	51.9	55.0	52.8	27.8	52.5	52.8	51.1
2425	50.5	7.0	52.8	1.7	51.4	51.7	54.7	52.8	27.8	52.5	53.1	51.1
2430	50.4	6.9	52.7	1.6	51.6	51.8	55.2	52.7	28.6	52.4	53.0	51.3
2435	50.5	7.3	52.8	1.7	51.7	51.9	55.3	53.3	29.9	52.5	53.1	51.4
2440	50.5	7.3	52.8	1.7	51.7	51.9	55.3	52.8	30.2	52.5	53.1	51.4
2445	50.4	7.2	52.7	1.6	51.6	51.8	55.2	52.7	30.7	52.4	53.3	51.3
2450	50.5	7.0	52.8	1.7	51.7	51.9	55.3	52.8	30.8	52.5	53.1	51.4

2455	50.5	7.0	52.8	1.4	51.7	52.2	55.3	52.8	30.5	52.8	53.1	51.4
2460	50.5	7.3	52.8	1.4	51.7	52.2	55.3	52.8	30.5	50.3	53.1	51.4
2465	50.5	7.3	52.8	1.7	51.7	51.9	55.3	53.1	30.5	52.5	53.1	51.4
2470	50.5	7.3	52.8	1.4	51.7	51.9	55.3	53.1	31.1	52.8	53.3	51.4
2475	50.7	7.2	52.7	1.6	51.6	51.8	55.8	53.0	31.6	52.7	53.0	51.3
2480	50.8	7.3	53.1	1.7	51.7	52.2	55.3	53.1	31.4	52.8	53.1	51.4
2485	50.8	7.0	53.1	1.7	54.5	52.2	55.6	53.1	21.2	52.8	53.3	50.5
2490	50.8	7.3	53.1	1.7	51.7	52.2	55.3	53.1	23.0	52.8	53.3	51.4
2495	50.8	7.3	53.1	1.7	51.7	52.2	55.6	53.1	23.9	52.8	53.3	51.4
2500	50.8	7.3	52.8	1.7	51.7	52.2	55.3	53.1	25.4	52.8	53.3	51.4
2505	50.8	7.0	53.1	1.7	51.7	51.9	55.6	53.1	27.2	52.8	53.3	51.4
2510	50.8	7.3	53.1	1.7	51.9	52.2	55.6	53.1	29.0	52.8	53.3	51.4
2515	50.7	7.2	53.0	1.6	51.8	52.1	55.5	53.3	27.1	52.7	53.3	51.6
2520	50.7	7.2	53.0	1.6	51.8	52.1	55.8	53.3	31.3	52.7	53.5	51.6
2525	51.0	7.2	53.3	1.6	51.8	52.4	55.8	53.3	29.8	53.0	53.5	51.6
2530	51.1	7.3	53.3	1.7	51.9	52.5	56.2	53.3	30.8	53.1	53.6	51.7
2535	51.1	7.3	53.9	1.7	52.2	52.5	56.2	53.6	31.1	52.8	53.6	51.7
2540	51.1	6.1	53.3	1.7	52.2	52.5	56.2	53.6	31.1	53.1	53.6	51.9
2545	51.1	7.3	53.6	1.4	53.9	52.8	56.2	53.6	30.8	53.3	53.9	51.9
2550	51.3	7.2	53.5	1.6	52.4	52.7	56.1	53.5	31.0	53.3	53.8	51.8
2555	51.4	7.0	53.6	1.7	52.5	52.8	56.2	53.9	31.1	53.3	53.9	51.9
2560	51.4	7.3	53.6	1.7	52.5	52.8	56.4	53.6	31.1	53.6	53.9	51.9
2565	51.4	7.3	53.6	2.7	52.5	52.8	56.4	53.9	31.4	53.6	53.9	52.2
2570	51.4	7.3	53.9	1.7	52.5	53.1	56.7	53.9	26.6	53.3	54.2	52.2
2575	51.7	7.3	53.9	1.7	52.5	53.1	56.7	53.9	26.3	53.3	54.2	52.2
2580	51.6	3.8	53.8	1.6	52.7	53.0	56.9	53.8	23.5	53.3	54.1	52.1
2585	51.7	7.3	53.9	1.7	52.8	53.1	57.0	53.9	24.2	53.6	54.2	52.2
2590	51.7	4.9	53.9	1.7	52.8	53.1	57.0	54.2	25.1	53.9	54.2	52.5
2595	51.7	7.3	54.2	1.7	52.8	53.3	57.3	54.2	27.5	53.6	54.2	52.5
2600	51.9	7.3	54.2	1.7	53.1	53.3	57.0	54.2	29.9	53.9	54.5	52.5
2605	51.9	7.3	54.2	1.7	53.1	53.6	57.6	54.2	30.5	54.2	54.2	52.8
2610	51.9	7.3	54.5	1.7	53.3	53.6	57.6	54.5	30.8	54.2	54.7	52.8
2615	52.2	7.0	54.5	1.7	53.3	53.6	57.6	54.7	31.7	54.2	54.7	52.8
2620	52.2	7.3	54.5	1.4	53.6	53.9	57.6	54.7	31.1	54.2	55.0	53.1
2625	52.2	7.3	54.7	1.7	53.6	53.9	57.8	54.7	26.9	55.0	55.0	53.1
2630	52.4	7.2	54.7	1.6	53.5	53.8	57.7	54.7	27.4	53.8	54.9	53.0
2635	52.5	7.3	54.7	1.7	53.6	53.9	58.1	54.7	28.7	53.9	55.0	53.1
2640	52.5	7.3	54.7	1.7	53.9	54.2	58.1	55.3	29.0	53.9	55.3	53.1
2645	52.8	7.3	55.0	1.7	53.6	54.2	58.1	55.0	30.8	53.9	55.3	53.1
2650	52.5	7.3	55.0	1.4	53.9	54.2	58.1	55.0	30.2	53.9	55.3	53.3
2655	52.4	7.2	54.9	1.6	55.2	54.1	58.3	54.9	30.1	54.7	54.9	53.3
2660	52.4	7.2	54.9	1.6	53.8	54.1	58.0	54.9	30.7	54.7	55.2	53.3
2665	52.8	7.3	55.0	1.7	53.6	54.2	58.1	55.0	31.7	54.7	55.3	53.3
2670	52.8	7.3	55.0	1.7	53.9	54.2	58.1	55.3	31.4	54.7	55.6	53.3
2675	52.8	7.7	55.0	1.7	53.9	54.5	58.4	55.0	31.7	55.0	55.9	53.3
2680	52.8	7.3	55.0	1.7	54.2	54.5	58.1	55.3	31.4	55.0	55.6	53.3
2685	53.0	7.2	55.2	1.6	53.8	54.4	58.3	55.2	32.7	54.9	55.5	53.5
2690	53.1	7.3	55.3	1.4	54.2	54.5	58.4	55.3	31.4	55.0	55.9	53.6
2695	53.1	7.3	55.3	1.7	54.2	54.5	58.4	55.3	31.4	55.0	55.6	53.6
2700	53.1	7.3	55.3	1.7	54.2	54.5	58.4	55.6	31.4	55.0	55.6	53.6

2705	53.0	7.6	55.2	1.6	54.1	54.4	58.6	55.5	33.3	54.9	55.8	53.5
2710	53.1	7.3	55.6	1.7	54.2	54.5	58.7	55.6	31.7	55.0	55.9	53.6
2715	53.1	7.7	55.3	1.7	54.2	54.7	58.7	55.6	31.9	55.3	55.6	53.6
2720	53.1	7.7	55.6	1.1	54.2	54.7	58.7	55.6	31.4	55.3	54.7	53.6
2725	53.1	7.3	55.3	1.4	54.2	54.5	58.7	55.6	31.4	55.0	55.9	53.9
2730	53.1	7.3	56.2	1.7	54.5	54.7	58.7	55.6	32.2	54.2	55.9	53.9
2735	53.3	7.3	55.6	1.7	54.5	54.7	58.7	55.6	31.7	55.3	55.9	53.9
2740	53.3	7.0	55.6	1.7	54.5	54.7	58.7	55.6	31.1	55.3	55.9	53.9
2745	53.3	7.7	55.6	1.7	54.5	54.7	58.7	55.6	31.1	55.3	55.9	53.9
2750	53.3	7.3	55.6	1.7	54.5	54.7	59.0	55.6	31.7	55.3	55.9	53.9
2755	53.3	7.2	55.5	1.6	54.4	54.7	59.1	55.5	32.1	55.5	55.8	53.8
2760	53.3	7.7	55.6	1.7	54.5	55.0	59.0	57.0	32.5	55.6	56.2	53.9
2765	53.3	7.7	55.6	1.7	54.5	55.0	59.0	55.9	31.4	55.6	56.2	53.9
2770	53.3	7.7	55.9	1.7	54.5	55.0	59.0	55.9	31.9	55.6	56.2	53.9
2775	53.3	7.3	55.9	1.7	54.5	55.0	59.0	55.9	31.7	55.6	56.2	53.9
2780	53.3	7.7	55.9	1.7	54.5	54.7	59.0	55.6	31.7	43.4	56.2	53.9
2785	53.3	7.3	55.6	1.7	54.5	54.7	59.0	55.9	31.9	55.3	56.2	53.9
2790	53.3	7.7	55.6	1.7	54.5	54.7	59.0	55.6	31.9	55.3	56.2	53.9
2795	53.3	7.7	55.6	1.7	54.5	54.7	59.0	55.6	31.7	55.3	56.2	53.9
2800	53.3	7.3	55.6	1.7	54.5	54.7	59.0	59.2	31.9	55.3	55.9	53.9
2805	53.3	7.3	55.6	1.7	54.5	54.7	59.0	55.9	31.1	55.3	56.2	53.9
2810	53.3	7.7	55.9	1.7	54.5	54.7	59.0	55.9	31.4	55.6	56.2	53.9
2815	53.3	7.3	55.9	1.7	54.5	55.0	59.2	56.2	32.2	55.3	56.2	53.9
2820	53.3	7.2	55.8	1.6	54.4	54.9	59.4	56.1	32.1	55.5	56.1	53.8
2825	53.6	7.7	55.9	1.7	54.7	55.0	59.5	56.2	32.8	55.9	56.4	54.2
2830	53.5	7.2	56.1	1.6	54.9	54.9	59.4	56.1	32.1	55.8	56.3	54.1
2835	53.9	7.3	56.2	1.7	55.0	55.3	59.8	56.4	31.9	55.9	56.7	54.5
2840	53.9	7.3	56.4	1.7	55.0	55.6	59.8	56.4	33.1	56.2	56.7	54.5
2845	54.2	7.7	56.4	1.7	55.3	55.6	60.1	56.7	33.4	56.2	56.7	54.5
2850	54.2	7.7	56.4	1.7	55.3	55.9	60.1	56.7	32.5	56.2	57.0	54.7
2855	54.2	7.7	56.7	1.7	55.6	55.9	60.4	57.0	32.8	56.4	57.0	54.7
2860	54.2	7.3	56.7	1.7	55.6	56.2	60.6	57.0	31.7	56.4	57.3	55.0
2865	54.5	7.7	57.0	1.7	55.6	56.2	60.6	57.0	31.9	56.4	57.3	55.0
2870	54.5	7.7	57.0	1.7	55.9	56.2	60.9	57.0	31.7	56.7	57.3	55.0
2875	54.4	7.6	56.9	1.6	55.8	56.1	60.8	57.2	31.8	56.6	57.5	54.9
2880	54.5	7.3	57.0	1.7	55.6	56.4	60.9	57.3	31.7	56.7	57.6	55.0
2885	54.7	7.3	57.0	1.7	56.2	56.4	60.9	57.3	32.2	57.0	57.6	55.3
2890	54.7	7.7	57.3	1.7	56.2	56.4	61.2	57.6	32.2	57.0	57.8	55.3
2895	55.0	7.7	57.3	1.4	56.2	56.4	61.2	57.6	31.9	57.0	57.8	55.6
2900	55.0	8.0	57.6	1.7	56.2	47.7	61.5	57.6	32.2	57.3	57.8	55.3
2905	55.0	7.7	57.6	1.7	56.2	56.4	61.5	57.8	31.7	57.3	57.8	47.1
2910	55.0	7.7	57.6	1.7	56.2	56.7	61.5	57.8	31.9	57.3	57.8	55.6
2915	55.0	7.3	56.7	1.7	56.4	56.7	61.5	57.8	32.8	57.3	57.8	55.9
2920	55.3	7.7	57.8	1.7	56.4	57.0	61.8	58.1	31.4	57.6	58.1	55.9
2925	55.3	8.0	57.8	1.7	56.7	56.7	61.8	58.1	31.9	57.0	57.8	55.9
2930	55.3	8.0	57.8	2.3	56.4	57.0	62.0	58.1	31.4	57.3	58.1	55.9
2935	55.3	8.0	57.8	1.7	56.4	57.0	62.0	58.1	31.7	57.0	58.1	55.9
2940	55.3	7.7	57.8	1.7	56.7	57.0	61.8	58.1	32.8	57.3	58.4	55.9
2945	55.3	7.7	58.1	1.7	56.7	57.3	61.8	58.1	32.5	57.3	58.4	56.2
2950	55.6	8.0	58.1	1.7	56.7	57.3	61.8	58.4	32.2	57.8	58.4	56.2

2955	55.6	7.7	58.1	1.7	57.0	57.3	61.8	58.4	32.8	57.6	58.4	56.2
2960	55.9	7.7	58.4	1.7	57.0	57.3	62.0	58.4	32.5	57.8	58.7	56.2
2965	56.0	7.8	58.8	1.8	57.4	57.6	62.4	58.8	33.5	57.9	58.8	56.5
2970	55.9	7.7	58.7	1.7	57.8	57.6	62.3	58.4	31.9	57.8	58.7	56.4
2975	55.9	7.0	58.4	1.7	57.3	57.6	62.3	58.4	32.2	57.6	58.7	56.4
2980	55.8	7.6	58.6	1.6	57.2	57.5	62.5	58.6	32.4	57.7	58.6	56.3
2985	55.9	8.0	58.7	1.7	57.3	57.8	62.6	62.0	32.8	57.8	58.7	56.4
2990	55.9	8.0	58.7	1.7	57.3	57.8	62.9	58.7	31.9	57.8	58.7	56.4
2995	55.9	8.0	58.7	1.7	57.3	57.8	62.9	58.7	32.5	58.1	58.7	56.4
3000	55.9	7.7	58.7	1.7	57.3	57.8	62.9	58.7	31.9	58.1	59.0	56.4
3005	56.2	7.7	58.7	1.7	57.3	57.8	62.6	58.7	31.9	57.8	58.7	56.4
3010	56.0	7.8	58.8	1.8	57.4	57.6	63.0	58.8	32.6	58.2	59.1	56.5
3015	56.2	7.7	58.7	1.7	57.6	57.8	62.9	59.0	32.8	58.1	59.0	56.4
3020	56.2	8.0	59.0	1.7	57.6	57.8	62.9	58.7	31.7	58.4	59.0	56.7
3025	56.2	8.1	59.1	1.8	57.6	58.2	63.0	59.1	31.5	58.5	59.1	56.8
3030	56.2	7.7	59.0	1.7	57.6	57.8	63.2	59.0	31.7	58.4	59.2	56.7
3035	56.2	7.8	58.8	1.8	57.6	57.9	63.0	59.1	31.7	58.5	59.3	56.8
3040	56.2	8.0	59.0	1.7	57.6	58.1	62.9	59.0	32.2	58.4	59.2	56.7
3045	56.2	7.7	59.0	1.7	57.6	57.8	62.9	59.0	31.9	58.4	59.2	56.7
3050	56.2	7.7	59.0	1.7	57.6	57.8	63.2	59.0	31.9	58.4	59.2	56.7
3055	56.2	8.0	59.0	1.7	57.6	58.1	63.2	59.0	32.2	58.4	59.2	56.7
3060	56.2	7.7	59.0	1.7	57.6	57.8	63.2	59.0	31.9	58.4	59.2	56.7
3065	56.2	8.0	59.0	1.7	57.6	58.1	63.2	59.0	32.2	58.4	59.2	56.7
3070	56.4	7.7	59.0	1.7	57.6	58.1	63.2	59.0	33.1	58.4	59.2	56.7
3075	56.4	7.7	59.0	1.7	57.6	58.1	63.5	59.0	32.8	58.4	59.2	56.7
3080	56.2	8.0	59.0	1.7	57.8	58.1	63.5	59.0	31.9	58.4	59.2	56.7
3085	56.2	8.0	59.0	1.7	57.8	58.1	63.5	59.2	32.2	58.4	59.2	56.7
3090	56.4	8.0	59.0	1.7	57.8	58.1	63.2	59.0	32.8	58.4	59.2	57.0
3095	56.4	7.7	59.2	1.7	57.8	58.1	63.5	59.0	33.1	58.7	59.2	56.7
3100	56.5	7.8	59.3	1.8	57.9	58.2	63.5	59.3	32.0	58.8	59.6	57.1
3105	56.4	8.0	59.2	1.7	57.8	58.1	63.5	59.2	33.4	58.7	59.2	57.0
3110	56.4	8.0	59.2	1.7	58.1	58.4	63.5	59.2	33.1	58.7	59.5	57.0
3115	56.6	7.9	59.4	1.6	58.0	58.3	63.6	59.4	32.7	58.9	59.4	57.2
3120	56.8	7.8	59.6	1.8	59.6	58.5	64.1	59.6	33.2	59.1	59.9	57.4
3125	56.7	7.7	59.5	1.7	58.1	58.4	64.0	59.8	33.1	58.7	59.8	57.3
3130	57.0	8.0	59.8	1.7	58.4	58.7	64.3	59.8	33.7	59.0	60.1	57.3
3135	57.1	8.1	60.2	1.8	58.5	59.1	64.7	59.9	33.5	59.1	60.2	57.6
3140	57.3	8.0	60.1	2.1	58.4	59.0	64.9	59.8	32.5	58.7	60.4	57.6
3145	57.4	8.1	60.5	2.2	60.7	59.1	65.2	60.2	32.6	59.1	60.5	56.5
3150	57.3	8.0	60.4	1.7	58.7	59.0	65.1	60.1	32.5	59.2	60.4	57.6
3155	57.3	2.7	60.4	1.7	58.7	59.0	65.7	60.1	31.9	59.2	60.4	57.8
3160	57.3	7.7	60.4	1.7	58.7	59.2	66.0	60.1	33.7	59.5	60.4	57.8
3165	57.6	8.0	60.6	1.7	59.0	59.2	66.0	60.4	34.9	59.8	60.6	57.8
3170	57.6	7.7	60.6	1.7	59.0	59.5	66.3	60.4	32.5	59.8	60.6	58.1
3175	57.9	7.8	60.2	1.8	59.1	59.6	66.4	60.7	33.5	63.5	61.0	58.2
3180	57.9	8.1	61.3	1.8	59.3	59.9	66.4	60.7	33.5	59.9	61.0	52.6
3185	58.2	7.8	61.3	1.8	59.3	60.2	66.6	61.0	33.5	59.9	61.3	58.5
3190	58.2	8.1	61.3	1.8	59.6	60.2	66.4	61.0	34.4	60.7	61.6	58.8
3195	58.1	8.0	61.5	1.7	59.5	60.1	67.9	60.9	33.7	60.6	61.5	58.4
3200	58.2	8.1	61.6	1.8	59.6	60.2	67.5	61.0	32.6	60.7	61.6	58.5

3205	58.2	8.1	61.6	1.8	59.6	60.5	67.5	61.0	32.9	60.7	61.6	58.8
3210	58.4	8.0	61.5	1.7	59.8	60.1	67.9	61.2	33.1	60.6	61.5	58.7
3215	58.5	8.1	61.6	1.8	59.9	60.5	68.0	61.3	32.9	60.7	61.6	58.8
3220	58.4	8.3	61.8	1.7	59.8	60.4	68.2	62.6	32.8	60.9	61.5	58.7
3225	58.5	8.1	61.9	1.8	60.7	60.7	68.3	61.3	33.2	61.0	61.9	56.0
3230	58.4	3.6	62.0	1.7	60.1	60.6	68.5	61.5	33.1	61.2	61.8	59.0
3235	58.8	8.1	62.1	1.8	60.2	60.7	68.3	61.6	32.6	60.2	61.9	59.1
3240	58.8	8.1	62.1	1.8	60.2	60.7	68.6	61.9	33.5	60.5	62.1	59.1
3245	58.7	8.0	62.0	1.7	60.1	60.6	68.7	61.5	32.2	60.4	61.8	59.0
3250	58.8	8.1	62.1	1.8	60.2	60.7	68.8	61.6	32.3	60.5	61.9	59.1
3255	58.8	8.1	62.4	1.8	60.5	60.7	68.8	61.6	33.2	60.5	62.1	59.1
3260	58.7	8.0	62.3	1.7	60.4	60.9	69.0	61.8	34.0	60.4	62.0	59.2
3265	58.8	8.1	62.4	1.8	60.5	60.7	68.8	61.9	33.2	60.7	62.4	59.3
3270	59.1	8.1	62.4	1.8	60.5	61.3	68.8	61.9	34.1	60.7	62.4	59.3
3275	59.0	8.3	62.3	1.7	60.4	60.9	69.0	61.8	33.4	60.4	62.0	59.2
3280	59.1	8.1	62.7	1.8	60.7	61.0	69.1	61.9	33.2	60.7	62.1	59.3
3285	59.0	8.3	62.3	1.7	60.4	60.9	69.3	61.8	32.5	60.6	62.0	59.2
3290	58.8	8.4	62.4	1.8	60.5	61.0	69.4	61.9	33.2	60.7	62.4	59.3
3295	58.8	8.4	62.4	1.8	60.5	61.0	69.4	61.9	33.5	60.5	62.4	59.3
3300	58.9	8.2	62.5	2.3	60.6	61.1	68.9	62.0	33.3	60.6	62.5	59.4
3305	59.1	8.1	62.4	1.8	60.7	61.0	69.4	61.9	25.8	60.5	62.4	59.3
3310	59.1	8.4	62.4	1.8	60.5	61.0	69.4	61.9	28.2	60.5	62.4	59.3
3315	59.0	8.0	62.6	2.1	60.4	60.9	69.3	62.0	28.1	60.4	62.3	59.2
3320	58.8	8.1	62.7	2.2	60.5	61.0	69.4	61.9	27.9	60.7	62.4	59.3
3325	59.1	8.1	62.7	2.2	60.5	61.0	69.4	61.9	29.1	60.7	62.4	59.3
3330	59.1	8.1	62.7	1.8	60.7	61.3	69.6	62.1	34.4	61.0	62.4	59.3
3335	59.1	8.4	62.7	2.2	60.7	61.3	69.4	62.1	33.8	61.0	62.4	59.6
3340	59.1	8.4	62.7	1.8	60.7	61.3	69.4	62.1	34.4	61.0	62.4	59.6
3345	59.0	8.3	62.6	1.7	60.4	61.2	69.5	62.0	34.0	63.2	62.6	59.5
3350	59.3	8.1	62.7	2.2	60.7	61.3	69.4	62.1	35.0	61.3	62.7	59.6
3355	59.3	8.1	63.0	1.8	61.0	61.6	69.6	62.4	34.4	61.9	62.7	59.6
3360	59.2	8.3	62.6	1.7	60.6	61.2	69.5	62.3	34.3	61.5	62.6	59.5
3365	59.3	8.4	63.0	1.8	61.0	61.3	69.9	62.1	34.4	61.6	62.7	59.6
3370	59.3	8.1	63.0	2.2	60.7	61.3	69.6	62.4	34.4	61.6	62.7	59.6
3375	59.4	8.2	63.1	2.3	60.8	61.4	70.0	62.5	35.1	61.7	62.8	59.7
3380	59.3	8.4	63.0	2.2	61.0	61.6	69.9	62.1	34.4	61.9	62.7	59.6
3385	59.3	8.4	63.0	2.2	61.0	61.3	69.9	62.4	34.4	61.9	62.7	59.6
3390	59.3	8.1	63.0	2.2	60.7	61.6	70.2	65.5	34.7	62.1	63.0	59.6
3395	59.3	8.1	63.0	1.8	60.7	61.6	70.2	62.4	34.4	62.1	63.0	59.6
3400	59.3	8.4	63.0	2.2	61.3	61.6	70.2	62.4	34.4	62.1	62.7	59.6
3405	59.3	8.4	63.0	2.2	61.0	61.6	69.9	62.4	35.0	62.1	62.7	59.6
3410	59.3	8.1	63.0	2.2	61.0	61.6	70.2	62.4	35.0	62.1	62.7	59.6
3415	59.5	8.0	62.9	1.7	61.2	62.3	70.1	62.3	34.9	62.0	62.9	59.8
3420	59.7	8.2	63.4	2.3	61.4	62.0	70.5	62.5	34.2	62.8	63.1	60.0
3425	59.6	8.1	63.3	2.2	61.3	61.9	70.4	62.7	33.8	62.4	63.3	60.2
3430	59.6	8.4	63.3	1.8	61.6	61.9	70.7	62.7	34.1	62.4	63.3	60.2
3435	59.9	8.7	63.5	2.2	61.6	61.9	71.0	63.0	33.5	62.4	63.3	60.2
3440	59.9	8.4	63.8	2.2	61.6	61.9	71.2	63.0	34.1	62.4	63.3	60.2
3445	59.9	8.1	64.1	2.2	61.6	62.1	71.8	63.0	33.5	62.7	63.3	60.2
3450	59.9	8.4	64.7	2.2	61.6	62.1	72.0	63.0	33.8	62.7	63.5	60.2

3455	60.2	8.4	64.9	2.2	61.9	62.1	72.0	63.3	34.7	62.7	63.5	60.5
3460	60.2	8.4	64.7	2.2	61.9	62.4	72.3	63.3	34.7	63.0	63.8	60.5
3465	60.5	8.4	65.2	2.2	62.1	62.4	72.3	63.5	35.0	63.3	63.8	60.7
3470	60.5	8.4	65.5	2.2	62.1	62.7	72.6	63.5	34.4	63.5	64.1	60.7
3475	60.6	8.5	65.3	2.3	62.5	62.8	73.0	63.9	35.1	63.6	64.2	60.8
3480	60.7	8.4	66.1	2.2	62.4	63.0	73.1	63.8	35.0	63.5	64.1	61.0
3485	60.7	8.4	66.4	2.2	62.4	63.0	73.7	63.8	35.0	63.5	64.1	61.0
3490	60.7	8.4	67.2	2.2	62.4	63.0	74.5	63.8	34.7	63.8	64.4	61.0
3495	60.6	8.0	67.7	2.1	62.3	62.9	75.0	63.7	34.6	63.7	64.3	60.9
3500	60.8	8.8	68.1	2.3	62.8	63.1	75.4	63.9	34.5	63.9	64.5	61.1
3505	61.0	8.4	69.6	2.2	62.7	63.0	76.2	63.8	36.4	63.8	64.7	61.0
3510	60.7	8.4	71.5	2.2	62.4	63.0	77.0	63.8	35.3	63.8	64.4	61.0
3515	60.7	8.7	73.7	2.2	62.4	63.0	77.8	69.6	35.6	63.8	64.7	61.0
3520	60.7	8.4	74.2	2.2	62.7	63.0	78.1	63.8	35.3	63.5	64.7	60.2
3525	61.0	8.4	74.2	2.2	62.7	63.0	78.9	64.1	35.6	63.8	64.7	61.0
3530	60.7	8.7	75.9	2.2	62.7	64.1	79.4	63.8	34.4	63.8	64.7	61.3
3535	61.0	8.4	76.4	2.2	62.7	63.3	79.7	64.1	35.0	64.1	64.7	61.3
3540	61.0	8.7	77.0	2.2	62.7	63.3	80.2	64.1	35.0	63.8	64.9	61.3
3545	60.9	8.3	78.0	2.1	62.6	62.9	80.7	64.0	34.3	63.7	65.1	61.2
3550	61.0	8.4	78.6	2.2	62.7	63.3	81.3	64.1	34.7	63.8	64.9	61.3
3555	61.0	8.4	78.6	2.2	63.0	63.3	81.8	64.1	34.7	63.8	64.9	61.3
3560	61.0	8.4	79.9	2.2	63.0	63.3	82.4	64.1	35.9	64.1	65.2	61.3
3565	60.9	8.6	80.4	2.1	62.6	63.2	82.8	64.0	34.3	63.7	65.1	60.9
3570	60.9	8.3	81.2	2.1	62.9	63.2	83.6	64.0	34.6	63.7	65.1	61.2
3575	60.8	8.5	81.9	2.3	62.8	63.1	84.3	64.2	34.5	63.9	65.3	61.4
3580	61.0	8.7	82.4	2.2	62.7	63.3	84.8	64.1	35.0	63.8	65.2	61.3
3585	60.9	8.3	82.8	2.1	62.6	63.2	84.9	64.0	35.5	64.0	65.1	61.2
3590	61.3	8.1	83.2	2.2	63.0	63.5	85.6	64.1	35.9	64.1	65.2	61.3
3595	61.3	8.1	83.4	2.2	63.0	63.5	85.6	64.4	35.9	64.4	65.5	61.6
3600	61.3	8.4	83.2	2.2	63.0	63.5	85.3	64.4	36.4	64.1	65.2	61.6
3605	61.0	8.7	79.7	2.2	62.4	63.0	83.2	64.1	34.7	63.8	64.4	61.3
3610	60.3	8.5	68.4	2.3	61.7	62.5	77.6	63.1	34.2	63.1	63.4	60.6
3615	58.8	8.4	61.6	2.2	59.9	61.0	69.4	61.9	33.5	61.6	61.6	59.3
3620	56.8	8.4	58.8	2.2	57.6	58.8	62.7	59.3	33.2	59.1	59.1	57.4
3625	54.6	8.1	56.2	2.2	55.1	56.0	58.5	56.8	31.7	55.7	56.5	55.1
3630	52.0	8.1	53.7	2.2	52.3	53.4	55.1	54.0	31.2	54.0	53.7	52.9
3635	49.5	7.4	51.2	2.2	49.8	50.9	51.5	51.8	30.3	51.2	51.2	49.8
3640	46.9	7.4	48.7	2.2	47.2	48.4	48.9	48.9	28.8	48.1	48.4	47.8
3645	44.6	7.1	46.1	2.2	44.9	45.8	46.4	46.6	28.5	46.4	46.1	45.5
3650	42.3	6.8	43.8	2.2	42.6	43.5	43.8	44.3	27.0	44.1	43.5	43.2
3655	40.0	6.8	41.4	2.2	40.2	41.1	41.4	41.7	26.4	41.7	41.4	41.1
3660	37.9	6.5	39.4	2.2	37.9	39.1	39.7	40.0	26.1	39.7	39.1	38.8
3665	35.8	6.1	37.2	2.1	36.0	36.9	36.9	37.5	23.6	37.2	36.9	36.9
3670	34.1	6.2	35.3	2.2	34.1	35.0	35.0	35.6	22.5	35.9	35.0	35.3
3675	32.3	5.9	33.2	2.2	32.3	32.6	33.5	33.8	21.0	33.5	32.9	33.5
3680	30.6	5.6	31.5	2.2	30.6	30.6	32.0	32.0	20.4	32.0	31.5	31.7
3685	29.1	5.3	29.7	2.2	29.1	28.8	30.3	30.6	19.5	30.6	29.7	29.7
3690	27.3	5.3	28.2	2.2	27.3	27.6	28.8	28.8	18.9	29.1	28.2	28.8
3695	26.1	5.0	26.7	2.2	26.1	26.7	27.0	27.3	17.7	27.6	26.7	27.3
3700	24.9	5.0	25.5	2.2	24.6	25.5	26.1	26.1	16.8	26.4	25.5	26.1

3705	23.7	5.0	24.0	2.2	23.4	24.0	24.3	24.6	16.1	25.2	24.0	24.9
3710	22.2	4.6	22.8	1.8	22.2	23.1	23.1	23.4	15.5	24.0	23.1	23.7
3715	21.6	4.3	21.6	1.8	21.3	21.9	22.2	22.5	14.9	22.8	21.9	22.8
3720	20.5	4.4	20.8	2.0	20.2	20.8	21.4	21.4	14.4	22.0	21.1	21.7
3725	19.6	4.4	19.9	2.0	19.0	19.9	20.2	20.5	13.2	20.8	19.9	20.8
3730	18.5	3.9	18.5	1.7	18.2	18.8	19.1	19.7	12.9	19.7	18.8	19.7
3735	17.8	4.1	17.8	2.0	17.2	18.1	18.4	19.3	12.5	19.3	18.1	19.0
3740	16.8	3.7	17.1	1.8	16.1	17.1	17.4	17.7	11.5	18.3	17.1	18.3
3745	16.0	3.6	16.0	1.7	15.4	16.4	16.4	17.0	11.4	17.3	16.0	17.3
3750	14.8	3.6	15.4	1.7	14.5	15.7	15.7	16.4	10.8	16.7	15.4	16.7
3755	14.9	3.4	14.9	1.8	14.0	15.2	15.2	15.8	10.3	16.1	14.6	16.1
3760	14.3	3.4	14.0	1.8	13.4	14.6	14.6	14.9	10.6	15.5	14.0	15.5
3765	13.6	3.3	13.3	1.7	12.6	13.9	13.6	14.5	9.8	14.8	13.3	14.8
3770	13.1	3.1	12.7	1.8	12.1	13.4	13.4	14.0	9.3	14.3	12.7	14.3
3775	12.4	3.1	12.4	1.5	11.5	12.7	12.7	13.7	9.0	13.7	12.1	13.7
3780	11.8	3.1	11.8	1.5	10.9	12.4	12.1	13.1	8.7	13.4	11.8	13.4
3785	11.7	3.0	11.1	1.4	10.5	11.7	11.4	12.3	8.0	12.6	11.1	12.6
3790	11.1	2.7	10.8	1.4	9.8	11.4	11.1	12.0	7.7	12.3	10.8	12.3
3795	10.3	3.1	10.3	1.5	9.3	11.2	10.6	11.5	7.4	11.8	10.3	11.8
3800	10.6	2.5	9.9	1.5	9.0	10.6	10.3	11.2	7.1	11.5	9.9	11.5
3805	10.3	2.5	9.3	1.5	8.7	10.3	9.6	10.9	6.8	11.2	9.3	11.2
3810	9.6	2.5	9.0	1.5	8.4	9.9	9.3	10.3	6.8	10.9	9.0	10.9
3815	9.3	2.5	8.7	1.5	8.1	9.6	9.0	9.9	6.5	10.6	8.7	10.6
3820	9.0	2.5	8.4	1.5	7.8	9.0	8.7	9.6	6.2	10.3	8.4	10.3
3825	8.6	2.4	8.0	1.4	7.0	8.6	8.3	9.2	5.8	9.8	8.0	9.5
3830	8.7	2.5	7.8	1.5	7.1	8.7	8.1	9.3	5.6	9.6	7.8	9.6
3835	8.5	2.6	7.6	1.3	6.9	8.5	7.9	9.1	5.4	9.4	7.6	9.4
3840	8.1	2.2	7.4	1.5	6.5	8.1	7.8	8.7	5.3	9.0	7.4	9.0
3845	7.8	2.2	7.1	1.5	6.2	7.8	7.1	8.4	5.0	9.0	7.1	8.7
3850	7.3	2.1	6.7	1.1	6.1	7.7	7.0	8.0	4.9	8.6	6.7	8.6
3855	7.3	2.1	6.4	1.1	5.8	7.3	6.7	8.0	4.5	8.3	6.7	8.3
3860	7.2	2.0	6.3	1.6	5.7	7.2	6.9	7.9	4.8	8.2	6.6	8.2
3865	6.8	1.8	6.2	1.2	5.6	6.8	6.5	7.8	4.3	8.1	6.2	8.1
3870	6.8	1.8	5.9	1.2	5.3	6.8	6.2	7.4	4.3	7.8	6.2	7.8
3875	6.5	1.8	5.9	1.2	5.3	6.5	5.9	7.4	4.3	7.8	5.9	7.4
3880	6.5	1.8	5.6	1.2	5.0	6.5	5.9	7.1	4.0	7.4	5.6	7.4
3885	6.1	1.7	5.5	1.1	4.5	6.4	5.8	6.7	3.9	7.3	5.5	7.0
3890	6.2	1.8	5.3	1.2	4.6	6.2	5.6	6.5	3.7	7.1	5.6	7.1
3895	5.8	1.7	5.2	1.1	4.2	6.1	5.2	6.4	3.6	6.7	5.2	6.7
3900	5.8	1.7	4.9	1.1	4.2	5.8	5.2	6.4	3.3	6.7	5.2	6.7
3905	5.9	1.8	5.0	1.2	4.3	5.9	5.0	6.5	3.4	6.8	5.0	6.8
3910	5.3	1.8	4.6	1.2	4.0	5.3	5.0	6.2	3.4	6.8	5.0	6.5
3915	5.5	1.7	4.5	1.1	3.9	5.5	4.5	6.1	3.3	6.4	4.5	6.4
3920	5.6	1.8	4.3	1.2	3.7	5.3	4.6	5.9	3.4	6.5	4.6	6.5
3925	5.3	1.5	4.3	1.2	3.7	5.6	4.6	5.9	3.1	6.2	4.3	6.2
3930	4.9	1.4	4.2	1.1	3.6	5.2	4.5	5.8	3.0	6.1	4.2	6.1
3935	5.0	1.5	4.3	0.9	3.4	5.3	4.3	5.6	3.1	6.2	4.3	6.2
3940	5.0	1.5	4.0	1.2	3.4	5.0	4.3	5.6	2.8	5.9	4.3	5.9
3945	5.0	1.5	4.0	1.2	3.4	5.0	4.0	5.6	2.8	5.9	4.0	5.9
3950	4.3	1.8	3.7	0.9	3.1	4.6	4.0	5.6	2.8	5.9	4.0	5.9

3955	4.2	1.4	3.6	1.1	3.0	4.5	3.9	5.2	2.7	5.8	3.9	5.8
3960	4.2	1.4	3.6	1.1	3.0	4.5	3.9	5.2	2.7	5.8	3.6	5.5
3965	4.2	1.4	3.6	0.8	3.0	4.5	3.9	5.2	2.7	5.5	3.6	5.5
3970	4.2	1.4	3.6	0.8	2.7	4.5	3.6	5.2	2.7	5.5	3.6	5.5
3975	3.9	1.4	3.6	0.8	2.7	4.5	3.6	4.9	2.4	5.5	3.6	5.5
3980	4.0	1.5	3.4	0.9	2.8	4.3	3.7	5.0	2.2	5.3	3.4	5.3
3985	3.9	1.4	3.3	1.1	2.7	4.2	3.6	4.9	2.4	5.2	3.3	5.2
3990	3.9	1.4	3.3	0.8	2.7	4.2	3.3	4.9	2.1	5.2	3.3	5.2
3995	4.0	1.5	3.1	0.9	2.5	4.3	3.4	4.6	2.2	5.3	3.4	5.3
4000	3.7	1.5	3.1	0.9	2.5	4.0	3.4	4.6	2.2	5.3	3.4	5.3
4005	3.6	1.4	3.0	0.8	2.4	4.2	3.3	4.5	2.1	4.9	3.3	4.9
4010	3.7	1.5	3.1	0.9	2.5	4.0	3.4	4.6	2.2	5.0	3.1	5.0

Appendix D: Uncertainty Analysis

A root-sum square uncertainty analysis was accomplished to compute the accumulated experimental error. The basic equation for the analysis was taken from Doebelin (12:63).

$$E_{rss} = \left[\left(\Delta u_1 \frac{\partial f}{\partial u_1} \right)^2 + \left(\Delta u_2 \frac{\partial f}{\partial u_2} \right)^2 + \ldots + \left(\Delta u_n \frac{\partial f}{\partial u_n} \right)^2 \right]^{1/2} \qquad \text{(D-1)}$$

where E_{rss} = Root-sum square (rss) value
f = function of independent variables
u_1 = first independent variable
Δu_1 = uncertainty in first independent variable
u_2 = second independent variable
Δu_2 = uncertainty in second independent variable
u_n = nth independent variable
Δu_n = uncertainty in nth independent variable

The function of interest for this experiment is the maximum heat throughput at dryout, Q_{max}. This was given by Eq. 3-1.

$$Q_{max} = \dot{m} C_p (T_o - T_i) \qquad \text{(3-1)}$$

Rewriting Eq. D-1, and using Eq. 3-1 as the function, f, gives:

$$\Delta Q_{max} = \left[\left(\Delta \dot{m} \frac{\partial Q_{max}}{\partial \dot{m}} \right)^2 + \left(\Delta C_p \frac{\partial Q_{max}}{\partial C_p} \right)^2 + \left(\Delta T_o \frac{\partial Q_{max}}{\partial T_o} \right)^2 + \left(\Delta T_i \frac{\partial Q_{max}}{\partial T_i} \right)^2 \right]^{1/2} \qquad \text{(D-2)}$$

where ΔQ_{max}= rss uncertainty in maximum heat throughput (W)
$\dot{m}$ = mass flow rate (kg/sec)
$\Delta\dot{m}$ = uncertainty in mass flow rate (kg/sec)
C_p = specific heat of coolant water (J/kg-K)
ΔC_p = uncertainty in specific heat of coolant water (J/kg-K)
T_o = coolant outlet temperature (K)
ΔT_o = uncertainty in coolant outlet temperature (K)
T_i = coolant outlet temperature (K)
ΔT_i = uncertainty in coolant outlet temperature (K)

Performing the partial derivatives of Eq. 3-1, and substituting the results into Eq. D-2, leads to

$$\Delta Q_{max} = \left[\left(\Delta\dot{m}C_p(T_o - T_i)\right)^2 + \left(\Delta C_p\dot{m}(T_o - T_i)\right)^2 + \left(\Delta T_o\dot{m}C_p\right)^2 + \left(T_i\left(-\dot{m}C_p\right)\right)^2\right]^{1/2} \quad \text{(D-3)}$$

The flow meter used in this experiment gave the volumetric flow rate, in terms of liters/minute. It was necessary to convert this to a mass flow rate using the equation;

$$\dot{m} = \rho_l\dot{v}C_1C_2 \quad \text{(D-4)}$$

where $\dot{m}$ = mass flow rate (kg/sec)
ρ_l = coolant density (kg/m^3)
$\dot{v}$ = volumetric flow rate (l/min)
C_1 = conversion factor (m^3/l)
C_2 = conversion factor (min/sec)

To find the uncertainty in the mass flow rate, the uncertainty in Eq. D-4 needed to be found. Using the rss method of Eq. D-1, Eq. D-4 becomes,

$$\Delta \dot{m} = \left[\left(\Delta \rho_1 \frac{\partial \dot{m}}{\partial \rho_1} \right)^2 + \left(\Delta \dot{v} \frac{\partial \dot{m}}{\partial \dot{v}} \right)^2 + \left(\Delta C_1 \frac{\partial \dot{m}}{\partial C_1} \right)^2 + \left(\Delta C_2 \frac{\partial \dot{m}}{\partial C_2} \right)^2 \right]^{1/2} \qquad \text{(D-5)}$$

The last two terms in the above equation are zero because the conversion factors were exact constants. Therefore, the mass flow rate uncertainty becomes,

$$\Delta \dot{m} = \left[\left(\Delta \rho_1 \dot{v} C_1 C_2 \right)^2 + \left(\Delta \dot{v} \rho_1 C_1 C_2 \right)^2 \right]^{1/2} \qquad \text{(D-6)}$$

The values for the density of water were computed using the equations in Physical and Thermodynamic Properties of Pure Chemicals. The authors reported the error of their equation as less than 0.2 percent (7). For conservatism, an uncertainty of 0.2 percent was used. The manufacturers of the flow meter specified the error of the flow meter as 1.0 percent of the reading. Incorporating these numbers into Eq. D-6 gives,

$$\Delta \dot{m} = \left\{ \left[(0.002 \rho_1) \dot{v} C_1 C_2 \right]^2 + \left[\left(0.01 \dot{v} \right) \rho_1 C_1 C_2 \right]^2 \right\}^{1/2} \qquad \text{(D-7)}$$

$$= \left[4 \times 10^{-6} \left(\rho_l \dot{v} C_1 C_2 \right)^2 + 1 \times 10^{-4} \left(\rho_l \dot{v} C_1 C_2 \right)^2 \right]^{1/2}$$

$$= \left[4 \times 10^{-6} \dot{m}^2 + 1 \times 10^{-4} \dot{m}^2 \right]^{1/2}$$

$$= 0.0102 \dot{m}$$

The values for the specific heat of water were based on interpolations of the saturated water tables presented by Incropera (16:A22). For the purpose of this investigation, the error associated with these tables was assumed to be no more than 1.5 percent, therefore:

$$\Delta C_p = 0.015 C_p \tag{D-8}$$

The calculation for the error associated with the measurements of the coolant manifold inlet and outlet temperatures was not as straight forward as the previous uncertainty calculations were. These measurements, T_o and T_i, involved the uncertainty of a series of components making up the DAS. The components included the thermocouple, the multiplexer, and the input/output board. The manufacturer of the multiplexer and the input/output board, Keithley MetraByte, specified the error of the series of components to be 1.9°C. This uncertainty value seemed excessively large so a method was sought to reduce the data imprecision due to the DAS.

The beginnings of this solution were presented in Chapter 3. As was mentioned there, the DAS was found to exhibit a distinct channel bias, with some channels being more accurate both in terms of true temperature measurement and in temperature measurement precision. To take advantage of those channels having the greatest reliability, a TC criticality analysis was performed and the most critical TCs were connected to the most precise DAS channels. These measures constituted the first step in improving the accuracy of the DAS data.

The second step involved data taken during the actual test runs. As part of each test run, bias readings were taken for each of the four most critical TC channels, TC5, TC6, TC11, and TC12. These TCs were used to measure the heat pipe operating temperature (TC5 and TC6), and the coolant manifold inlet and outlet temperatures (TC11 and TC12, respectively). This bias data was used to construct a correlation curve for each of the four critical TCs, for each test category, (static, 1.84g, 2.50g, and 3.27g). Fig. D.1 is an example of one of the correlation curves. Similar correlation curves were constructed for each of the four critical TCs, during each of the four test categories (static and three vibrational cases).

Fig. D.1 shows the bias measurements for the coolant manifold outlet temperature from the 3.27g test runs. The measured temperature, as recorded by the DAS is along the X-axis, while the true tempera-

ture, as recorded using the calibration unit is along the Y-axis. Along with the data points, a least squares linear curve fit is plotted. This line, along with the square of its' reliability (R^2) value were used to compute the coolant manifold temperature and uncertainty at wick dryout. The value for the coolant manifold outlet temperature was computed using the DAS measurement at wick dryout and the equation for the curve fit shown in Fig. D.1. The uncertainty associated with this calculated value is a function of the reliability of the curve fit, using the equation,

$$\Delta T_o = T_o\sqrt{1-R_o^2} \tag{D-9}$$

where ΔT_o= uncertainty associated with the coolant manifold outlet temperature ($^\circ$C)
T_o = calculated coolant manifold outlet temperature ($^\circ$C)
R_o^2 = square of the reliability of the least squares curve fit

The uncertainty associated with the coolant manifold inlet temperature is computed in a similar fashion. This method for computing the uncertainty associated with the coolant manifold temperatures resulted in data significantly more accurate than specified by the manufacturer. For Fig. D.1, the temperature uncertainty associated with the least squares curve fit line is less than 4.2 percent. Applying this over the range of data plotted, results in an outlet manifold temperature uncertainty between 0.20 and 0.95°C. This is an improvement of nearly 50 percent from the manufacturers specification at the upper end of the

plotted range. At the lower end of the plotted range, there is a reduction in error of nearly 90 percent.

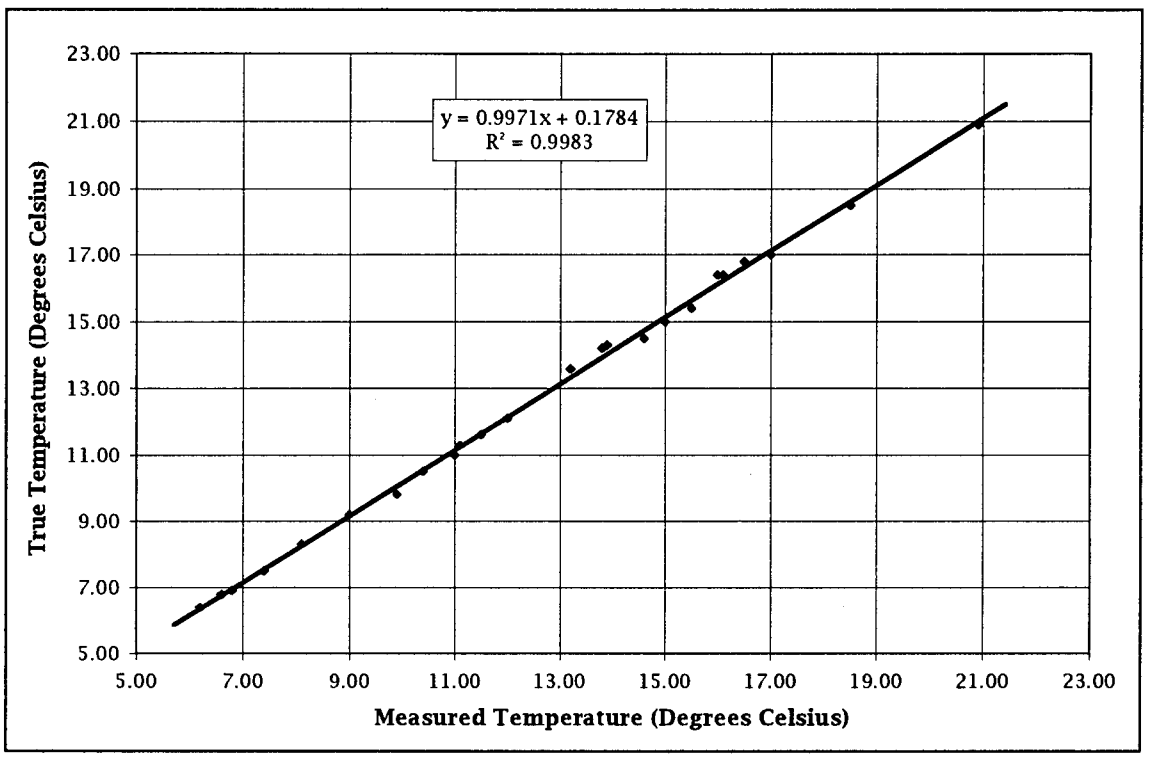

Figure D.1 Correlation Curve for Manifold Outlet Temperature (3.27G)

The individual uncertainty equations (Eqs. D-7, D-8, and D-9) can be substituted into Eq. D-3 to find the total uncertainty associated with maximum heat throughput.

$$\Delta Q_{max} = \left\{ \left[0.0102 \dot{m} C_p (T_o - T_i) \right]^2 + \left[0.015 C_p \dot{m} (T_o - T_i) \right]^2 + \left(T_o \dot{m} C_p \sqrt{1 - R_o^2} \right)^2 + \left[T_i \left(-\dot{m} C_p \right) \sqrt{1 - R_i^2} \right]^2 \right\}^{1/2} \quad \text{(D-10)}$$

$$= \left\{ \left(0.0102^2 + 0.015^2\right)\left[\dot{m}C_p(T_o - T_i)\right]^2 \right.$$
$$\left. + \left(1 - R_o^2\right)\left(T_o \dot{m} C_p\right)^2 + \left(1 - R_i^2\right)\left(T_i \dot{m} C_p\right)^2 \right\}^{1/2}$$

This equation can be simplified one step further to yield

$$\Delta Q_{max} = \left[\left(3.2904 \times 10^{-4}\right) Q_{max}{}^2 + \left(1 - R_o^2\right)\left(T_o \dot{m} C_p\right)^2 + \left(1 - R_i^2\right)\left(T_i \dot{m} C_p\right)^2 \right]^{1/2} \quad \text{(D-11)}$$

Eq. D-11 is used, in conjunction with the correlation curves for each test category, to compute the uncertainty associated with the maximum heat throughput at wick dryout, Q_{max}.

Bibliography

1. Adam, N. K. The Physics and Chemistry of Surfaces. New York: Dover Publishing Incorporated, 1968.

2. Brennan, Patrick J. and Edward J. Kroliczek. Heat Pipe Design Handbook: Volume II, NTIS N81-70112. Towson, Maryland: B & K Engineering, Inc., June 1979.

3. Charlton, Mark C. Effect of Transverse Vibration on the Capillary Limit of a Wrapped Screen Wick Copper/Water Heat Pipe. MS thesis, AFIT/GA/ENY/92D-02. School of Engineering, Air Force Institute of Technology (AU), Wright-Patterson AFB, OH, December 1992.

4. Cheng, K. C. and J. P. Zarling. "Applications of Heat Pipes and Thermosyphons in Cold Regions," Heat Pipe Technology, Volume II: Materials and Applications. 1-32. New York: Begell House Inc. Publishers, 1993.

5. Chi, S. W. Heat Pipe Theory and Practice: A Sourcebook. Washington: Hemisphere Publishing Corporation, 1976.

6. Clark, L. T. and G. S. Glenn. "Design Analysis and Testing of Liquid Metal Heat Pipes for Application to Hypersonic Vehicles," AIAA-88-2679. American Institute of Aeronautics and Astronautics, June 1988.

7. Daubert, T. R. and R. P. Danner. Physical and Thermodynamic Properties of Pure Chemicals. Washington: Hemisphere Publishing Corporation, 1989.

8. DeMeis, Richard. "Heat-pipe Cooled Rockets," Aerospace America, 25 [3]: 13-14, (March 1987).

9. Deverall, J. E. "The Effect of Vibration on Heat Pipe Performance," LA-3798. Los Alamos Scientific Laboratory, October 1967.

10. Deverall, J. E., E. W. Salmi, and R. J. Knapp. "Orbital Heat Pipe Experiment," LA-3714. Los Alamos Scientific Laboratory, June 1967.

11. Deverall, J. E. and J. E. Kemme. "Satellite Heat Pipe," LA-3278-MS. Los Alamos Scientific Laboratory, January 1965.

12. Doeblin, E. O. Measurement Systems: Application and Design. New York, McGraw-Hill Book Company, 1983.

13. Dunn, P. D. and D. A. Reay. Heat Pipes. Oxford: Pergamon Press, 1976.

14. Grover, G. M., T. P. Cotter, and G. F. Erickson. "Structures of Very High Thermal Conductance," Journal of Applied Physics, 35 [7]: 1990-1991, (July 1964).

15. Huber, Neil F. Effect of Longitudinal Vibration on the Capillary Limit of a Wrapped Screen Wick Copper/Water Heat Pipe. MS thesis, AFIT/GAE/ENY/93D. School of Engineering, Air Force Institute of Technology (AU), Wright-Patterson AFB, OH, December 1993.

16. Incropera, F. P. and D. P. DeWitt. Fundamentals of Heat and Mass Transfer. New York: John Wiley and Sons, 1990.

17. Ivanovskii, M. N., V. P. Sorokkin, and I. V. Yagodkin. The Physical Principles of Heat Pipes. Oxford: Clarendon Press, 1982.

18. Richardson, John W., Charles A. Whitehurst, and Gerald D. Whitehouse. "The Effect of Longitudinal Vibration on Heat Pipe Performance," The Journal of Astronautical Sciences, 17 [5]: 249-266, (March-April 1970).

19. Silverstein, Calvin C. Design and Technology of Heat Pipes for Cooling and Heat Exchange. Washington: Hemisphere Publishing Corporation, 1992.

20. Tawil, M., J. Alario, R. Prager, and R. Bullock. "Heat Pipe Applications for the Space Shuttle," Progress in Astronautics and Aeronautics: Thermal Control and Radiation. 103-112. Cambridge, Massachusetts: The MIT Press, 1973.

21. D250T Axially Grooved Aluminum-Ammonia Heat Pipe Qualification Data. Dynatherm Corporation, Cockeysville, MD, 1994.

22. Vibration Testing System. Operations and Maintenance Manual TA30-5-1. Wallingford, Conn.: Unholtz-Dickie Corporation, no date.

VITA

Captain Kenneth A. Carpenter was born 2 April 1963, in Coldwater, Michigan. He is married to Karen S. Carpenter and has an 18-month old daughter, Katherine. Kenneth graduated from Bronson High School in June of 1981, and enlisted in the United States Air Force in November 1981 as a Munitions Systems Specialist. As an enlisted member, he served tours of duty at Andersen AFB, Guam, and Loring AFB, Maine, and rose to the rank of Staff Sergeant. In April of 1986, he was selected for the Airman's Education and Commissioning Program (AECP) in the field of Aeronautical Engineering. The Air Force sponsored his undergraduate program at Purdue University, where he received his Bachelor of Science Degree in Aeronautical and Astronautical Engineering in May of 1988. He graduated from Officer Training School in September 1988, and was assigned to the 6595th Aerospace Test Group at Vandenberg AFB, CA. There he worked as a Titan Launch Systems Engineer, supervising the dismantling of the Titan 34D Launch Tower, and the construction of the new Titan IV Launch Tower. He was transferred to the Satellite Operations Division where he was chosen as a Satellite Launch Operations Engineer for the first West Coast Titan IV launch. In May 1993, he was selected to attend the Astronautical Engineering Program at the Air Force Institute of Technology (AFIT). Upon graduation, he will be tranferring to a Project Office in Washington DC.

Permanent Address: Kenneth Carpenter
1103 Carpenter Rd
Bronson, MI 49028

REPORT DOCUMENTATION PAGE

Form Approved
OMB No. 0704-0188

1. AGENCY USE ONLY (Leave blank)	2. REPORT DATE	3. REPORT TYPE AND DATES COVERED
	December 1994	Master's Thesis

4. TITLE AND SUBTITLE
The Effects of Transverse Vibration on the Performance of an Axial Groove Wick Heat Pipe

5. FUNDING NUMBERS

6. AUTHOR(S)
Kenneth A. Carpenter, Captain, USAF

7. PERFORMING ORGANIZATION NAME(S) AND ADDRESS(ES)
Air Force Institute of Technology/ENY
Wright-Patterson AFB, OH 45433

8. PERFORMING ORGANIZATION REPORT NUMBER
AFIT/GA/ENY/94D-5

9. SPONSORING/MONITORING AGENCY NAME(S) AND ADDRESS(ES)

10. SPONSORING/MONITORING AGENCY REPORT NUMBER

11. SUPPLEMENTARY NOTES

12a. DISTRIBUTION/AVAILABILITY STATEMENT
Approved for public release; distribution unlimited

12b. DISTRIBUTION CODE

13. ABSTRACT *(Maximum 200 words)*

An experimental investigation was performed to determine the effects of transverse vibrations on the performance of an ammonia/aluminum axial groove wick heat pipe. Theoretical calculations predicted a performance degradation due to the working fluid being shaken out of the upper capillary grooves. A benchtop shaker was used to apply transverse, sinusoidal vibrations of 30, 35, and 40 Hertz, corresponding to peak acceleration amplitudes of 1.84g, 2.50g, and 3.27g, respectively. Maximum heat throughput, Q_{max}, of the vibrating heat pipe was measured. A comparison of these values and static Q_{max} values indicated a degradation in heat pipe performance. A mean performance deterioration of 27.6 Watts was measured for the 1.84g case; an average degradation of 12.9 percent from static heat pipe performance. At 2.50g peak acceleration, the degradation rose to 37.3 Watts; an average decrease of 14.8 percent from static performance. An average deterioration in performance of 28.1 percent was recorded for the 3.27g case. This amounted to a mean performance degradation of 69.3 Watts. The results of this investigation revealed that transverse, sinusoidal vibrations have a detrimental impact on the performance of an ammonia/axial groove wick heat pipe. Further, the performance degradation increases with increasing vibrational peak acceleration amplitude.

14. SUBJECT TERMS	15. NUMBER OF PAGES
Heat Pipe, Vibration, Axial Groove	108
	16. PRICE CODE

17. SECURITY CLASSIFICATION OF REPORT	18. SECURITY CLASSIFICATION OF THIS PAGE	19. SECURITY CLASSIFICATION OF ABSTRACT	20. LIMITATION OF ABSTRACT
Unclassified	Unclassified	Unclassified	UL